1949

Investigation of physical and chemical effects of ion irradiation on different materials and their possible application.

(*Functionalization of microfluidic devices by microstructures created with proton beam lithography*)

Thesis for the Degree of Doctor of Philosophy (PhD)

Emad Nady Saad Ahmed

Supervisor: Dr. Róbert Huszánk

UNIVERSITY OF DEBRECEN

Doctoral Council of Natural Sciences and Information Technology

Doctoral School of Physics

Debrecen, 2022

Hereby I declare that I prepared this thesis within the Doctoral Council of Natural Sciences and Information Technology, Doctoral School of Physics, University of Debrecen in order to obtain a PhD Degree in Natural Sciences at Debrecen University.

The results published in the thesis are not reported in any other PhD theses.

Debrecen, 2022.

…….
Emad Nady Saad Ahmed
Doctoral candidate

Hereby I confirm that Emad Nady Saad Ahmed candidate conducted his studies with my supervision within the Physical Methods in Interdisciplinary Researches Doctoral Program of the Doctoral School of Physics between 2017 and 2022. The independent studies and research work of the candidate significantly contributed to the results published in the thesis.

I also declare that the results published in the thesis are not reported in any other theses.
I support the acceptance of the thesis.

Debrecen, 2022.

…….
Dr. Róbert Huszánk
Supervisor

Investigation of physical and chemical effects of ion irradiation on different materials and their possible application.

(Functionalization of microfluidic devices by microstructures created with proton beam lithography)

Dissertation submitted in partial fulfilment of the requirements for the doctoral (PhD) degree in **Physics**

Written by **Emad Nady Saad Ahmed** certified Physicist

Prepared in the framework of the Physics Doctoral School of the University of Debrecen

Physical Methods in Interdisciplinary Researches programme

Dissertation advisor: **Dr. Róbert Huszánk**

The official opponents of the dissertation:

Dr. ....

Dr. ....

The evaluation committee:

Chairperson:	Dr.	.....
Members:	Dr.	.....
	Dr.	.....
	Dr.	.....
	Dr.	.....

The date of the dissertation defence: ……20 …

Contents

Chapter 1

1. Introduction

The following dissertation summarizes the results that have been achieved during my PhD studies in the Doctoral School of Physics in Debrecen University.

In my work, I investigated the difficulty of the laminar flow mixing phenomena with fabricated microfluidic devices, functionalized them as passive micromixers. Our aim was to find structures, designs or any way to induce perturbation in the laminar flow, to make the mixing more efficient. This study includes the computer simulation, the design and manufacturing of different microfluidic devices with or without embedded microstructures. By coupling proton beam lithography (direct writing technique utilizing focused, few MeV proton beams, to create micro- and nanoscale structures) and conventional UV lithography fabrication techniques, Poly(dimethyl-siloxane) PDMS microstructures were incorporated into PDMS micro-devices, as a novel creation method. This allows microstructures and micro-devices to be created from the same material, which is not only beneficial but also necessary in some applications (e.g., cell separation, etc.).

1.1. Objectives

It is well known, that the mixing of two fluid flow at microscale, even if they are the same material (e.g., water and a diluted aqueous solution), is still a great challenge for researchers because of the behaviour of the laminar flow. Because of that, working with microfluidic devices, at certain applications, is still difficult, for example in chemical synthesis at microscale, analysis of

chemical content of biological or biochemical applications, which gives importance to this area of research.

During my doctoral work, my first aim was to learn the steps of the fabrication of a microfluidic device. The first step is applying only UV lithography method, using UV light and the negative SU-8 photoresist. The second step is applying the microlithography using the PDMS negative resist, to learn the microfabrication method using the microprobe instruments. Finally, the microfluidic devices were finalized by combining the two methods, where the created microstructures by proton microlithography were integrated to the created macro parts by UV lithography.

My goal was also, after a literature overviewing, to simulate microfluidic devices with different layouts, obstacles and designs to investigate the mixing properties of them using two different concentration liquids as inlets. After finding a good structure, layout or design candidates for mixing by simulations, I planned to fabricate them in real chips.

My final goal was, to investigate the mixing performance of the functionalized microfluidic devices (i.e.: the chips containing the microstructures) to compare their mixing efficiency values, then draw the conclusions of the obtained results.

For thesis structure, in the beginning brief summary was discussed for the literatures overviewing, introduction, advantages, principles and descriptions of microfluidics micromixer devices. Passive micromixers and their physical parameters were detailed in chapter 2. Then, the general theoretical background of proton microlithography and UV lithography techniques are illustrated through this chapter.

The used methods and materials in our research work are showed in chapter 3, in which the details of experimental facilities and procedures are described in two ways. Firstly, introduction and physics of the COMSOL simulation

using microfluidic module are introduced, then followed by computational fluid dynamics (CFD) simulations of different microstructures for mixing purposes. Secondly, the experimental steps for creating our microstructures are described in details.

The fabrication stages of microfluidic chips were discussed through chapter 3, where the details of the fabrication of the microstructures were showed using the proton beam lithography and the UV-lithography techniques, then the system for mixing test of our fabricated micromixers chips was described to investigate the mixing performance of those chips.

Chapter 4 discusses the obtained results of COMSOL simulations for different micromixers, and shows the calculated mixing efficiency values of the suggested microstructures. Then, the real different passive micromixers and their mixing performances and mixing efficiencies are reported.

Conclusions and summary of the scientific results obtained in our research work are shown in chapter 5.

Chapter 2

2. Theoretical background

2.1. Introduction to Microfluidics

The first microfluidic devices proved that fluidic components could be downsized and integrated together, giving rise to the concept that a full "lab on a chip" could be fitted, much like a microelectronic circuit is an entire computer on a chip. Since then, there has been a lot of interest in realizing the full potential of this approach, which has resulted in the creation of a variety of microfluidic devices and fabrication methods.

Poly(dimethyl-siloxane) (PDMS) and other elastomeric materials have already appeared as excellent competitors to the silicon and glass materials and actually used in MEMS (microelectromechanical systems) devices.[1,2] By which, simplified device fabrication and the ability to accept densely integrated microvalves into designs.[3,4] So the microfluidics devices have exploded into a ubiquitous technology with applications in a wide range of fields.

As numerous researchers have pointed out, that scaling down fluidic processes to the microscale offers many significant advantages[5,6,7,8,9,10,11,12,13], some stemming directly from the reduction in size and others a result of the ability to integrate at this scale.

One of the characteristics of microscale and nanoscale devices is the high surface to volume ratio (SVR), which is the result of the downscaling[14]. Surface tension and viscosity, rather than gravity and inertia, become the main characteristics in the micro domain of microfluidic devices. Electrokinetic pumping, surface tension-driven flows, electromagnetic forces, and acoustic streaming are examples of mechanisms that have no affect macroscopic

assessments but are crucial at the microscale[15,16].This property can result in different types of dominating forces. For example, large SVR typically make surface forces (such as surface tension) the dominant force, while significantly decrease the inertial and body force effects.

Because of the high surface-to-volume ratio, a high rate of heat and mass transfer is possible in microfluidic devices. "Digital microfluidic technology" is an example of a microfluidic design that takes advantage of this property, in which droplets of water/oil are produced and carried in a controlled manner to fulfil specific purposes like storage, mixing, chemical reaction, or analysis[17,18,19]. The SVR have also positive effects, especially on increasing the reaction rate in case of in microfluidic devices used for chemical reactions.

Since 1979, when the first micro-gas chromatograph was introduced[20], microfluidic technology has improved steadily, allowing numerous operations to be performed on a single small chip, including mixing, reaction, separation, and analysis.

The most important feature of the microfluidic devices to reduce the amount of reagent that is required for specific applications, increase reaction rates, and minimize sample handling, thereby reducing the risk of cross contamination. Commonly, microfluidic devices are used in drug synthesis, gene analysis, and cell analysis[21,22,23].

Micromixers are one form of microfluidic devices that are used to mix two or more fluids in micro scale, in order to handle small amounts of fluids for variety of applications. Micromixer technologies are described based on their applications. (1) chemical applications, such as synthesis, polymerization, and extraction; (2) biological applications, such as DNA analysis, biological screening enzyme tests, and protein folding; and (3) chemical or biochemical content detection/analysis using NMR, FT-IR, or Raman spectroscopies.[24]

Micro-mixing techniques, which were developed not only for laboratory study but also for industrial applications, are used in a number of chemical microfluidic systems.[24,25] Micromixers are crucial parts of microreactors, and they are used to manipulate reagent or catalyst concentrations, as well as for chemical synthesis. Chemical reaction processes in a chemical application can be divided into three types: combined, serial, or multi-mode mixing, as illustrated in Figure 2:1. Micro-mixing's advantage in these applications is that it takes less time to process than traditional methods, making production simpler.[24]

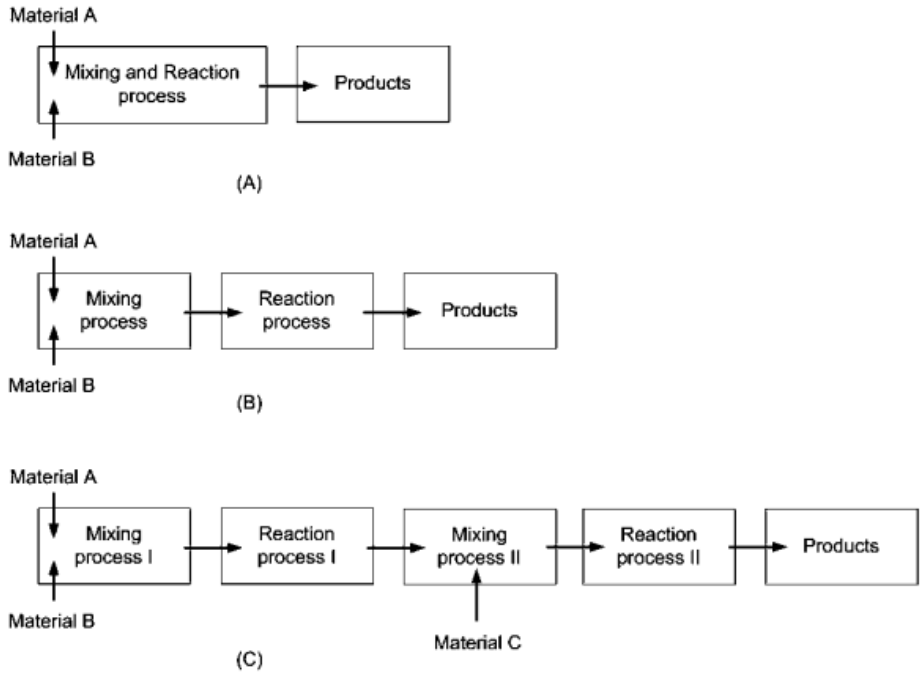

Figure 2:1 Schematic illustration of micro-mixing in chemical applications; (A) simultaneous model, mixing and reaction take place in the mixer; (B) serial model, mixing and reaction take place sequentially in the mixer and reactor; (C) multi model, initial mixing and reaction begin to happen, followed by other mixing and reaction.[24]

There are many applications of microfluidic devices in the branches of chemistry and biology, which lead to development in both research and industry fields. One of these applications, for a simple example, is a highly

selective acylation of ferrocene with various acid anhydrides performed in a microfluidic chip.[25] Acylation is one of the most important synthetic methods in ferrocene chemistry. The used design for this application is a microfluidic chip built in soda-lime glass, with channels created using photolithography and wet etching. The microfluidic chip's inner geometry is 500 μm× 100 μm× 1000 μm. In Figure 2:2, the chip's structure is shown. The final solution, containing ferrocene and the products were neutralized by saturated sodium bicarbonate solution and extracted with hexane. The conversion rate of acylated ferrocene were determined by High-Pressure Liquid Chromatography (HPLC).

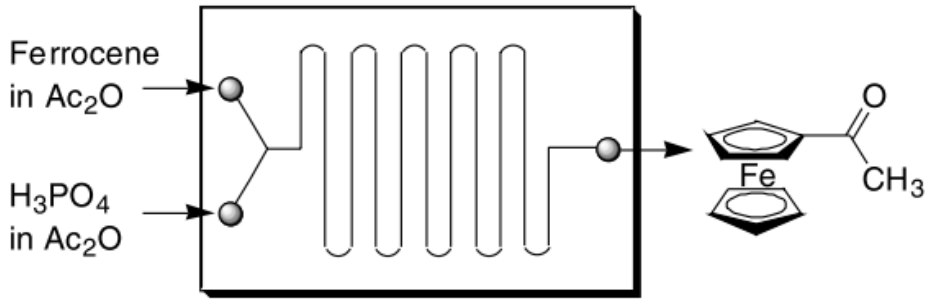

Figure 2:2 The microfluidic chip's schematic configuration for acylation of ferrocene. [25]

Microfluidic chip reactors require less space, energy, and reagents than traditional batch systems, and provide better yields and improved reaction selectivity in a shorter reaction time while producing less wastes due to their short diffusion distance, large specific surface area, and increased thermal transfer. The acetylation of ferrocene with acetic anhydride in the presence phosphoric acid was examined at different flow rates and temperatures. The reactions were carried out at *15* and *25*$^{\circ}C$, respectively. Two syringe pumps were used to introduce the acetic anhydride solution containing ferrocene (molarity = *0.15 M*) and the acetic anhydride solution containing phosphoric acid (molarity = *1.5 M*).

For the reactions at *15°C*, the conversion rate of ferrocene increased from *78%* to *98%* with the increase of flow rate and reached a peak at *35 µl/min* flow rate, and a decrease of conversions was found with increasing flow rate. For the reactions at *25°C*, the conversions in all cases were excellent (*96–99%*). The by-product diacetyl-ferrocene was not detected by HPLC in any case. Therefore, this microchip procedure gave excellent selectivity.[25] In comparison, a typical batch system with vigorous stirring was used to acetylate ferrocene at *55–60 °C* for *15* minutes, and the conversions were only *60–70%*. Lower temperatures reduced the process, while higher temperatures resulted in the creation of the by-product diacetylferrocene.[25]

The high heat exchange efficiency of microfluidic chips allows for rapid heating and cooling, allowing for precise temperature control. Improved mixing efficiency is responsible for the remarkable improvement in conversions at low flow rates. Because microfluidic chips have a high surface-to-volume ratio, viscose force is more relevant than other parameters.[25] Extending this system with a micromixer element, close to the inlets, would probably further increase the efficiency of this reaction, even at lower temperature and higher flow rate.

2.1.1. Reynolds Number and Diffusion.

Fluid flow is commonly categorized into two kinds of flow: laminar and turbulent. Laminar flow is described by smooth and steady fluid motion, whereas turbulent flow is characterized by vortices and variations in flow.

Physically, in terms of the relative value of the viscous and the inertial forces, the two flow types differ. The relative importance of these two types of forces for a given flow condition, or the degree to which the fluid is laminar or turbulent, is characterized by the Reynolds number (Re) as defined in *equation 1*,

$$Re = \frac{\rho u D_h}{\mu} = \frac{u D_h}{\nu} \quad (1)$$

Where ρ, μ, u *and* v are density, dynamic viscosity, the velocity and the kinematic viscosity of the fluid, respectively. And D_h is the hydraulic diameter of the channel, which is a characteristic number that depends on the cross-sectional geometry of the channel as shown in Figure 2:3.

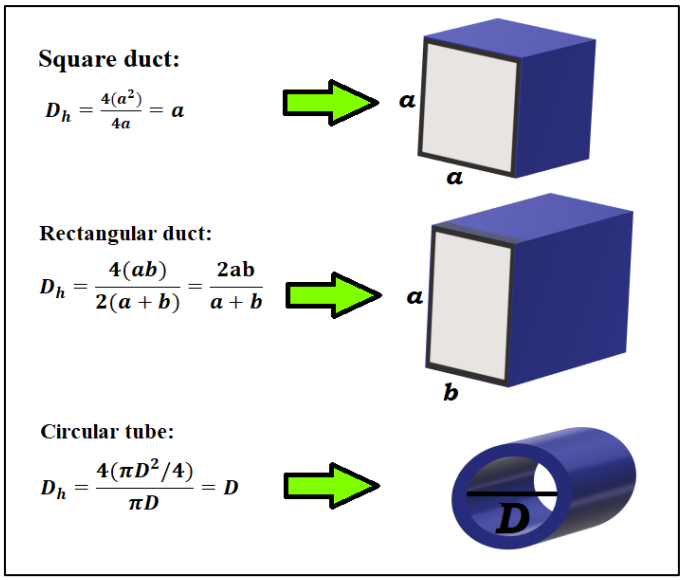

Figure 2:3 Hydraulic diameter calculation of different channels structures.

The low value of Re means that viscous effects of fluids are dominant comparing with inertial effects, and then, a fully laminar flow exists. In the laminar flow system, with time fluid, the velocity is invariant at every position within the fluid stream and streams flow parallel to each other while boundary conditions are constant. Thus, mixing can only be achieved by molecular diffusion due to convective mass transfer only in the direction of fluid flow.[26]

On the other hand, the opposite happens at high value of Re, where the flow is governed by inertial forces and represented by a turbulent flow. The fluid exhibits motion in a chaotic flow that is random in space and time and is characterized by convective mass transport in all directions.[27]

There is a transitional Re range between the laminar and turbulent flow regimes. Many parameters, such as channel form, surface roughness, and aspect ratio, are a function of the exact values of this Re number set. For most cases, the transition Re is usually assumed to be in the range between *1.500* and *2.500*.[28] In the case of microfluidic systems, the flow is known to be basically laminar, where *Re* is usually less than *100* and this characteristic has a direct consequence on mixing within microfluidic devices.

Mixing is largely dominated by passive molecular diffusion and advection in an environment where there is limited laminar fluid flow. Diffusion is characterized as the process of spreading molecules by Brownian motion from a region of higher concentration to a region of lower concentration, resulting in gradual material mixing. Using Fick's *equation* (*2),* diffusion is described mathematically.

$$j = -D\frac{d\varphi}{dx} \qquad (2)$$

Where *D* is the diffusion coefficient, *x* is the position of the species, and $d\varphi/dx$ is the concentration gradient of the species. *D* can be derived from the Einstein-Stokes *equation 3* for simple spherical particles.

$$D = \frac{kT}{6\pi\mu R} \qquad (3)$$

Where *k* is Boltzmann's constant, *T* is the absolute temperature, *R* is the radius of the particles (or molecules) and μ is the viscosity of the medium. The diffusion coefficient at room temperature for a small molecule in water has the typical value of $10^{-9} m^2/s$.[29]

Diffusion is a non-linear process, in which the time *t* taken for a species to spread the scales is proportional squarely with the distance *x* covered. A simple case of diffusion can be modelled by *equation 4* in one dimension.

$$x^2 = 2Dt \qquad (4)$$

Where *t* is the average time of the particles to be diffused over the distance *x* with respect to the microfluidic channel, *x* is the stream width of the fluid to be mixed along the microfluidic channel.[30] The diffusion distance can be extremely small on a microfluidic length scale[31], especially if the fluid streams are hydrodynamically concentrated as shown in Figure 2:4.

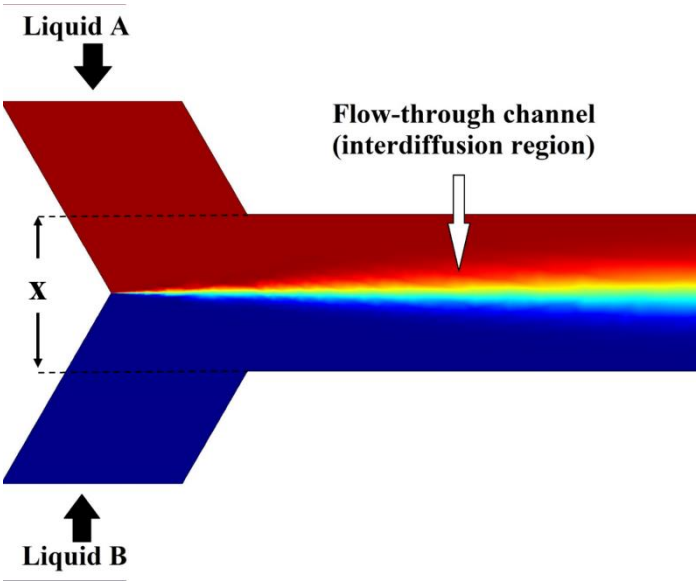

Figure 2:4 T-shaped micromixer with two input fluids, each containing one diffusing species. L and x represent the length and width of the mixing channel, respectively.

At a fixed flow rate, *x* is the transverse distance over which a molecule, with a diffusion coefficient *D*, travels by passive diffusion as it flows a longitudinal distance of *L*.[30] Since *x* varies with the square power, the time needed for complete mixing is reduced drastically by the decrease in distance (*x*). Diffusion is therefore the main way of moving particles and mixing fluids in microfluidic devices.

2.1.2. Types of Micromixers and Mixing in Microfluidic Devices.

Micromixers can generally be grouped into two different types: active[32,33,34,35,36] and passive[37,38,39,40,41,42,43,44,45,46,47,48,49,50,51,52]. Active

micromixers require external turbulence effects during the mixing process, which caused/ evolved by electrokinetic, dielectrophoretic, electrohydrodynamic, temperature, pressure or other forces.

In order to accelerate the mixing phase, active micromixers use both external energy input and fluid pumping energy to produce time-dependent disruptions that stir and disrupt the fluid[53]. Many types of external force employed by active micromixers can be further classified as pressure field-driven[54], acoustic (ultrasonic) driven[55], temperature-induced[56] or magneto-hydrodynamic[57]. Generally, the advantage of active micromixers is obviously the higher mixing efficiency[58]. However, their disadvantages are the need to incorporate peripheral devices such as external power source and the complicated and costly manufacturing process. This may limit the use of such devices in practical applications. Moreover, biological fluids may be harmed by using ultrasonic waves or high temperature gradients in active mixing mechanisms. Therefore, when applying microfluidics to chemical and biological applications, active mixers are not a common option[59].

In order to restructure the flow in a way that decreases the diffusion length, passive mixing devices rely entirely on the use special channel designs. The first microfluidic device reported was passive mixer, which require less cost and more convenient manufacturing than active micromixers, and can be relatively easier integrated into devices. Fabrication of passive type micromixer is generally not difficult, they don’t require external force for its operation and hence very easy to implement. Hence, the structures of active micromixers are often complicated, on the other hand the passive-type mixers are mainly based on breakup, folding, fluid stretch, and molecular diffusion. Some features like simple fabrication, very easy to implement, absence of moving components and no requirement for an external energy source were

discussed in many essays[37,38,39,40], which makes passive mixers more interesting than active mixers.

The significant decrease of mixing time can usually be obtained if the liquid stream is divided into serial or parallel lamination[60,61], mixing streams hydrodynamically focused[62], gas (slug) or liquid (droplet) bubbles established into the flow[63,64], or chaotic advection is reinforced by ribs and grooves created at the channel walls. [65,66]

As mentioned in the previous section, the Re is small in microfluidic systems, meaning that hydrodynamic instability does not develop, so the flows is not turbulent. Because of the micro-meter size dimension of the channels, the flow type in a micromixer is laminar, and mixing through such micromixers is achieved through molecular diffusion, which is normally slow, especially for macromolecules. As a result, in order to accomplish efficient mixing for micromixers based purely on diffusion, the molecule diffusion lengths (channel cross dimensions) must be greatly decreased.[38]

The mixing efficiency in microscale devices can be determined using a number of different methods. They can be (a) direct methods of measurement, which are usually experimental, for example: flow visualization and mixing performance techniques such as titrimetric, radioactive tracer and different optical analytical techniques; or (b) indirect approaches from which the degree of mixing can be quantified including Poincare section analysis, residence time distribution and numerical particle tracking method[67].

The Mixing Efficiency (*M*) of the micromixers applied in our study is defined using *equation 5*[68],

$$M = \left[1 - \sqrt{\left(\frac{c_{out} - \bar{c}_{out}}{\bar{c}_{out}}\right)^2}\right] \times 100\ \% \qquad (5)$$

Where c_{out} is one of the outlet concentrations and $\bar{c}_{\mathrm{out}}$ is the average concentration of the two outlet concentrations.

2.1.3. Passive Micromixers.

Most passive micromixers have various micro-structures that achieve high mixing performance with low pressure and a short mixing length. Passive micromixers rely on the molecular diffusion and chaotic advection phenomena of mass transport. The best way to maximize the mixing efficiency of a micromixer is to decrease the diffusion path and to increase the surface contact area between the various fluids. By varying the design to allow the manipulation of the laminar flow within the channels, the enhancement of chaotic advection can be realized. A shorter diffusion path will increase the mixing efficiency.

Different types of mixing mechanisms can be found in literature for different mixing modes of passive micromixers as shown in Figure 2:5.

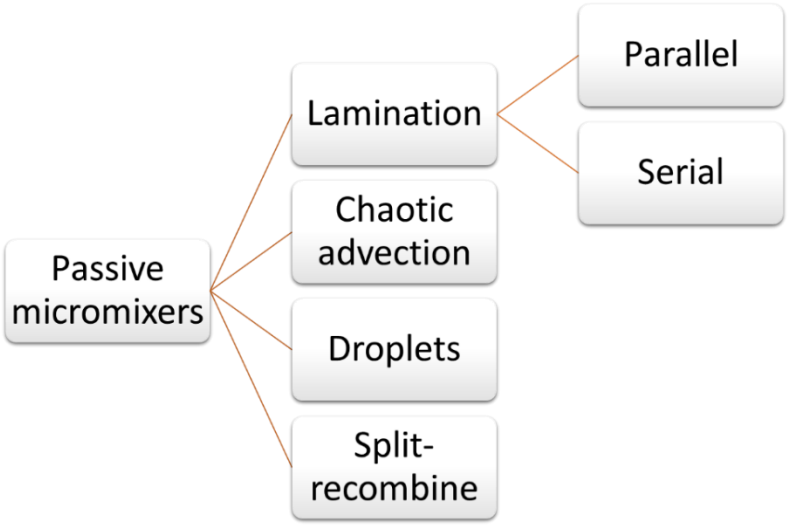

Figure 2:5 Schematic diagram of different types of passive micromixers.

There are many studies about passive micromixers utilizing simple planar structures such as obstacles, unbalanced collisions, convergence–divergence, and spiral channel layouts, among others, and their results shows acceptable range for mixing efficiency (*79-95%*).

Table 1. Passive micromixers reported in recent years.[68]

Dimension	Structure	Characteristic	Re	Mixing Length (μm)	Mixing Efficiency	Reference
2D	Unbalanced Collisions channel	Unbalanced three-split recombine sub-channels	30–80	8275	90%	[69]
		Dislocation structure	<80	8000	85%	[70]
	Embedded Barrier channel	Triangle baffle	1	6400	85.5%	[71]
		Curved micromixers with cylindrical obstructions	0.1–60	8280	88%	[72]
	Spiral	Single logarithmic spiral	67	12,000	86%	[73]
		Double logarithmic spirals	50	5000	80%	[74]
	Convergent–Divergent channel	Sigma channel	0.91	8000	79.1%	[75]
		Semi-elliptical walls	35.5	-	80%	[76]
		Convergent–divergent walls	10–70	6720	90%	[77]
		Ellipse-like micro-pillars	≤1	9000	80%	[78]
		Reversed flow in square wave channel	≤0.1 or ≥10	3710	95%	[79]
		Reversed flow in zigzag channel	≤0.5 or ≥5	-	93%	[80]
3D	Chamber	Trapezoidal chambers	0.5–60	3870	80%	[81]

		Trapezoidal-zigzag channels	0.1–0.9 or 20–80	3610	90%	[82]
		Unbalanced split and cross collision chambers	0.5–100	5000	80%	[83]
		Circular mixing chambers	0.1	6400	88%	[84]
		Split and recombine chambers	1–100	-	90%	[85]
	3D Spiral	Three dimensional spirals	40	2340	90%	[86]
		Cross-linked dual helical	0.003–30	320	99%	[87]
		Tapered structures	50	10,500	90%	[88]
	Overbridge	Overbridge-shaped channel	0.01–50	2000	90%	[89]
		Tesla structures	0.1–100	10,700	94%	[90]
		X-shape structures combined with H-shape structures	0.3–60	102,500	87.7%	[91]
		X-shape structures combined with O-shape structures	0.3–60	102,500	72.9%	91
		Serpentine crossing channels	0.2–10	7500	99%	[92]

Several experimental and theoretical investigations have been carried out for different passive micromixers, as following:

a. flow lamination, which is used in basic T-mixer and Y-mixer[93,38,94,95], using different geometries: zig-zag, square-wave, rhombic and similar[96], in serial multi-stage and multi-layer mixers[97];
b. chaotic mixing by eddy or swirl formation, stretching and folding [98,99,100,101,102,103,43];
c. split-and-recombine concepts (SAR) [104,105,106,107,108], etc.

Mixing performance enhancement in passive micromixers is achieved by optimizing the structural dimensions of the microchannel in such a way that the mixing performance is improved. There are various structural dimensions that can be used to improve the mixing efficiency.[68]

The design of a Y-shaped micromixer, with rectangular and triangular barriers, was designed and introduced to mix fluids with small diffusion coefficient molecules, and the resulted mixing efficiency is *100 %* at a flow rate corresponding to the Reynolds number (Re) of *25*.[109]

An experimental study was performed employing split and recombination micromixer, *T*-type and *O*-type mixers, with Reynolds number ranging from *0.083* to *4.166* and the corresponding mixing efficiency can be reached to *90 %* in a short length.[110]

A numerical evaluation of a passive micromixer with Reynolds numbers ranging from *0.1* to *60*, using cylindrical restrictions within a curved microchannel, found that the mixing efficiency values were *72 % - 88 %*.[72]

The three-dimensional staggered herringbone micromixer shape optimized for mixing of two fluids, one of them with a solved molecule with low diffusion coefficient, and obtained an efficiency less than *90 %*.[111] T type three-dimensional designs of twisted microchannels were constructed and

numerically simulated as a chaotic mixers.[112] Numerical calculations and practical tasks on a planar serpentine micromixer have been evaluated using chaotic mixing, and yielded *90%* of mixing efficiency at Re of *2*.[113]

A passive micromixer with deformable baffles was examined numerically and the achieved mixing efficiency was *98%* at the *Re* from *0.01* to *300*.[114] Micromixer was fabricated using PDMS as material by a lithography process, in which, the staggered herringbone chaotic layout was designed and experimented, and the mixing efficiency of *99.7* % at *20 µl/min* and *99.2% at 100 µl/min* was resulted.[115]

Numerical simulation and experimental study of split and recombine micromixer have also been studied and *84%* of mixing efficiency was achieved.[116] Numerical simulation and experimental study of tesla valve micromixer was investigated and mixing efficiency of *95.3% was* achieved at Re of *1*.[117]

A three-dimensional chessboard shape novel micromixer and developed a new bonding technique using PDMS to PDMS bonding was reported and achieved a *95%* of mixing efficiency at *12.7 µl/min*.[118] A micromixer device for lab on chip application was developed by UV cured adhesive bonding technique.[119] SU-8 used to fabricate a micromixer device where a bonding process was developed using SU-8 coated over the substrate.[120]

A three-dimensional spring like micromixer device was experimented and it was bonded to the substrate using a controllable furnace.[121] The results of mixing efficiency using different passive mixing systems can be summarized in the following Table 2.

Table 2. Mixing efficiency (%) of different types passive micromixers

Structure	Compact shapes	Flow rate (µl/min)	Reynolds number (Re)	Mixing Efficiency (%)
Y-type	rectangular and triangular barriers	____	25	100
***T*-type and *O*-type**	____	____	0.083 - 4.166	≤ 90
Curved microchannel	cylindrical restrictions	____	0.1 - 60	72 - 88
3D-staggered herringbone	____	____	____	≤ 90
Planar serpentine	____	____	2	90
Microchannel	deformable baffles	____	0.01 - 300	98
Straight channels	staggered herringbone	20/100	____	99.7 / 99.2
Split-recombine	____	____	____	84
Tesla valve	____	____	1	95.3
3D-chessboard	____	12.7	____	95

2.1.3.1. Pressure drop

In general, in the field of laminar flow the relationship is linear between the pressure drop and the Reynolds number (or the volume flow rate), as stated in the Hagen-Poiseuille equation.

In fluid dynamics, the Hagen-Poiseuille law is universally applied to describe the pressure drop in a fluid flowing through a cylindrical pipe. The fluid is assumed to be viscous and incompressible, and the pipe has constant circular cross-section which diameter is substantially shorter than its length. The Hagen-Poiseuille equation is defined in standard fluid dynamics notation as follows in *equation 6*:

$$\Delta P = \frac{8\mu L Q}{\pi R^4} \qquad (6)$$

Where ΔP is the pressure drop, R is the radius, μ is the dynamic viscosity, π is the mathematical constant, L is the passage length and Q is the volumetric flow rate.

Pressure drop is also an important design parameter of the micromixer for power consumption. Good mixing efficiency and low pressure drop are two essential aspects of a mixer's design. Good mixing efficiency is particularly important for microfluidic devices applied for chemical reactions, where the reaction yields are strongly affected by the mixing efficiency. Low pressure drop is useful in industrial applications since it lowers energy consumption.

2.2. Lithography

Lithographic techniques are intensively applied in both industry and in research. Lithography allows the push of ever-decreasing dimensions of semiconductor devices and is thus the keystone of the nanotechnology revolution.

They can be categorized into parallel and serial lithography. Parallel lithography uses suitable masks and projects an image of the mask onto the resist layer to form the desired patterns. Just like as in this work, in the formation of SU-8 patterns on glass sheet using mask by UV-lithography to be used for microfluidic caps which will be discussed in details in *section 2.3*.

Serial lithography is a direct writing technique that exposes the resist point-by-point using heavy particle electron beam and laser light.

Lithography is a procedure that uses chemical modifications to precisely and repeatedly construct designed patterns in a specialized layer of material on a substrate. Usually, this pattern is then transferred to another usable layer via a conventional etching or removal procedure.[122]

In the proton beam lithography (direct writing), the resist is exposed to the focused energetic protons as shown in Figure 2:6, by which the beam can be

scanned over the resist and the pattern is directly traced out by a focused beam (PBL on PDMS).

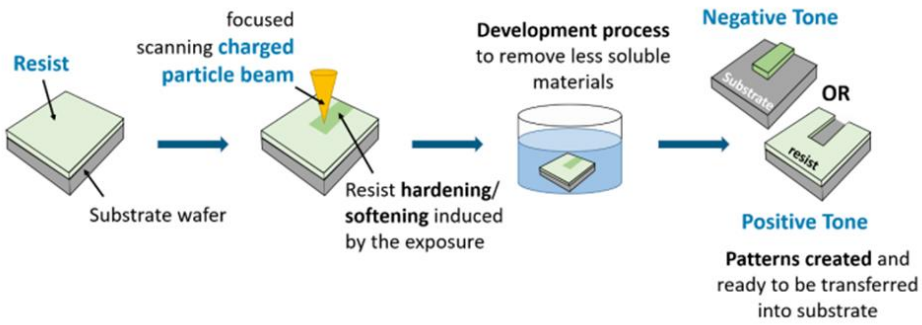

Figure 2:6 Main manufacturing processes in resist-based lithography: Coating the resist material, exposing the resist with a charged particle beam, and eventually generating structures in negative and positive tone resists during the development process.[123]

Resists are categorized into two types: positive tone resists undergo polymeric chain scission when exposed to radiation and become more soluble in the developer. Polymethyl methacrylate (PMMA) is an example of a high-resolution positive tone resist because it is made up of long chain polymers that break down into smaller fragments when exposed and become more soluble.[124] On the other hand, the second resists type is the negative tone, which become less soluble after radiation exposure due to the cross-linking reactions, where smaller molecules combine into larger ones, leading to a decrease in solubility.[125] Hydrogen silsesquioxane (HSQ), SU-8 and PDMS are good examples of high-resolution negative tone resists.

2.2.1. Factors of lithography and development process

Resist materials are suitable for a certain set of lithography procedures due to a number of chemical and mechanical features. The contrast of a resist refers to the rate of changes in material solubility upon exposure, i.e., polymer chain scission/cross-linking. High-contrast resists can be patterned with limited

parameters than low-contrast resists. Figure 2:7 shows the dose response curve of a hypothetical positive tone resist, where in a logarithmic scale, the residual thickness of resist after the development process, normalized to the original resist thickness, is plotted versus the exposure dosage.

It can be seen that at low doses, the resulting resist thicknesses remain relatively unchanged. However, as the dose rises from below to over the threshold value, a nonlinear and abrupt transition occurs, causing a rapid change in the thickness of the resist layer. The slope of the linear section of the dose response curve determines the resist contrast (γ), and a steeper edge gives a greater, and hence a higher contrast value. Traditional resists, such as PMMA, have a contrast value of $\gamma = 2$, while modern chemically amplified resists have a contrast value of $\gamma = 15$.[126]

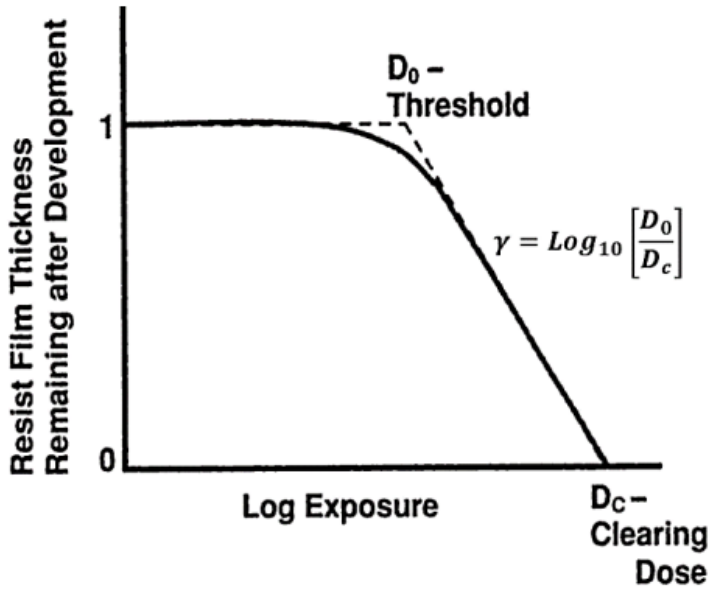

Figure 2:7 The characteristic curve of a hypothetical positive tone resist, with the slope of the transition curve proportional to the resist contrast value. [122]

Sensitivity and throughput are also crucial aspects in lithography. The required exposure dose to induce specific chemical reactions in the resist for

pattern definition is known as sensitivity. The definition of the sensitivity depends on the resist type, where it is defined as the dose required to totally clear the resist material for positive-tone resist, and the dose required to produce *50%* of the ultimate fully-exposed thickness for negative-tone resist. Type and energy of radiation, resist thickness and development processes, are known to have an impact on the sensitivity of a resist.

Throughput is referred to the number of features patterned per second, and it shows the lithographic technique's speed. Because a high resist sensitivity requires less exposure time, faster beam lithography is possible, resulting in improved throughput and lithography efficiency.

The development process is following to the exposure, either the (exposed) fragments from the positive tone resist or the (unexposed) non-crosslinked molecules from the negative tone resist are removed with a developer. The pattern development, removing process, can be achieved by immersing the sample in the developer solution.

Longer polymers are less mobile and more resistant to the developer, thus, they dissolve more slowly.[127,128] The process can speed up by employing a developer with a higher concentration, but the resolution will suffer as a result. Beside the developer's strength, the temperature and duration of the development are additional aspects that can influence the development's outcome.

Because exposure and development are strongly associated, underexposure may be the cause of underdevelopment in a pattern. A pattern that looks to be overdeveloped may also be overexposed.

The mentioned parameters for lithography and development were the guide to our experiments for forming the appropriate patterns, which used in our designed micromixers, as it will discussed in details in *sections 3.4.3* and *3.4.2*.

2.3. SU-8 UV lithography

Ever since its first introduction[129], the negative-tone resist, the epoxy-based SU-8 has got a lot of interest from the micro-fabrication community. The important reasons for the popularity of it are the stable mechanical, thermal and chemical properties.[130] It can be layered and patterned with high thicknesses, greater than *1 mm*[131], to create tall microstructures with high aspect ratios[132] , which are obviously unprecedented features in traditional photoresists. Using these special characteristics, the cross-linked SU-8 has been used as a micro-mould for electroplating and final microstructures in a wide variety of applications including micro gears[133], micro cantilever for scanning force microscopy[134], microfluidic channel[135], optical waveguide[136], and neural probe[137], to name a few.

Several lithography techniques have been used to design various tall and high aspect ratio microstructures as well as deep sub-micron scale structures in SU-8, such as conventional ultraviolet (UV) lithography[129], deep X-ray lithography[138], electron-beam lithography[139], and proton beam lithography.[140]

Usually, photoresist is coated on a substrate (e.g., silicon or glass), and the top surface of the coated photoresist is irradiated normally, using energetic beam (e.g., UV, e-beam, and proton beam). This is a so-called front-side exposure method, regardless of the chosen types of photoresists and lithography techniques used. [141]

2.4. Direct-write techniques

Direct-write methods have been regarded as potential alternatives to masked techniques[142], and when they are used to write stamps or moulds and paired with nanoimprinting and pattern transfer, they have certain significant advantages.[143,144]

In Figure 2:8 comparison of different types of direct-write techniques e.g. Proton beam lithography (PBL), slow heavy ions (focused ion beam technology – FIB) and electrons (e-beam writing).

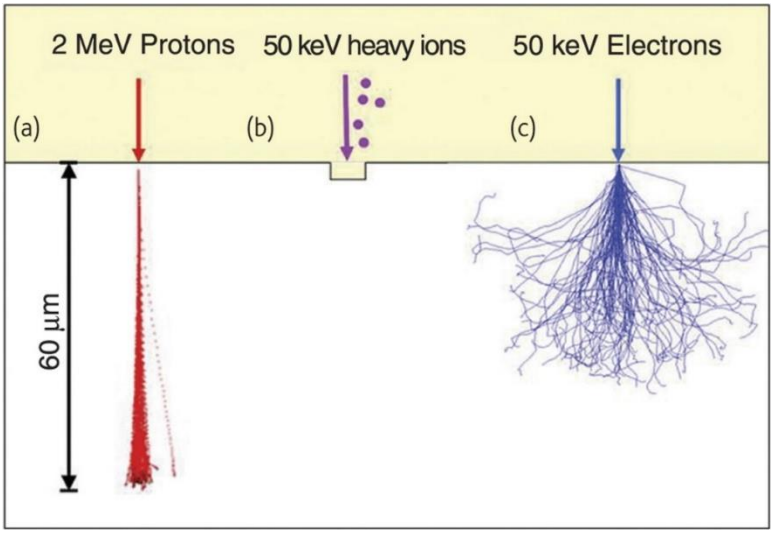

Figure 2:8 Comparison of (a) p-beam, (b) FIB, and (c) e-beam writing techniques. The differences between the three approaches are depicted schematically in this diagram. SRIM and CASINO software packages were used to predict the p-beam and e-beam outputs, respectively. [145]

One of the direct-write technologies is the PBL, where *1-2 μm* size focused protons are scanned serially over a resist. Furthermore, this technique developed so much in the last decades, that nowadays even *~50 nm* focused beam size can be reached, so even Nano structures can be realized.[146]

2.4.1. Properties of MeV protons

The advantages of interaction of protons with matter, is shown in Figure 2:8, and can be described as follows:

a. Fabricating high aspect ratio three-dimensional structures where MeV protons travels in a straight line apart from a small amount of end-of-range broadening comparing to focused electron beam which spreads rapidly as it enters the resist material.

b. In contrast to EUV or X-ray lithography, which exhibit an exponential drop in dose with depth, the proton penetration rate through material is generally constant along its range (apart from a ten-fold increase at the end of range).
c. By varying the proton beam energy, the penetration depth can be varied, which allows formation of multilevel structures in one layer of resist.
d. Lithography with protons also provides a virtual lack of high-energy secondary electrons, which could normally cause undesirable exposure to the resist material (proximity effects). In contrast, a little but noticeable fraction of secondary electrons are created in e-beam writing, with energies that potentially contribute to the micron-scale proximity effect.

2.4.2. Proton beam interaction with resist material

In a resist substance, the track of a MeV proton is determined by the interactions of protons with both the atomic electrons and nuclei in the material. For most of the proton path through the material, the probability of a proton interacting with an electron is several orders of magnitude higher than the probability of nuclear scattering. As the energy of the protons decrease, the nuclear collisions increase, especially at the end of range region.[147]

Because of the large mass difference between the proton and the material's electrons ($m_p/m_e \approx 1800$), proton collisions with electrons do not cause any significant deviation in a proton's track from a straight-line path. Additionally, due to the momentum mismatch, each proton/electron collision has a slight energy transfer from the proton to electron, leading to many thousands of collisions before the protons stop. [145]

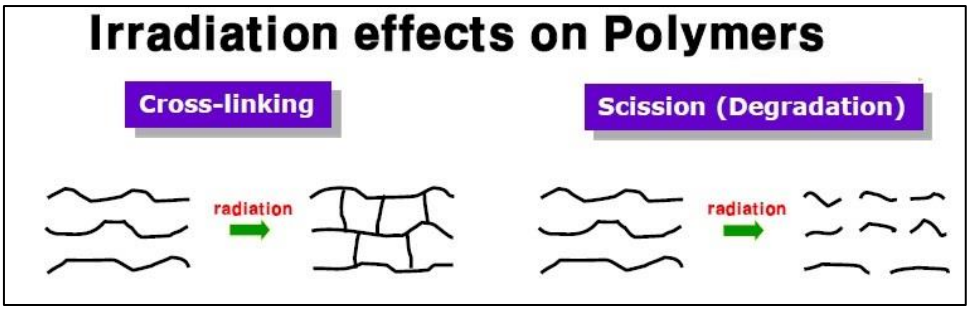

Figure 2:9 types of irradiation effects on resist materials

The primary mechanisms for producing structures in resist materials depends on the type of effect of irradiation on polymer shown in Figure 2:9 , in general, the effect in positive resists such as PMMA and CR-39 is the bond scission, while in negative resists such as SU-8 and PDMS is cross-linking.

In positive resists the irradiated regions, caused by the radiation, can be removed by chemical development to produce structures, whereas in negative resists the development procedures remove the uncross-linked resist leaving the cross-linked structures behind (Figure 2:10).

In proton beam lithography, the chemical change (scission or cross-linking) is caused by proton beam-induced ionizations, excitations and direct bond scission reactions. During these processes, free radicals form, which have high reaction rate with oxygen or other radicals initiating a complex reaction mechanism. In positive resist, such as in PMMA, the reactions quickly cause the leave of carbon dioxide and other small molecule fragments, making it positive resist. In case of PDMS, almost only the methyl side groups change and leaving the material, while vast amounts of crosslinks occur causing the quick solidifying in the material (leading to a glass state at high dose).[148]

The proton dose required for exposure varies from *30-150 nC/mm*^{2}, depending on the resist material[149], and is around *80-100* times less than that required by e-beam writing.[150,151,152]

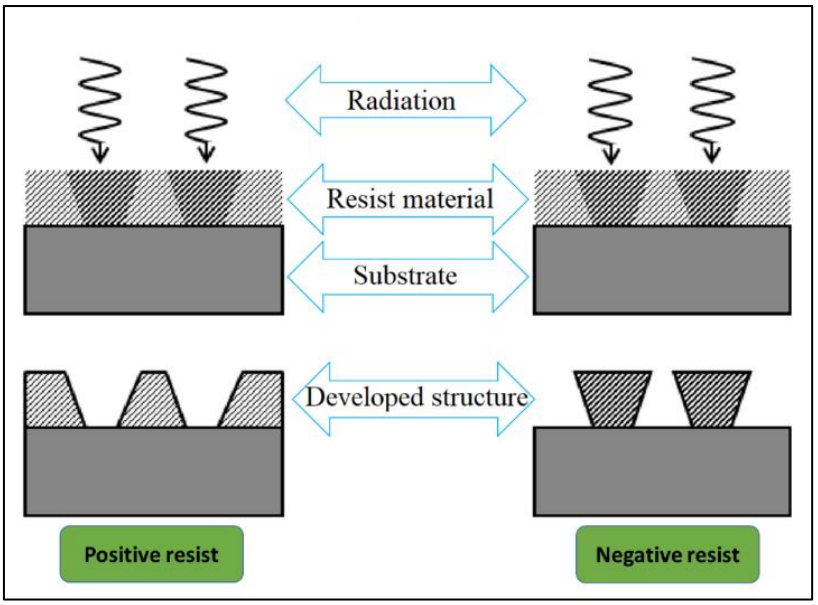

Figure 2:10 types of resist polymer to radiation effect

2.5. Chemical effects on PDMS due to proton exposure

Poly(dimethyl-siloxane) (PDMS) is a commonly applied polymer nowadays, serving as a base material for many applications. As shown in Figure 2:11, its chemical structure is based on a silicon main chain (–Si–O–Si–) with methyl side groups (–CH_3). In elastomeric form it has been widely used to fabricate Micro-Electro-Mechanical Systems (MEMS), microfluidic devices, micro-stamps by moulding techniques[153,154,155,156,157,158,159], micro optical devices using developer-less PBW method[160], or HAR wrinkles by pre-stretch method.[161] Moreover, many papers reporting about measuring of cell adhesion and traction forces by elastomeric PDMS micropillar arrays.[162,163,164] However, microstructures can be created in PDMS directly by PBW.[165,166,167] Irradiating this polymer with protons (typically *1–3 MeV*) will initiate cross-linking process without affecting the main Si–O–Si chain[168], while the degree of cross-linking is related to the proton fluence. [169]

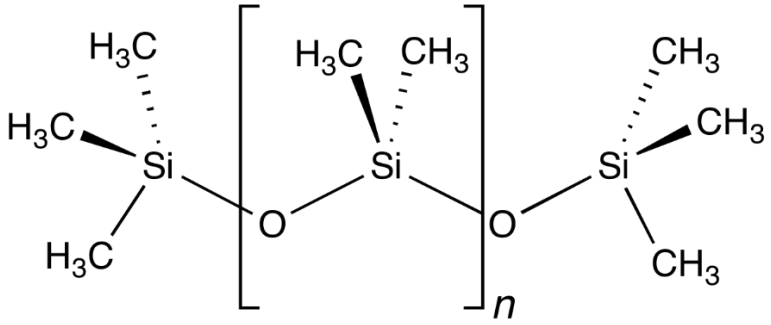

Figure 2:11 Chemical structure of poly(dimethyl-siloxane) (PDMS).[170]

Radiation of organic materials is accompanied by radiation-induced effects, i.e., those changing the chemical structure and physical properties. Polymers, as organic macromolecules, can be sensitive to ionizing radiations such as accelerated ions, gamma rays, X-rays, UV/UVO or laser radiation. The molecular chain or the bonds in the side groups can be easily cleaved by receiving a certain level of energy, causing main chain scissions, breakage of bonds, free radical formations and the release of gaseous degradation products, depending on the chemical groups attached to the main chain of the polymer.[165]

Radiation-induced processes have many advantages compared to other conventional methods. During radiation processing of polymers, the reaction is initiated by the radicals induced by the radiation itself, so there is no need for further catalysts or additives. The free radical forms when the polymer absorbs the radiation energy and gets excited or ionized. In the chemically initiated process, free radicals are produced by the decomposition of an initiator to fragments which attack the base polymer leading to free radicals. In addition, the concentration and purity of the initiators are a limiting factor as well. In the case of radiation initiation, with the variation of the dose rate, an easier and better reaction control can be realized. Furthermore, the radiation processing is temperature independent, so there is no need for activation energy for process initiation.[165]

Irradiation of polymers and elastomers with ionizing radiation (gamma rays, X-rays, UV, electron beams, ion beams) leads to the formation of reactive intermediates such as excited states, ions and free radicals. The excited-state molecules may return to the ground state through radiation less decay or form free radicals by homolytic dissociation reactions. Finally, the free radicals cause a number of chemical reactions in polymers such as recombination, new radical formation, gas yielding and many other reaction pathways. The final effects of these reactions are the formation of grafts, crosslinks and scissions of the main chains or side groups. In the case of silicones, we can divide the main irradiation-induced chemical effects the same way to the crosslinking and scission. Generally, the dominance of crosslinking or chain scission depends on the main chain and the side groups of the polymer and the irradiation condition (i.e., the radiation source, dose, temperature, etc.).[165]

Furthermore, there can be significant differences in chemical mechanism occurred by usage of different radiation conditions, i.e., low or high LET radiation. Following, the radiation-induced chemical processes will be demonstrated on the most commonly used silicone polymer/elastomer, the poly(dimethyl-siloxane).

Generally, organic materials are sensitive against high-energy ionizing radiations (e.g., accelerated ions, gamma ray, X-ray). The minimum energy required to cleave a covalent bond of a carbon chain is in the range of approximately $3-6\ eV$. This energy range is easily surpassed by ionizing radiations, representing high probability of degradation to organic materials. The linear energy transfer is defined as the average energy loss of the particle per unit path length (dE/dx). During ion-irradiation, the energy transfer to the surrounding medium increases along the ion track, according to the Bragg equation, and it has a local maximum value around the end of range region (Bragg peak). This increase in local energy transfer leads to higher

concentrations of reactive species, which can affect the radiation chemical yield.[171,172]

However, the reaction mechanism and the forming products may vary along the ion track as well, which process can hardly be explained by the LET value. Instead, this is probably due to the changes in the way of the ion − molecule interactions, that is, ionization versus excitation of the molecules, which is probably more related to the actual energy of the irradiating ion then to the deposited energy density.

Poly (dimethyl-siloxane) (PDMS) is a promising polymer, serving as a base material for many applications nowadays.[173,174] Its chemical structure is based on a silicon main chain (−Si−O−Si−) with methyl side groups (−CH_3). The siloxane bonds have some special features, which strongly influence the chemistry of the PDMS. The Si−O bond distance is shorter than the sum of the covalent radii, *1.64 Å*, instead of *1.76 Å*, which suggests a partial double bond character of the Si−O bond. Furthermore, the barrier of the rotation around the Si−O axis, as well as the linearization of the Si−O−Si angle, is very low.[175] Consequently, the chain is unusually flexible; the Si−O−Si angle is between *140°−180°*, which is significantly wider than the tetrahedral angle. In addition, there is a significant difference in the bond energies and electronic characters between the main chain and the side groups, making this polymer ideal to test the qualitative chemical changes in the function of the energy of the irradiating ion.[168]

Silicones are synthetic polymers whose chemical structure is based on a siloxane main chain (-Si-O-Si-) with organic side groups (i.e., methyl, ethyl, phenyl, etc.). The most common member of the siloxane family is poly (dimethyl-siloxane) (PDMS), when both the attached side groups are methyl groups.

Silicone polymers are available in elastomeric form, which can be easily formed from linear silicones through a number of different crosslinking reactions. As most of the useful applications of the silicones are in their elastomeric form, it is important to understand the effect of ionizing radiations on the properties of these polymers/elastomers.[165]

In the liquid-phase PDMS, the polymer chains are able to move, so the radicals formed during irradiation can interact with another chain or radicals so crosslinking process will dominate. However, in the case of the already crosslinked PDMS elastomer, the chains have significantly less freedom, so the formed excited states and radicals are more likely to release their excess energy by bond scissions reactions resulting the leaving of side groups and gas yielding. Though crosslinking of the neighbouring groups and chains still takes place, it plays a less important role.[165]

Various very smooth, high aspect ratio 3D microstructures were designed and fabricated in liquid PDMS polymer by the irradiating proton microbeam.[169]

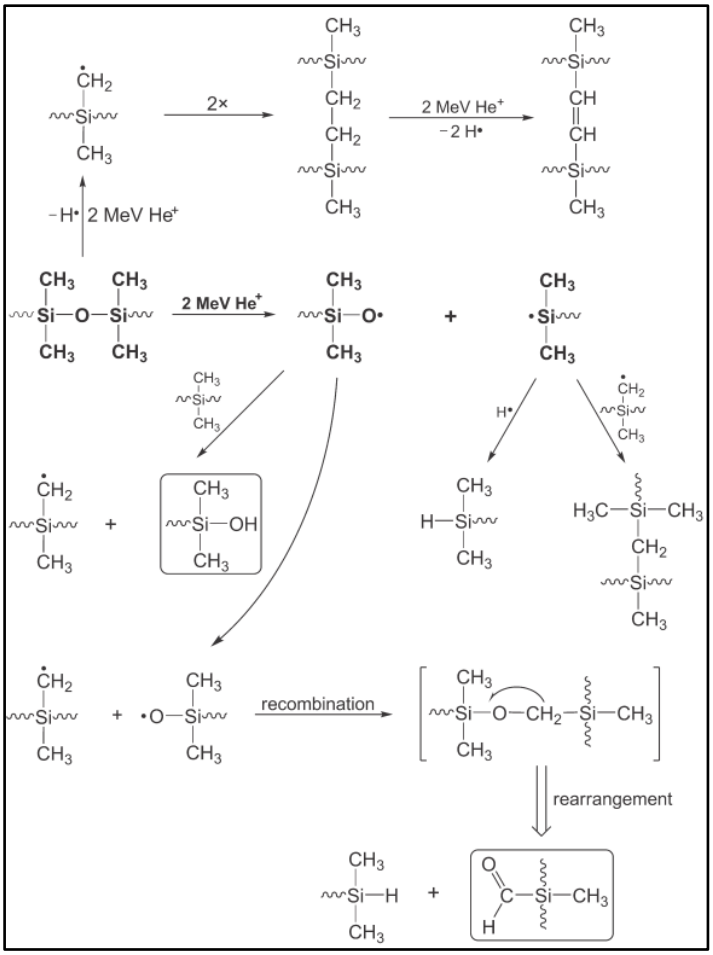

Figure 2:12 Scheme of the Proposed Mechanism for the Reactions Taking Place in the PDMS Polymer Induced by a 2.0 MeV He^+ Ion Irradiation.[176]

So the idea of our research point is to enhance the mixing efficiency of passive micromixers using different microstructures. In the beginning, Computational fluid dynamics (CFD) simulations were studied for the proposed microstructures, to investigate the mixing efficiency of all of our microstructures theoretically. Then, it was followed by the fabrication of the real microfluidic chips for mixing purposes.

For this purpose, the performance characteristics of our proposed micromixers, especially the mixing efficiency, have been studied for different microfluidic devices: straight channel, empty circle and circle with

micropillars, which work as a passive micromixer. Also, an efficient microstructure, circle with different walls was proposed, which can be described as a circle with overlapped parallel walls. The fabricated walls aim to force the fluid to move in a narrow channel serpentine shape, which enhance the mixing efficiency comparing to the used simple channel or circle with and without micropillars.

The mentioned different microstructures were fabricated using the previously discussed two techniques the proton beam lithography and the UV-lithography. Our microfluidic chips for passive micromixers were created by fabricating *PDMS* cap and *PDMS* microstructure, which bonded together by air plasma treatment using corona discharge. Then finally, the mixing efficiency for all the above micromixers have been simulated and discussed, beside the calculation of some characteristics of our fabricated micromixer, like Reynolds number and fluid velocity, have been reported at a range of the flow rate.

Chapter 3

3. Experimental procedures and CFD simulations

In methodology, there are two methods for studying the mixing performance of different passive micromixers. One of the methods is the computational fluid dynamics (CFD) simulations of the various designs of micromixers using COMSOL software[177] (*COMSOL Multiphysics version 5.3*) and the other one is the fabrication of the designed micromixers chips. For both methods, the mixing efficiency was investigated and discussed in details in chapter 4.

My studies were done in two ways, different microstructure shapes and different walls microstructure, both of them were simulated by finite element method (FEM) and were fabricated by lithography techniques to be used as a passive micromixer. The first way of this study was carried out using different microstructures (*see Figure 3:4*, will be detailed in *section 3.2.2*) for passive mixing like straight channel, circle, circle-with-pillars and circle-with-walls. The results of different microstructure (the first way of studying) showed a good mixing of the micromixer circle-with wall structure, which was achieved theoretically and experimentally.

This good mixing performance of circle-with-walls structure was the key to initiate the second way of study. The second way was performed using different walls microstructures (*see Figure 3:5*, will be detailed in *section 3.2.3*) like (e.g. simple circle [SC], circle with low number and same level walls [CLSW], circle with high number and same level walls [CHSW], circle with low number and tall (length) walls [CLTW] and circle with high number and tall (length) walls [CHTW]), all of the achieved results will be discussed in chapter 4.

3.1. Introduction of COMSOL simulation

Engineers and scientists utilize the Microfluidic Module of the COMSOL Software package to construct, simulate, and analyse microfluidic systems. Simulation technologies are increasingly being used in the design cycle because they can improve understanding, minimize prototyping costs, and accelerate development.

Using the Microfluidic Module of the COMSOL Software package, the users can model efficiently and precisely single-phase flows. In two-dimensional and three-dimensional domains, the Microfluidic Module can solve stationary and time-dependent flows. Predefined physics interfaces, also known as Microfluidics physics interfaces, are used to create formulas suitable for various forms of flow. To define a fluid-flow problem, the Fluid Flow interfaces use physical values such as pressure and flow rate, as well as physical characteristics such as viscosity and density.

For a variety of microfluidic flows, several physical interfaces are offered. Forms of flow are Laminar flow, creeping flow, two-phase flow (phase field, level set, and moving mesh), porous media flow (Darcy's Law[178], the Brinkman equations[179], or Free and Porous Media Flow — which combines the Brinkman equations with laminar flow), and slip flow. The Transport of Diluted Species interface can be used to handle the transportation of numerous species. These physics interfaces can be easily used with COMSOL's Electrostatics or Electric Currents interfaces to handle multimodal problems such as electrokinetic flows.

The basic physical principles are given in the form of partial differential equations coupled with appropriate initial and boundary conditions for every one of the Microfluidic physics interfaces. COMSOL's function creates physics by giving users access to the underlying equation system as well as the equations solved by each component. Also, there is enormous flexibility to

include user-defined equations and idioms to the system. For example, to make the transport of a species model, which significantly affects the viscosity of the fluid, one can actually input in a concentration “dependent viscosity”, so there is no requirements of scripting or coding.

The complex couplings formed by these user-defined equations are directly represented in the equation system when COMSOL builds the equations. Then the equations are solved using a variety of industrial-strength solvers and the finite element methodology. Once a solution is found, a wide selection of post-processing tools is available to examine the data, and pre-defined plots are easily handled to demonstrate the device responses.

COMSOL allows flexibilities to estimate a wide range of physical parameters including the predefined quantities like the pressure, velocity, shear rate, or the vorticity (available through easy-to-use menus), in addition to optional user-defined variables.

To simulate a microfluidic device, firstly the geometry must be established in the software. Then the proper materials are chosen, and a suitable microfluidics physics interface is applied. Within the physics interface, initial and boundary conditions are defined. Next, the mesh is defined, in many circumstances COMSOL’s default mesh is used, which is appropriate for some problem and can be produced from physics-dependent defaults. The default mesh is Normal, which is not good enough in our calculation, so the highest mesh size will be used. A solver is selected, the problem is solved after selecting a solver with defaults adapted for the relevant physics interface. Finally, the results are represented graphically. The COMSOL Desktop is used to perform all of these processes.

3.2. Computational fluid dynamics (CFD) simulations

COMSOL Multiphysics' microfluidics module (*software version 5.3a*) was used to carry out the CFD estimations. By which, the simulations of our designs have been computed by successive three main steps: model building, solving, and then evaluating the results.

In model building the geometry, equations and physics (parameters and boundaries) were specified, then creating mesh parameters for solving and finally the results were evaluated. All suggested designs were simulated in COMSOL to evaluate mixing performance in this study. To run the mixing simulations in two-dimensional designs, the “creeping flow” and “transport of diluted species” modules were used.

The Navier-Stokes equation and the continuity equation, stated in *equations 7* and *8*, respectively, describe the flow of an incompressible Newtonian liquid in a micromixer.

$$\nabla[-pI + \mu(\nabla u + (\nabla u)^T)] + F = 0 \qquad (7)$$

$$\rho\, \nabla(u) = 0 \qquad (8)$$

Where the used fluid characteristics in equations *7* and *8* are ρ, μ and p (the fluid density, the fluid dynamic viscosity, and the fluid pressure, respectively). And other important factors are described as following: u is the flow velocity, I is the identity matrix, T is viscous stress tensor and F is the body force.

The convection – diffusion equation, as given in *equation 9*, can be used to characterize species transportation in systems.

$$\nabla(-D\nabla c) + u\nabla c = R \qquad (9)$$

Where the species parameters are c and D, the concentration and diffusion constant, respectively, and R is the source term.

3.2.1. Mesh size selection

Finding the suitable mesh size of finite element method simulation is very important for more accurate and precise simulation to emulate the mixing efficiency of the real experiments of our designs. So different mesh sizes were simulated by simple Y channel as shown in Figure 3:1, in which there is an arbitrary fixed cut line at the end of the Y channel and its importance to compare the concentration variations (referred to the mixing efficiency) through the points of the drawn cut line for the different simulated mesh sizes.

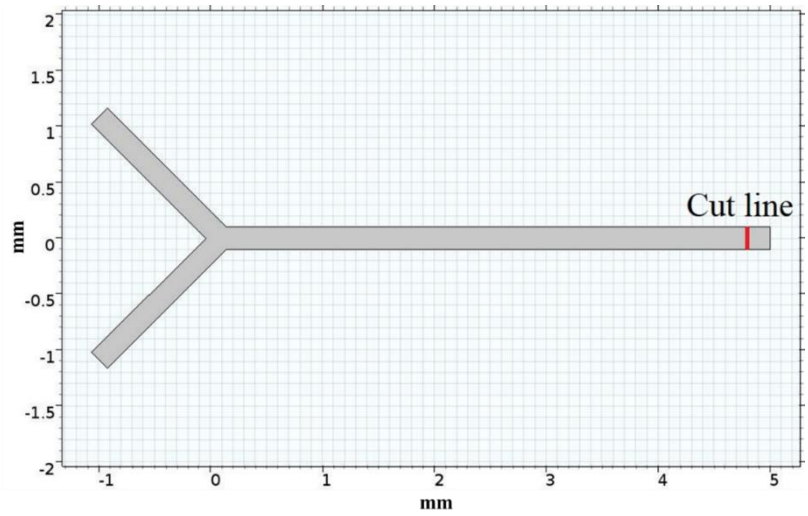

Figure 3:1 Y channel for mesh size testing and cut line at the end of the channel.

Using the Y channel structure (length = *6 mm* and width = *0.2 mm*) and different mesh sizes, the COMSOL simulations were carried to investigate the mixing efficiency corresponding to the used mesh size. The elemental size of different default mash (Extremely coarse, Extra coarse, Coarser, Coarse, Normal, Fine, Finer, Extra fine, and Extremely fine) can be observed in different maps shown in Figure 3:2, and the different default values of customized settings or parameters (maximum element size (mm), minimum element size (mm), maximum element growth rate, curvature factor and

resolution of narrow regions) were described in Table 3 for different “mesh” sizes. .

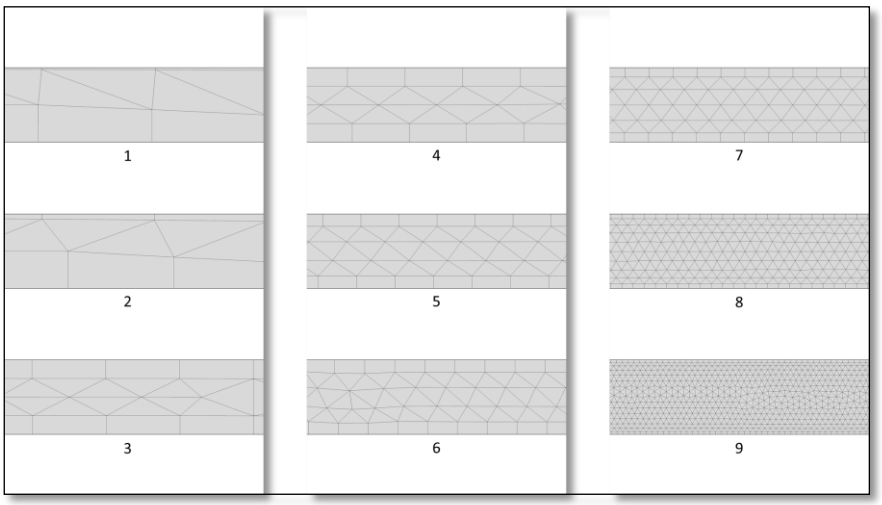

Figure 3:2 Different mesh sizes: 1. Extremely coarse, 2. Extra coarse, 3. Coarser, 4. Coarse, 5. Normal, 6. Fine, 7. Finer, 8. Extra fine, and 9. Extremely fine.

Table 3. Mesh parameters for the finite element method study on Y channel.

Mesh name	Maximum element size (mm)	Minimum element size (mm)	Maximum element growth rate	Curvature factor	Resolution of narrow regions
Extremely coarse	0.489	1550×10^{-5}	1.4	1	0.9
Extra coarse	0.289	1110×10^{-5}	1.3	0.8	1
Coarser	0.193	888×10^{-5}	1.25	0.6	1
Coarse	0.149	666×10^{-5}	1.2	0.4	1
Normal	0.0999	444×10^{-5}	1.15	0.3	1
Fine	0.0777	222×10^{-5}	1.13	0.3	1
Finer	0.0622	88.8×10^{-5}	1.1	0.25	1
Extra fine	0.0289	33.3×10^{-5}	1.08	0.25	1
Extremely fine	0.0149	4.4×10^{-5}	1.05	0.2	1

The modules (creeping flow and transport of diluted species) and the governing equations mentioned in the previous section were used to study the influence of the mesh size on the mixing behaviour of Y channel micromixer for all the different mesh size. In these modules, the used parameters are diffusion coefficient $D_c = 1\times10^{-10}\ [m^2/s]$, input velocity $U_0 = 0.001\ [m/s]$ and different parameters values of elemental size.

The value of concentration refers to the mixing efficiency. So, using the cut line and the concentration profiles in Figure 3:3, it can be observed easily that the concentration value around *50* refers to a very good mixing while the far values from *50* means a weak mixing at any point of y coordinate (the cut line).

The results show the dependence of concentration value on the used mesh size as shown in Figure 3:3, where the low mesh size (Extremely coarse, Extra coarse, Coarser and Coarse) gives an excellent mixing while the high mesh size (Normal, Fine, Finer, Extra fine, and Extremely fine) gives poor mixing. Values of the concentration are around *50* for the low mesh sizes (Extremely coarse, Extra coarse, Coarser and Coarse) at the end of Y channel as illustrated in Figure 3:3, which means an excellent mixing through the used channel. But on the other hand, experimentally this not happen, due to this, those low mesh size will not be useful for our simulation.

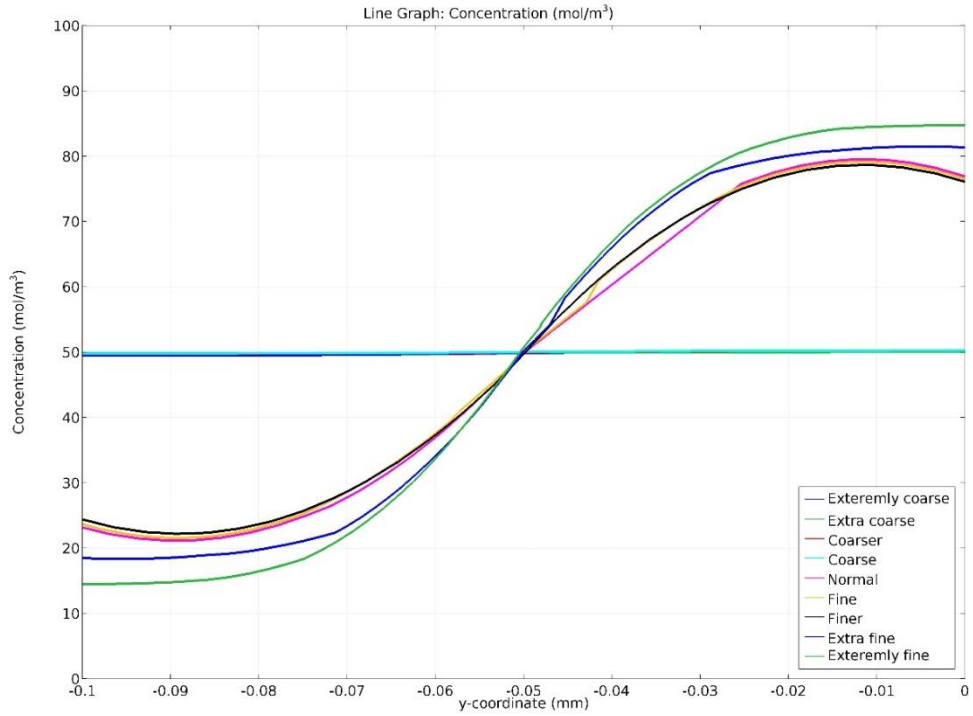

Figure 3:3 Concentration dependence with different mesh size at fixed cut line at the end of Y channel.

By changing the mesh size to high values for Y channel, the concentration values went so far from *50*, which means a very poor mixing as shown in Figure 3:3 for mesh sizes (Normal, Fine, Finer, Extra fine, and Extremely fine). This result agrees too much extent with the experimental result of poor mixing during the real test of Y channel micromixer. Which means the best mesh size for our simulation is the lowest value of concentration (Extremely fine).

The reason of this, is that at low mesh size, the used elements by the finite element method have large size and too low number of (*see maps 1, 2 and 3 in Figure 3:2*). So, the high level of averaging occurs or the numerical diffusion may induce significant error in the estimation of the resulting concentration field in the lowest resolution numerical solution[180], which will cause incorrect calculations. On the other hand, the 9^{th} map (*see also*

Figure 3:2) has small size and a lot of elements, which gives a good averaging and will result in an appropriate and reliable calculations. That is why selecting the suitable mesh size for accurate investigation is necessary at the very beginning of the simulations.

The default mesh in a COMSOL simulations sizes is set up of for normal, which is not acceptable. In every calculation we used the maximum resolution, the extremely high mesh size.

3.2.2. CFD of different structures

The presented two-dimensional designs' geometries for different structures (channel, circle, pillars and walls) are shown in Figure 3:4. Two inlet channels, two outlet channels, and the mixing unit area are the important components of our micromixers. As shown in Figure 3:4, the design and number of inlets and outlets are similar in all our proposed micromixer systems, where the dimensions are length *(L) = 2 mm* and width *(W) = 0.2 mm* of both the inlets and outlets. But the mixing unit area varies like:

a- straight channel, with length *(L) = 6 mm* and width *(W) = 0.2 mm*

b- circle, with diameter = *2 mm* (radius *(R) = 1 mm*)

c- circle-with-pillars, pillar diameter = *0.005 mm* (radius *(R) = 0.0025 mm*) and interstitial distance between the pillars *(D) = 0.045 mm*

d- circle-with-walls, wall thickness *(T) = 0.03* mm and interstitial distance between the walls *(D) = 0.17 mm.*

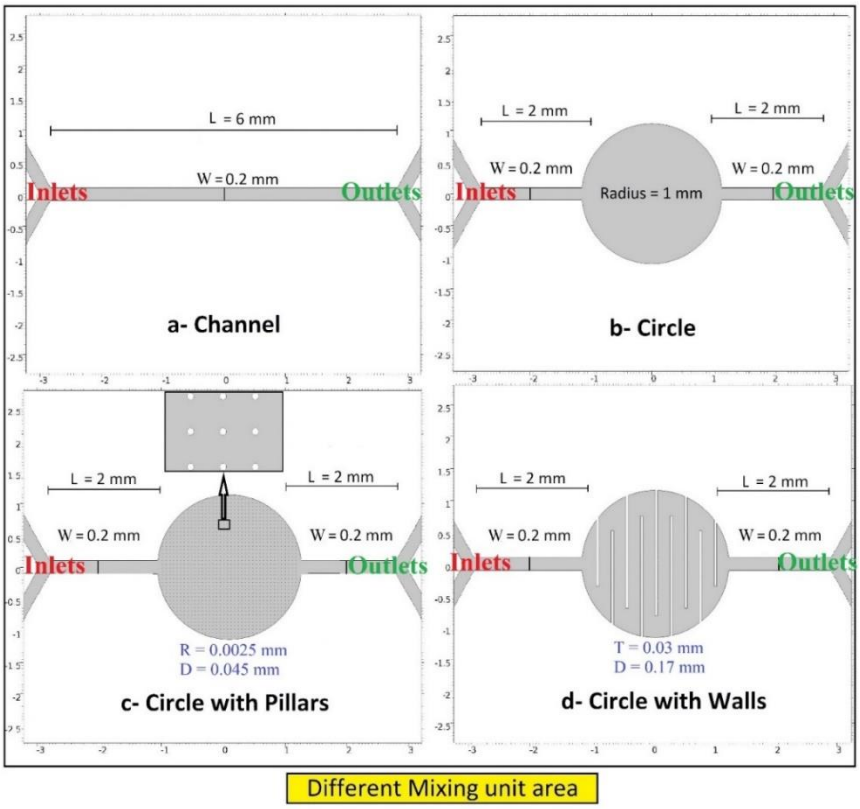

Figure 3:4 Different mixing unit geometrical structures: a) straight channel, b) circle, c) circle-with-pillars, and d) circle-with-walls.

3.2.3. CFD of different walls structures

The good results of fluid mixing obtained using CFD for the array of walls, was the key to the current study. With which the CFD calculations of the designs of our passive micromixers, with different walls structures, showed an improvement of the mixing efficiency comparing to the presented ones in previous section. During the simulation, water and a diluted aqueous solution is injected to the mixer through two inlets. They flow through the chip, including the mixing unit area, where they start to mix. The level of the mixing depends on the mixer designs and parameters.

The geometrics and dimensions of two-dimensional proposed designs of different walls structures for passive micromixers are shown in Figure 3:5. The

main parts of the proposed designs for the micromixers are *2* inlets, *2* outlets and mixing unit area. All structures have the same inlets and outlets (geometry and number) where both *2* inlets and *2* outlets are *2* circles of radius *(R) = 1 mm* connected to *2* channels of length *(L) = 2 mm* and width *(W) = 0.2 mm*, but all structures have different mixing unit area as following:

a. Simple circle [SC] of radius *(R) = 1 mm*, circle with low number and same level walls [CLSW] of wall thickness *(T) = 0.03 mm* and gap between walls *(G) = 0.17 mm*.
b. Circle with high number and same level walls [CHSW] of wall thickness *(T) = 0.03 mm* and gap between walls *(G) = 0.07 mm*.
c. Circle with low number and tall (length) walls [CLTW] of wall thickness *(T) = 0.03 mm* and gap between walls *(G) = 0.17 mm*.
d. Circle with high number and tall (length) walls [CHTW] of wall thickness *(T) = 0.03* mm and gap between walls *(G) = 0.07 mm*.

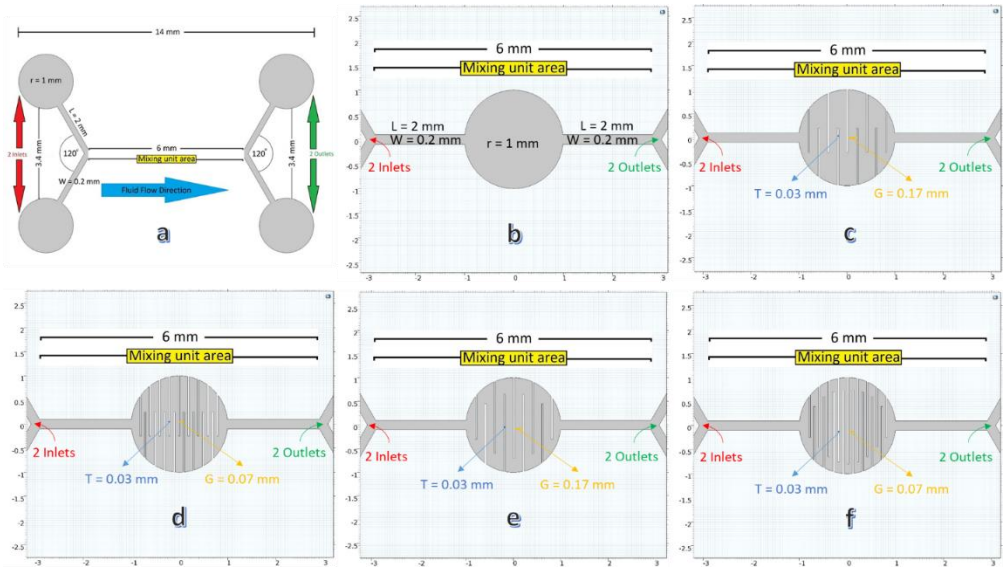

Figure 3:5 Geometry of main parts of COMSOL simulation micromixers: a) inlets, outlets and mixing unit area, b) simple circle [SC], c) circle with low number and same level walls [CLSW], d) circle with high number and same level walls [CHSW], e) circle with low number and tall (length) walls [CLTW], and f) circle with high number and tall (length) walls [CHTW].

3.3. High-aspect-ratio structures

Proton beam lithography is a technique that make use of a focused beam of several (MeV) protons written directly into a resist to produce a 3D latent image in a resist material. The several MeV energy protons have high penetration depth into the resist (e.g. a *2 MeV* proton will penetrate *84.2 μm* into PDMS). Proton beam lithography is the only technique that offers the capability of direct-write, high aspect ratio microstructures.[181] With this method, a complicated pattern of a maximum area *of 2.5 × 2.5 mm²* can be exposed down to a depth of *150 μm* in a few seconds.

3.3.1. Three-dimensional micro lithography facility

The proton beam lithography equipment works at the Institute for Nuclear Research at Debrecen (*Atomki*), using the *5 MV* Van de Graaff accelerator.

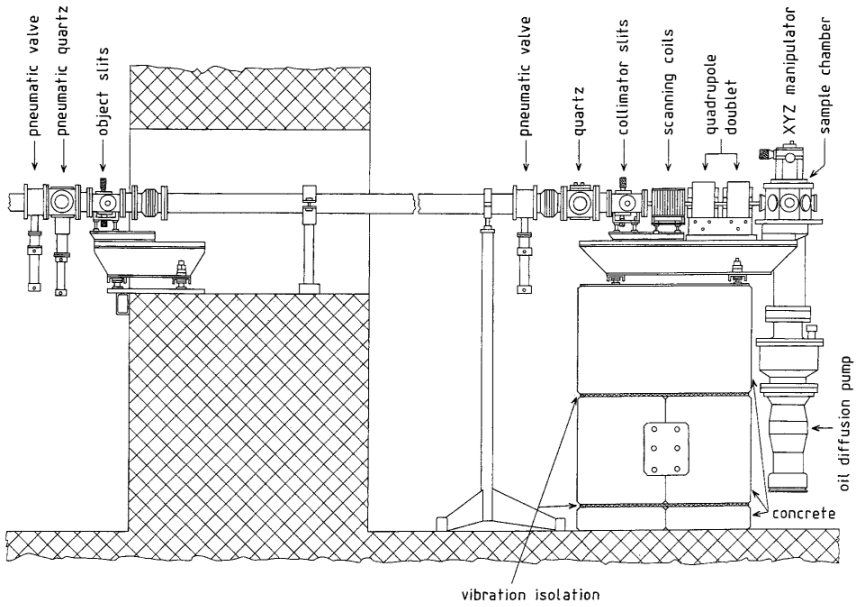

Figure 3:6 Schematic diagram of scanning proton microprobe facility in ATOMKI. [182]

Figure 3:6 depicts the arrangement of the proton microprobe setup, which used in combination with the *5 MV* single-ended vertical Van de Graaff

machine[183]. The accelerator can be used to generate ion beams of p (proton), d (deuterium) and ^{4}He (helium) employing an RF ion source capable of producing a single charged particle.

The vertical beam is switched to a horizontal plane of the accelerator using an analysing magnet, which is also useful for the stabilization of the beam energy. Initially, the accelerator was used to produce high current beams (*10-20* μA) of light ions in multiple beam lines. Large collimators were thus utilized because of the less important impact played by beam emittance and brightness characteristics.

In setting up the microprobe beam line, after the beam analysing and switching magnets, there are the beam analysing and transportation system that includes installed asymmetrically fed magnetic quadrupole doublet beam focusing and steering lenses[184]. The *0°* beam line was selected for the microprobe installation to avoid using the switching magnet.

Ion source's pre-focusing element can produce a beam spot (with a diameter of less than *4 cm*) on a quartz-plate positioned in the plane of the object slits at 10 *m* from the analysing magnet. Thereafter the asymmetrical quadrupole doublets of the transport channel and the microbeam facility itself have been adjusted to match the optical axis.

The Grime and Watt available system[185] was chosen because it has a strong reputation and is utilized in various laboratories. Oxford Microbeams Ltd provide microbeam facility as following: two sets of slit units for object and collimator slits, magnetic quadrupole doublet lenses, scanning coils (two pair of ferrite core coils, pre lens scanning with a maximum scanning area (*2.5 x 2.5* mm^2), and power supply. The object is *6* meters away, and the demagnification ratios are around *5* in the horizontal and *50* in the vertical.

The end stage has been fixed tightly on *1.4* tons total weight concrete cast blocks and *1 cm* thick cork-boards between them and below them, to

decrease the mechanical vibration. The object slit unit is housed in a window in the *1.1m* thick concrete wall that separates the main target hall from the microbeam system (Figure 3:6).

The Oxford type octagonal target chamber is ideal for controlling target movement from the top with an XYZ sample holding stage, while a binocular optical viewing microscope and detectors are in the vertical plane.

The vacuum system consist of turbo pumps and a sample chamber. The high pumping speed of the turbo pumps permits fast recovering of the vacuum in the small volume of the sample chamber after changing the sample. The beam current is collected and measured by an ultra- sensitive current digitizer also from Oxford[182].

3.4. Microfluidic Chip fabrication.

The structures suggested by the simulations were fabricated in real microfluidic chip, using lithography techniques, for mixing purposes. The main processes in chip fabrication are as follows:

1. *Preparation the samples for proton beam irradiation*
2. *Proton beam lithography (PBL) of PDMS microstructures.*
3. *SU-8 photolithography of PDMS cap.*
4. *Bonding the PDMS cap onto the PDMS microstructures by plasma treatment.*

After bonding and finalizing the chip fabrication, the mixing efficiency for the different fabricated micromixers were calculated using a system described in *4.5.2 section*.

3.4.1. Preparation the samples for proton beam irradiation

Before scanning the desired patterns on samples using proton beam facility, the samples should be prepared through two sequential steps: PDMS elastomer

layer was created on the conductive glass substrate then liquid PDMS layer was coated above the elastomer layer, which will be discussed in details through the following subheadings. Finally, the prepared samples should be taken directly to the irradiation chamber for proton beam scanning.

i. Creation of PDMS base polymer rubber layer

The liquid PDMS was added to curing agent in Petri dish, then mixed well to form homogeneous mixture (Sylgard 184 kit, Dow-Corning, base polymer: curing agent volume ratio *10:1*), bubbles were initiated during the mixing so it is recommended to wait *30-60* minutes until those bubbles disappear. The mixed composition (liquid PDMS and curing agent) was coated on the conductive glass substrate by a spin coater, then the samples were put on hotplate at temperature *85°C* for *30 min*. to form a cross-linked PDMS layer on the surface, forming a PDMS rubber layer of thick about *30 μm*.

ii. Coating liquid PDMS on rubber layer

On the crosslinked rubber layer, a new liquid PDMS layer of thickness *25 μm* can be coated using spin coater which was adjusted to fixed parameters (speed = *2600 RPM*, coating time = *60 s, see Figure 3:7*).

Finally, after coating, the sample was moved directly to the irradiation chamber where the proton beam was prepared and set up previously with special parameters will be discussed in the next section.

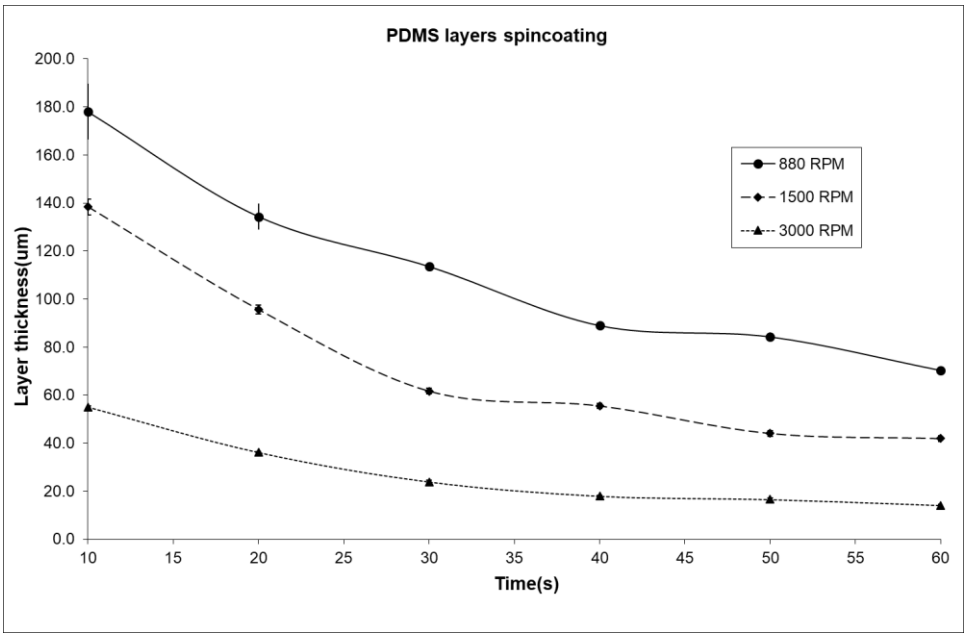

Figure 3:7 Variation of PDMS thickness (μm) with time (s) at different spin coater speed.

3.4.2. PDMS microstructures using Proton beam lithography (PBL).

Within the suggested micromixers that use microstructures for mixing (i.e., micro pillars or walls), a topmost layer of liquid PDMS was coated as a negative resist for proton beam irradiation. Where a fresh layer of around a *25 μm* base polymer was spin-coated on top of the cross-linked rubber layer, detailed procedure can be found in the work of *Huszank et al.*[169]

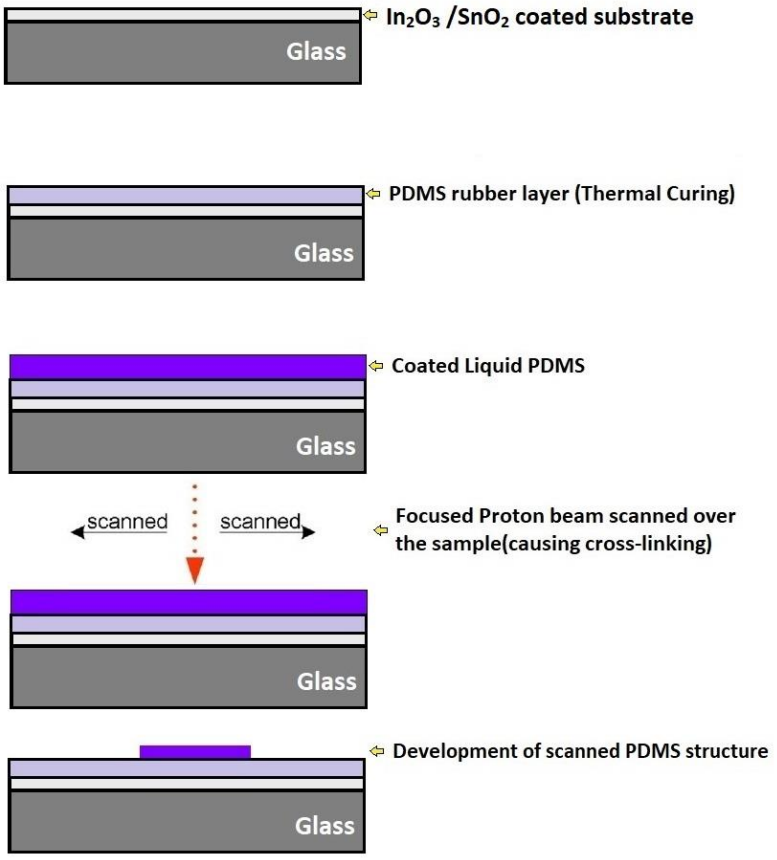

Figure 3:8 PBL procedure scheme diagram (side view). 2 mm × 2 mm portion of the resist was magnetically scanned by the proton beam.

For the fabrication process of the microstructures (Figure 3:8), proton beam assisted lithography process was used, with the setup of the proton microprobe. Their radiation was performed by protons of energy *2.0 MeV* with a beam current of typically *500 pA*, focusing on approximately $2\ \mu m \times 2\ \mu m$.

The focused proton beam was magnetically scanned over the resist material, according to the given scan pattern. Ionscan program or a bitmap manipulator graphical software can be used to build the patterns. Micro-pillar array and a circle with structured walls are two examples of these patterns (*see Figure 3:9*). The delivered fluence of electric charge to the PDMS samples ranged from *3000* to *10000 nC/mm*^{2}. After the direct irradiations, the scanned

structures were developed immediately using chemical compounds to remove the non-irradiated parts[169], then finally the samples were rinsed with ethanol to remove the impurities and visualize the scanned patterns smoothly without distortions.

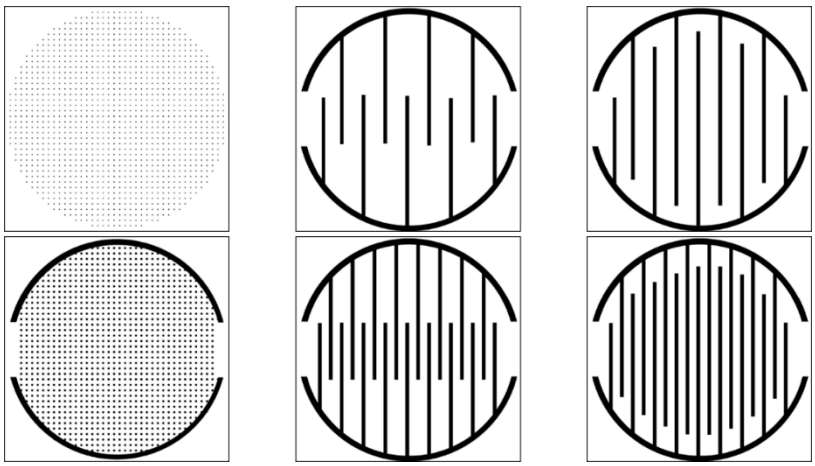

Figure 3:9 Different patterns for PBL scanning

The development should be done after the irradiation process directly. After this, the sample was rinsed in ethanol for some seconds to dry the samples.

The structures can be checked by optical microscope and should be clear as shown in (Figure 4:1 - Figure 4:3), and the previous steps can be repeated if some parts of non-irradiated areas still exist and the structure is not clear. Finally, the formed patterns are ready to be embedded in a micromixer chip for mixing efficiency test.

3.4.3. PDMS caps using SU-8 photolithography.

Photolithography method was used to create the chip's cap. The used system of UV-irradiation, shown in Figure 3:10, can be described as follows: an UV lamp was in a vertical direction at a fixed distance from the mask

(contains the desired pattern). The coated SU-8 substrate (a cleaned glass substrate was coated by SU-8 photoresist) was put under the mask directly.

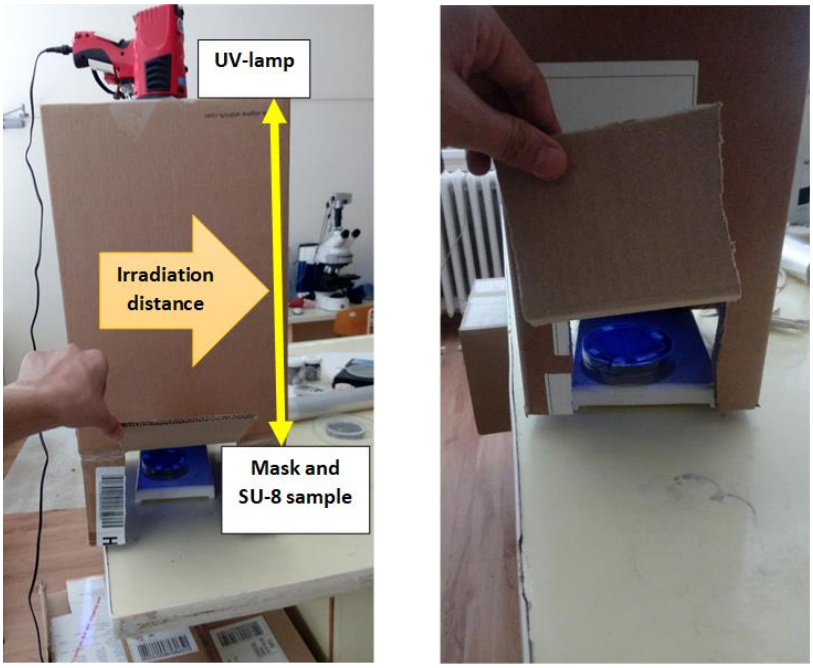

Figure 3:10 The system of UV-irradiation for SU-8 photolithography.

Some of parameters should be taken in account during creation the fine structure of the SU-8 master like: cleaning the glass substrate carefully, choosing the desired SU-8 layer thickness from the SU-8 calibration curve (Figure 3:11) and optimizing the irradiation time of UV and the development time of the structure.

Many attempts were done by changing those parameters to optimize the best conditions to create the fine pattern of SU-8 master, and the results are shown in Figure 3:12. Where the bad patterns appeared at the first trials because the used parameters (irradiation distance, irradiation time and development time) are not efficient to fit the optimized conditions for the fine pattern, then at the end the fitting parameters were reached for the good pattern when the optimized conditions were used.

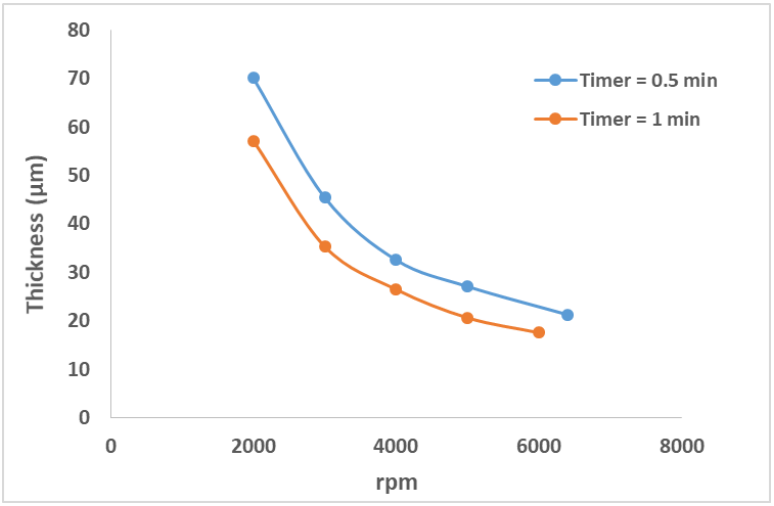

Figure 3:11 Variation of SU-8 thickness (µm) with spin coater speed at different times (0.5 and 1 min).

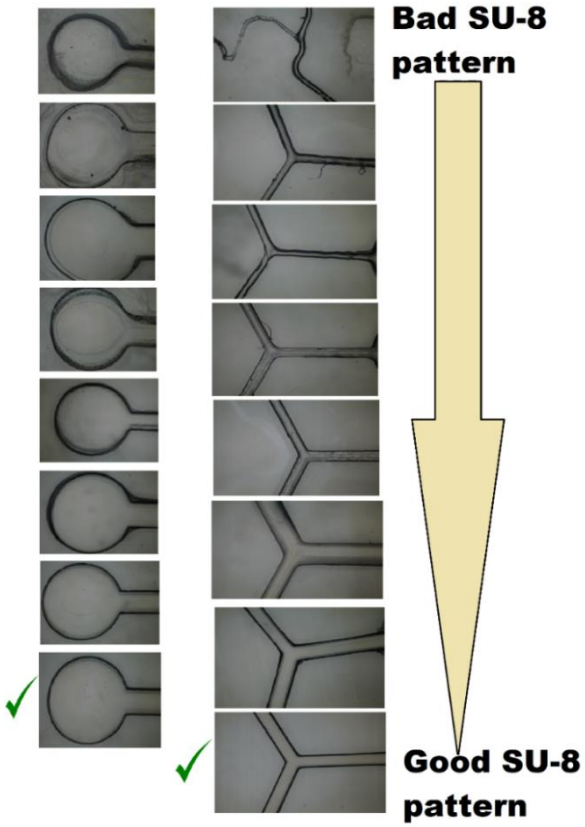

Figure 3:12 Trials for optimization the suitable parameters (UV irradiation time, irradiation distance and the development time) to obtain the good SU-8 pattern.

Using the previous optimized condition, the SU-8 sample was irradiated using UV through the cap mask, and the needed pattern can be stamped on the glass substrate by development process. The mixture of liquid PDMS and curing agent was poured onto the SU-8 pattern, then was allowed to crosslink freely.

The moulding process of the PDMS can be described as following: firstly, an amount of liquid PDMS was prepared (according to the *1/10* ratio of the PDMS liquid and the curing agent), and then were poured on SU-8 master and let it to crosslink, forming the PDMS cap. The created PDMS cover was finally peeled off, as seen the formation scheme in Figure 3:13.

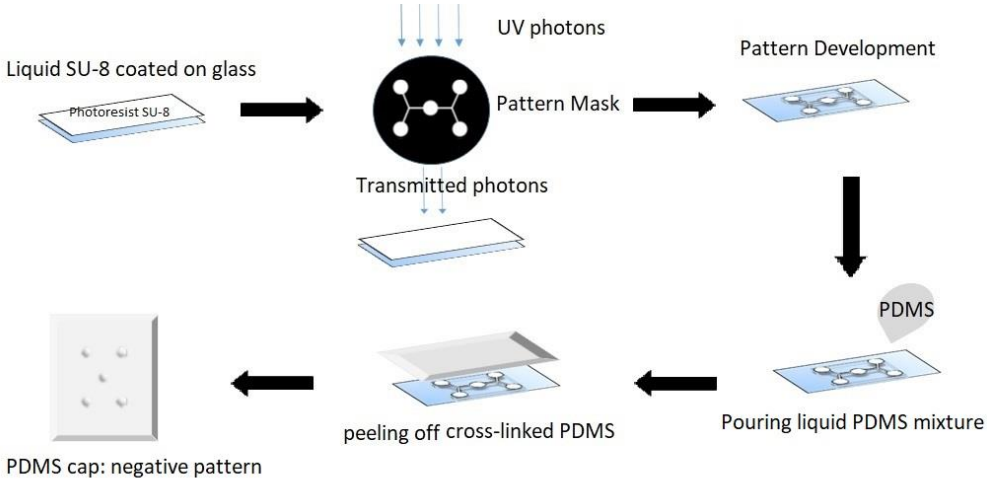

Figure 3:13 PDMS cap formation scheme with SU-8 master and UV lithography.

3.4.4. Plasma treatment for bonding the PDMS cap and microstructures.

A good mixing performance using low flow rates as well as less pressure drop without causing damage to the device bonding is critical for any micromixer. At just about the same point, micromixer channel sealing is an

essential part of the fabrication process. The bonding process can be accomplished using a variety of different approaches.[186]

The complete form of the microfluidic chip can be achieved using plasma-bonding equipment (corona plasma treater) shown in Figure 3:14, where the PDMS cap was bonded to the PDMS microstructure pattern. After chemically activating the PDMS surfaces using air plasma treatment, the two surfaces were aligned and squeezed. Following that, two inlet and two outlet holes were carved into the top. Finally, flexible pipes were attached to the inlets and outlets.

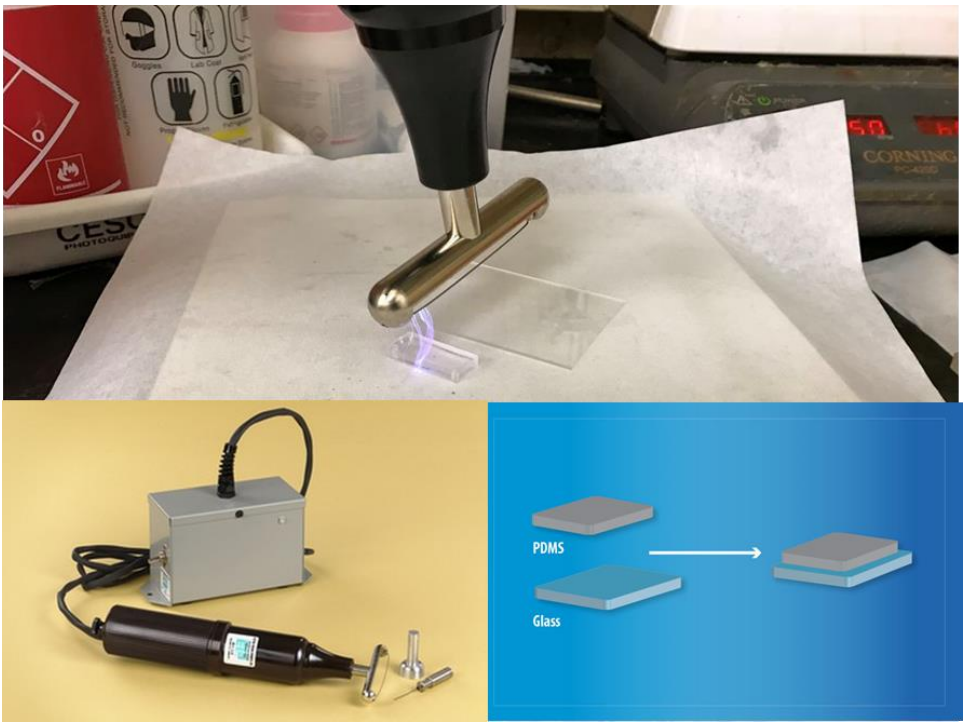

Figure 3:14 Plasma treatment using corona plasma treater for PDMS bonding.

3.5. Mixing test system and concentration measurements

The system shown in Figure 3:15 was used for mixing test. A syringe pump was used with two syringes filled with a) water and b) aqueous solution of methylene blue. The two syringes were connected to the fabricated micromixer

chips by two pipes through the two inlets of the micromixer. The flow rate was adjusted and controlled by syringe pump, where the flow rates ranged from *1* to *6 μl/min*.

The two fluids were pumped in the inlets and pass through the designed micromixer, and the mixed fluid was collected at the outlets. Then the concentration of the collected samples was investigated by UV/Vis spectrophotometry. Due to the type of the micromixer, the concentrations of the two fluids will change, and consequently the mixing efficiency of the applied micromixer can be calculated.

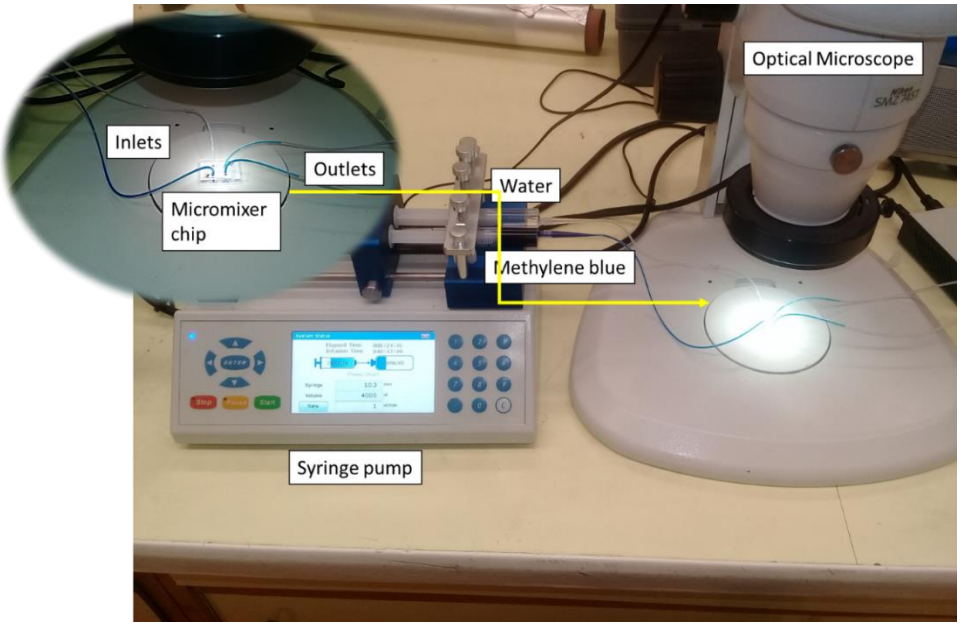

Figure 3:15 the system for mixing two fluids using the fabricated chip.

UV/Vis spectrophotometry was used to study the absorbance spectrum of the collected samples for different types of micromixers. The linear relationship between the absorbance (*A*) and the concentration (*c*) of a solution was defined by Beer-Lambert law[187,188] in *equation 10*:

$$A = \varepsilon c l \qquad (10)$$

Where (ε) is the molar absorption coefficient and (I) is the optical path length in cm. Also, the absorbance (A) can be defined via the incident intensity I_o and transmitted intensity I as described by *equation 11*,

$$A = log_{10} \frac{I_0}{I} \qquad (11)$$

Due to the direct proportionality of light absorbance and the solution concentration, the absorbance spectrum of the mixed samples was measured then the concentrations were calculated.

Chapter 4

4. Experimental results and discussion

Through chapter 4, the details of the results of COMSOL simulations of the different designed micromixers, and the results of successive experimental steps of the fabrication process of our microfluidic chip will be described. The mixing efficiency of the simulated and fabricated micromixers will be also discussed through this part, based on two different ideas of micromixers.

4.1. Different PDMS microstructures created with PBL for passive micromixers

PBL is the ideal method for writing fine 3D microstructures on PDMS. Using the detailed method of PBL, mentioned in *section 3.4.2*, different microstructures have been manufactured for various applications, such as passive micromixers (recent application). For mixing purposes, the fabricated microstructures are circle with micropillars and circle with different wall.

Figure 4:1 shows the created PDMS circle with PDMS micropillars by PBL and its dimensions as following: (circle diameter *2 mm*, micropillars diameter *0.005 mm*, height *0.025 mm* and distance *0.045 mm*). Figure 4:2 describes the PDMS circle with different PDMS walls and their characterization as following: a) low number and same level walls [CLSW] (wall thickness *(T) = 0.03 mm* and gap between walls *(G) = 0.17 mm*), b) high number and same level walls [CHSW] (wall thickness *(T) = 0.03 mm* and gap between walls *(G) = 0.07 mm*), c) low number and tall (length) walls [CLTW] (wall thickness *(T) = 0.03 mm* and gap between walls *(G) = 0.17 mm*), and d) high number and tall (length) walls [CHTW] (wall thickness (*T) = 0.03 mm* and gap between walls *(G) = 0.07 mm*).

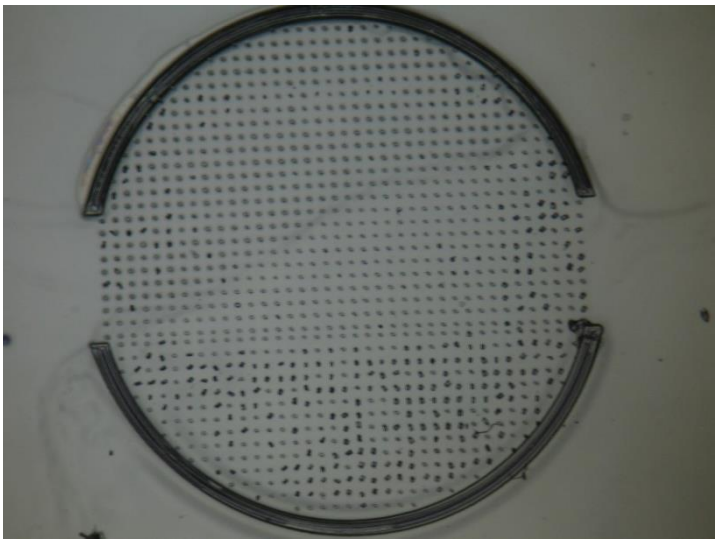

Figure 4:1 Optical microscopic view of a pillar type micromixer. (Top view)

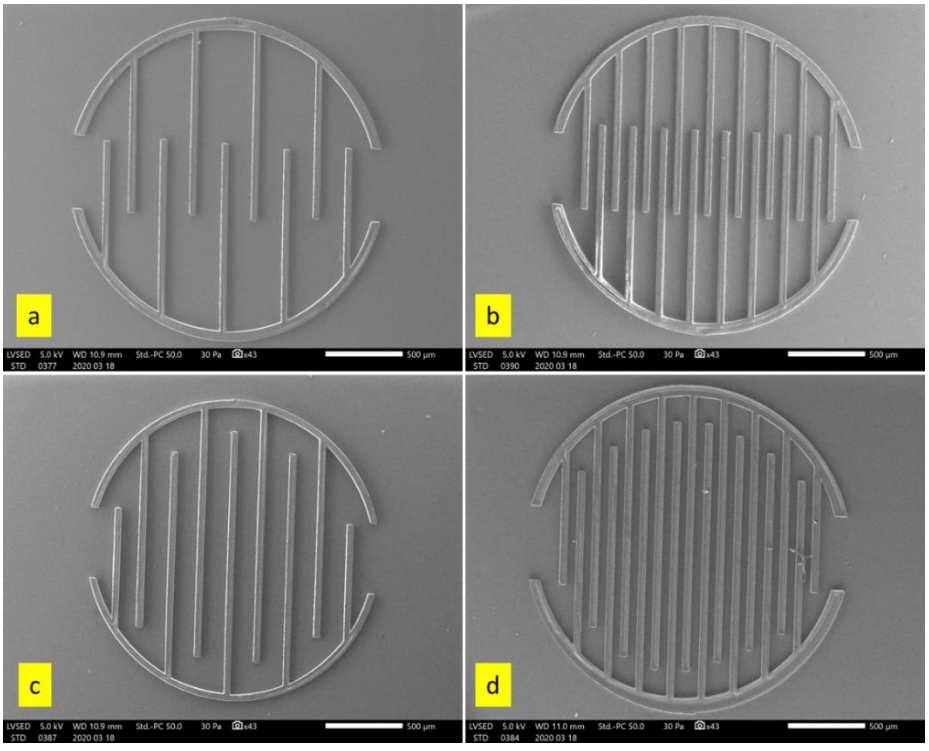

Figure 4:2 SEM of the PDMS microstructure on glass substrate showing circle with different walls, a. low number and same level walls [CLSW], b. high number and same level walls [CHSW], c. low number and tall (length) walls [CLTW] and d. high number and tall (length) walls [CHTW]. (Top view)

4.2. Different PDMS micropillar created with PBL

PBL was used to fabricate PDMS microstructures, forming PDMS micropillar array in a circle area. The mixing unit area (circle area of the created micropillar) has a diameter 2 mm, as shown in Figure 4:3. Creation of different sizes micropillars depends on dimensions of the drawn shapes in the scanning pattern file (drawn by Ionscan program, or a bitmap manipulator graphical software for scanning), which was used for proton beam scanning as mentioned in *section 3.4.2*.

There are two different sizes of pillars, the thin pillars are characterized by pillar diameter about *0.005 mm (~5 μm)* and spacing distance between the centres of two successive pillars about *0.045 mm (~45 μm)*, and the thick pillars is characterized by pillar diameter about *0.02 mm (~20 μm)* and spacing distance between the centres of two successive pillars about *0.03 mm (~30 μm)*.

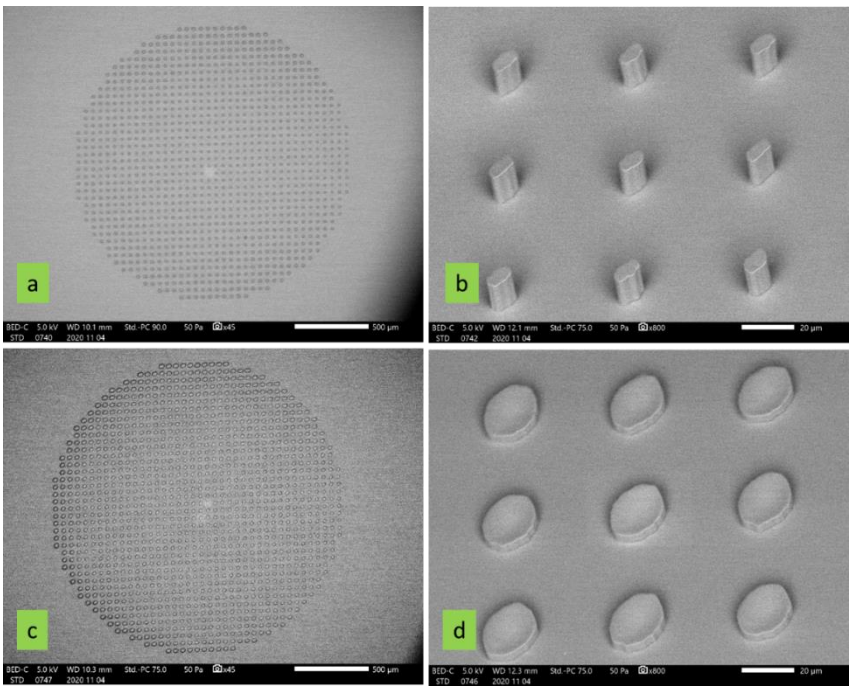

Figure 4:3 SEM of the PDMS micropillars on glass substrate showing a. full array of thin micropillars, b. focused image of thin pillars, c. full array of thick micropillars and d. focused image of thick pillars (top view).

4.3. Different PDMS caps of microfluidic chips

One important part of the chip is the cap, which forms the top part of the micromixer chip. And it can be formed using the SU-8 patterns which were created by UV lithography method (*described in section 3.4.3*). By which SU-8 master of different patterns can be fabricated as shown in Figure 4:4 (Long channel, circle or elliptic with different inlets/outlets).

Those SU-8 moulds were used to create the desired cap by pouring liquid PDMS on the designed SU-8 mould as illustrated in the method of *PDMS caps using SU-8 photolithography*..

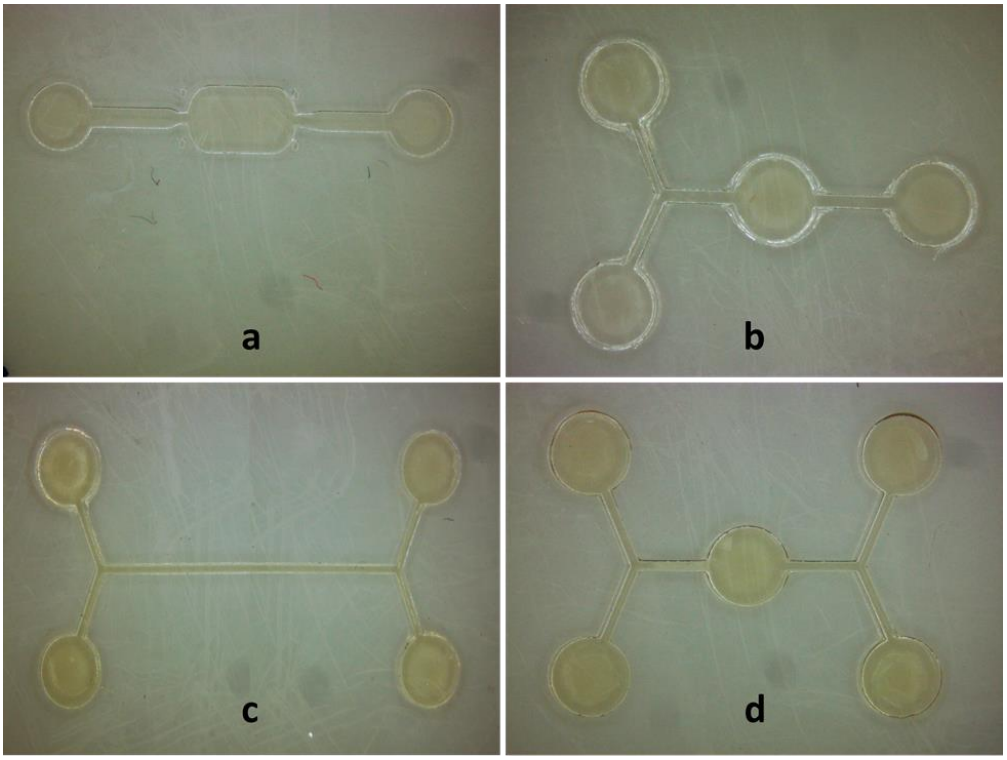

Figure 4:4 SU-8 master of different structures (channel, elliptic and circle) on glass by UV lithography with different inlets and outlets (a. 1 inlet and 1 outlet, b. 2 inlets and 1 outlet, c. and d. 2 inlets and 2 outlets)

Long channel SU-8 master shown in Figure 4:4, was used only to create the cap for channel micromixer. Other different caps can be created using

different SU-8 masters (shown in Figure 4:4), those caps have different number of inlets and outlets (*1* inlet and *1* outlet, *1* inlet and *2* outlets or *2* inlets and *1* outlet, and *2* inlets and *2* outlets). In the fabrication process of the real micromixers, the cap can be used as the cover of the microstructure beside it contains the inlets and outlets of the micromixer.

Focusing on the *2* inlets and *2* outlets SU-8 master for channel and circle, PDMS caps were fabricated as shown in Figure 4:5 (long channel and circle) where the formed shape is carved on one side of the cap and the other side is flat.

Later the formed caps (from the direction of the carved shape) were bonded to the created microstructures by PBL to get fully chip for passive micromixers application.

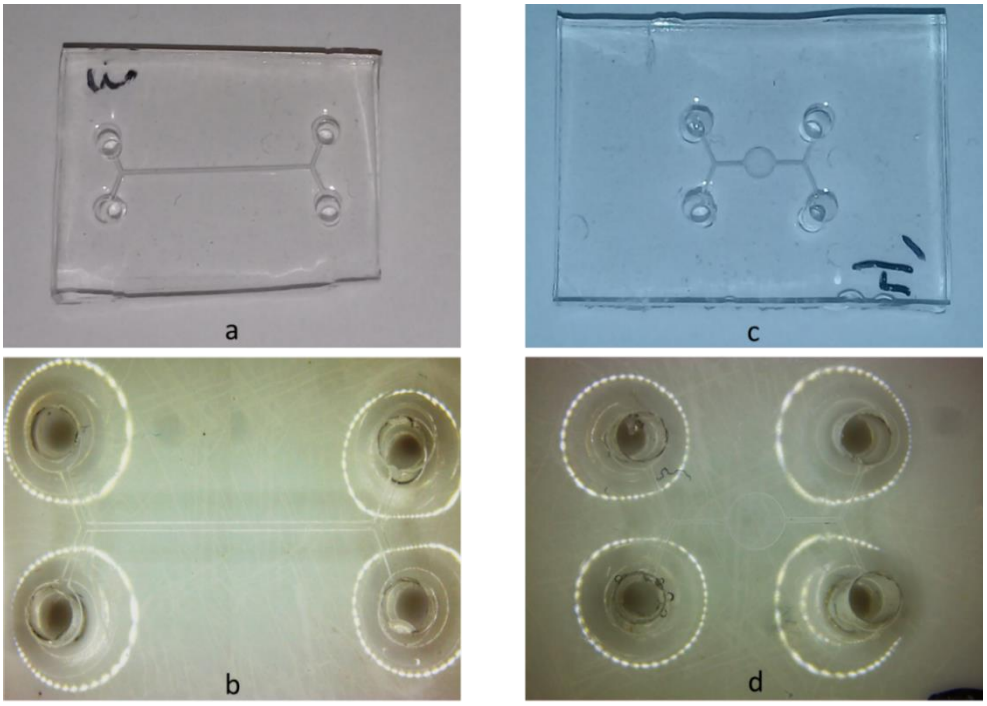

Figure 4:5 PDMS caps for micromixers with 2 inlets and 2 outlets of long channel (a. top view of upper level and b. top view of bottom level containing the sculpted long channel structure) and circle (c. top view of upper level and d. top view of bottom level containing the sculpted circle structure)

4.4. The creation of the microfluidic chip

To finalize the whole shape of the microfluidic chip, the PDMS structures and the PDMS cap should be bonded together. For that, both parts should be treated by air plasma, described in the methodology *section 3.4.4.* After proper bonding flexible silicone pipes was connected to the inlets and outlets as illustrated in Figure 4:6.

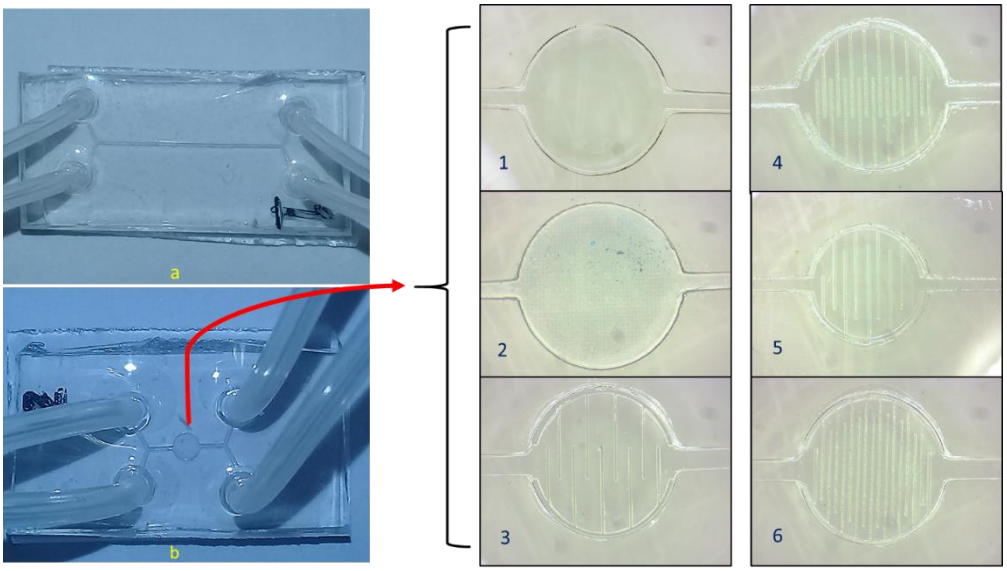

Figure 4:6 Final form of micromixers chips for mixing test, a. long channel micromixer and b. circle micromixer with different mixing unit areas (1. Simple circle [SC], 2. Pillars, 3. Low number and same level walls [CLSW], 4. High number and same level walls [CHSW], 5. Low number and tall (length) walls [CLTW] and 6. High number and tall (length) walls [CHTW]).

4.5. Mixing performance of passive micromixers

4.5.1. COMSOL simulation and mixing efficiency of different micromixers structures.

The mixing efficiencies of the different walls designs, which were illustrated in Figure 3:4, were simulated using the presented equations and physics (parameters and boundaries) previously in *section 3.2*.

The molecular diffusion coefficient in this model was set to 10^{-11} m^2/s. The fluid concentrations entering the two inlets were set to *0* and *100 mol/m^3*, as indicated by the blue and red colours in (Figure 4:7 - Figure 4:10). At the two inlets, the model boundary conditions have a constant velocity of *0.01 m/s*. Two cut lines at the inlets and outlets were arbitrarily established to identify absolute concentrations before and after the mixing unit area. The positions (inlet: distance = *0*, outlet: distance = *5*) of the two cut lines are indicated in (Figure 4:7 - Figure 4:10), and the mixing efficiencies are calculated using concentration across the y direction of these two cut lines.

The graphs (Y-coordinate vs Concentration) represent the concentration through the used two cut lines. In which, the blue line represent the concentration of the two fluids through the inlet cut line (distance = *0*, refers to the x coordinate value (*-2.5 mm*) according to the origin point, *see Figure 3:4*) and the green line for the outlet cut line (distance = *5*, refers to the x coordinate value (*+2.5 mm*) according to the origin point, *see Figure 3:5*). And it is obvious that the concentrations of the two fluids at inlets are unchanged for all the different used micromixers, which means no mixing for all micromixers and in case of perfect mixing, the edges of the green lines in (Figure 4:7 - Figure 4:10) should tend toward *50 mol. m^{-3}*.

The simulation results show that the mixing efficiency of the channel and the circle micromixers was very low, due to the little change of the concentration of the two fluids through the micromixers especially at the used two cut line.

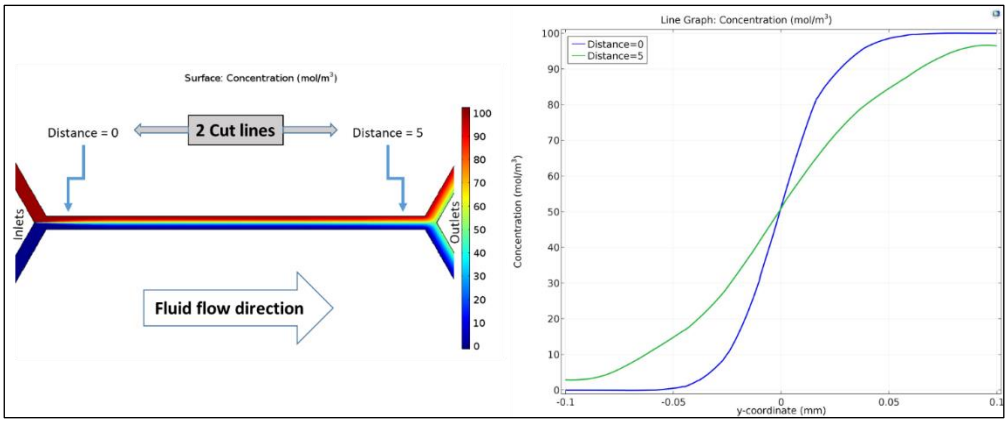

Figure 4:7 Left: the mixing performance results using COMSOL simulation for channel structure micromixer. 2 cut lines are indicated at distances of 0 (near inlets) and 5 (near outlets). Right: Concentration profiles (concentration vs y- coordinate of the cut lines).

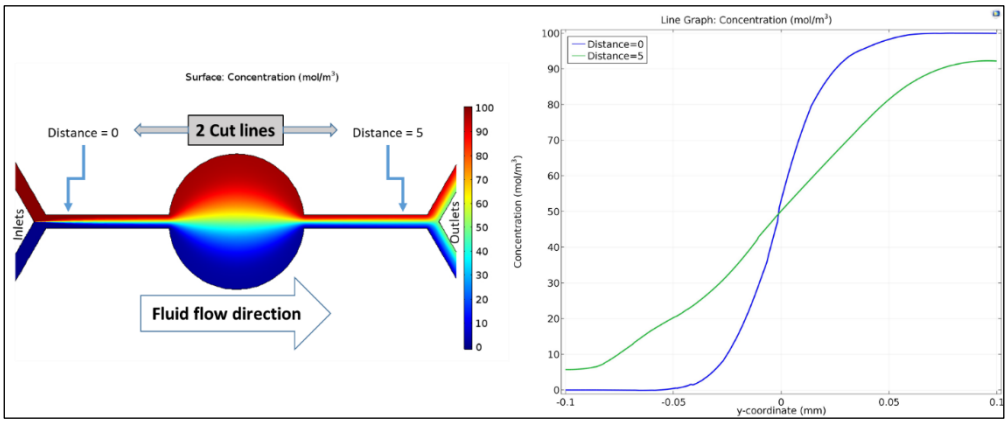

Figure 4:8 Left: the mixing performance results using COMSOL simulation for circle structure micromixer. 2 cut lines are indicated at distances of 0 (near inlets) and 5 (near outlets). Right: Concentration profiles (concentration vs y- coordinate of the cut lines).

However, Figure 4:9 shows improvement in the mixing efficiency using pillars rather than the channel or the circle micromixers for the same mixing conditions. As it is indicated by the green line in Y-coordinate vs Concentration graph of pillar micromixer, the concentration of the two fluids is changed a little bit due to the slightly increase in the mixing of the two fluids. The mixing was improved through the pillars as it works to spilt and recombine the fluids molecules, which increase the molecular diffusion.

The best mixing results were obtained using the circle-with-walls structure as shown in Figure 4:10, where the concentrations of the two fluids at outlets becomes nearly similar as indicated by the tendency of the green line (Y-coordinate vs Concentration graph) towards the mean concentration value (around *50 mol. m*$^{-3}$).

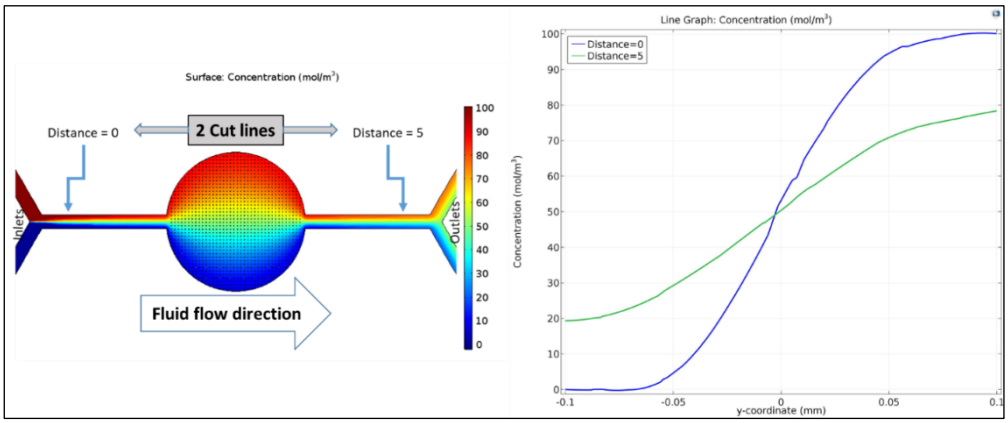

Figure 4:9 Left: the mixing performance results using COMSOL simulation for circle-with-pillars micromixer. 2 cut lines are indicated at distances of 0 (near inlets) and 5 (near outlets). Right: Concentration profiles (concentration vs y- coordinate of the cut lines).

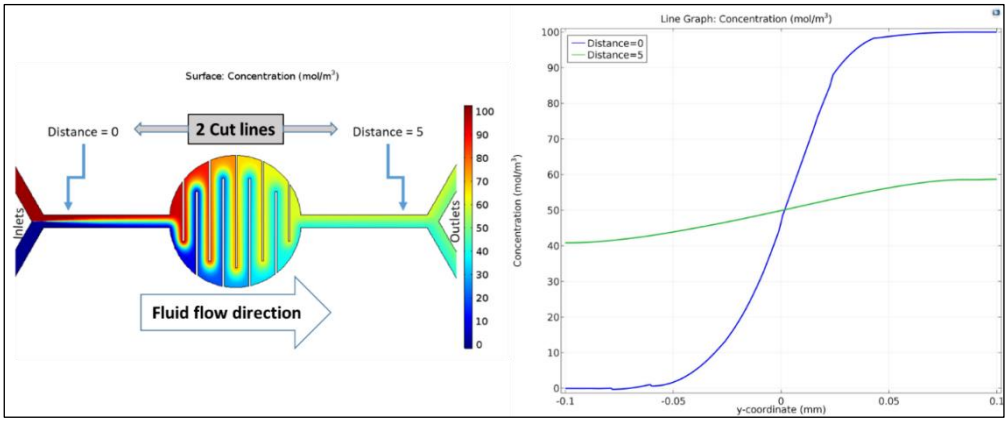

Figure 4:10 Left: the mixing performance results using COMSOL simulation for circle-with-walls micromixer. 2 cut lines are indicated at distances of 0 (near inlets) and 5 (near outlets). Right: Concentration profiles (concentration vs y- coordinate of the cut lines).

The mixing efficiency can be considerably enhanced by utilizing microstructures in microfluidic chips, notably in the case of micro-wall

structures, as shown by the concentration profiles. Where the walls behave as an obstacle to restructure the path of fluids flow in a narrow channel serpentine shape which enhance the mixing efficiency.

These simulated designs were used to build and fabricate the real chips. As a baseline, the less efficient chips were manufactured.

4.5.1.1. Pressure drop values in different micromixer

Good mixing performance and low pressure drop are two important design factors of any mixer. Low pressure drop is very important for industrial production because it decreases energy requirements[189].

Another feature of the COMSOL simulation, beside the mixing efficiency investigations, is the pressure drop calculations for our simulated micromixers, where the simulations of different structures were done at flow velocity *0.01 m/s*. The pressure drop through the different micromixer structures can be shown in Figure 4:11, in which the pressure drop of the walls structure is higher than the other structures (channel, circle or pillars). The results showed that the pressure drop values ranges (*0.139 - 1.74 kPa*) for all the mentioned structures, and the variation of the pressure drop depends on the dimensions of the micromixer

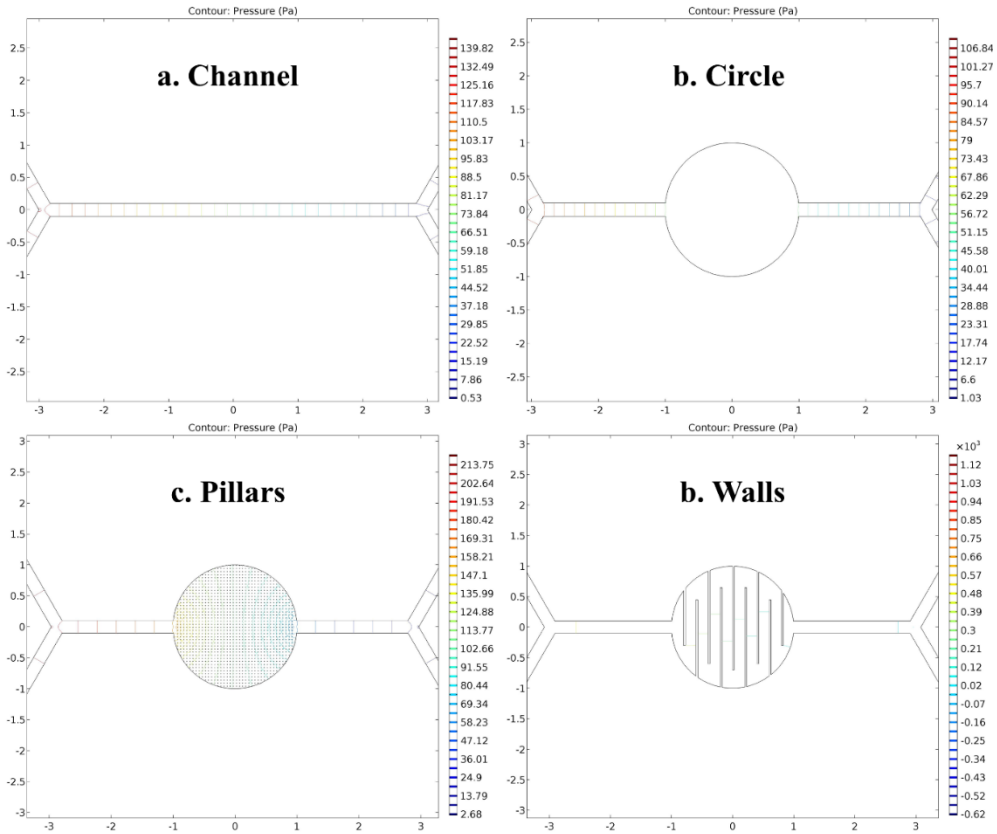

Figure 4:11 Pressure contour and the bar of pressure change for different shape micromixers: a) Channel, b) Circle, c) Pillars and d) Walls.

On the other hand, the pressure drop was calculated for the real fabricated micromixers using *equation 6*, which help to find the values of pressure drop at different flow rate using the exact dimensions of the micromixers. The calculated drop pressure with flow rate (*1-6 µl/min*) was listed in Table 4 for the different micromixers chips (channel, circle, pillars, and walls), the results show a high pressure drop of the walls micromixer which match to some extent with the simulated pressure drop results. It is obvious the dependency of the pressure drop on the flow rate.

Table 4 the calculated pressure drop at different flow rates for different shape micromixers.

Micromixer type	Flow rate (µl/min)	Pressure drop ΔP (kPa)	Micromixer type	Flow rate (µl/min)	Pressure drop ΔP (kPa)
Channel	1	0.05	Circle	1	0.01
	2	0.09		2	0.01
	3	0.14		3	0.02
	4	0.18		4	0.02
	5	0.23		5	0.03
	6	0.27		6	0.03
Pillars	1	0.03	Walls	1	1.19
	2	0.06		2	2.38
	3	0.1		3	3.56
	4	0.13		4	4.75
	5	0.16		5	5.94
	6	0.19		6	7.13

4.5.2. Mixing test of the fabricated chips of different structures micromixers

To evaluate the mixing efficiency, all of the created microfluidic chips of channel, circle, circle-with-pillars, and circle-with-walls were tested using mixing test system (*see section 3.5*), and it is illustrated in (Figure 4:12-Figure 4:15).

For the mixing test, two fluids, a) water and b) aqueous solution of methylene blue, were used in the two inlets as shown in Figure 3:15, then the mixed samples are collected at outlets for flow range *1 - 6 µl/min* for different micromixers. For a mixing efficiency of *100 %*, at both outlets the concentration value is expected to be exactly half of the original's methylene blue concentration. The intensity change of an absorption peak (*664 nm*) was

determined using spectrophotometry to examine the concentrations of the methylene blue solutions.

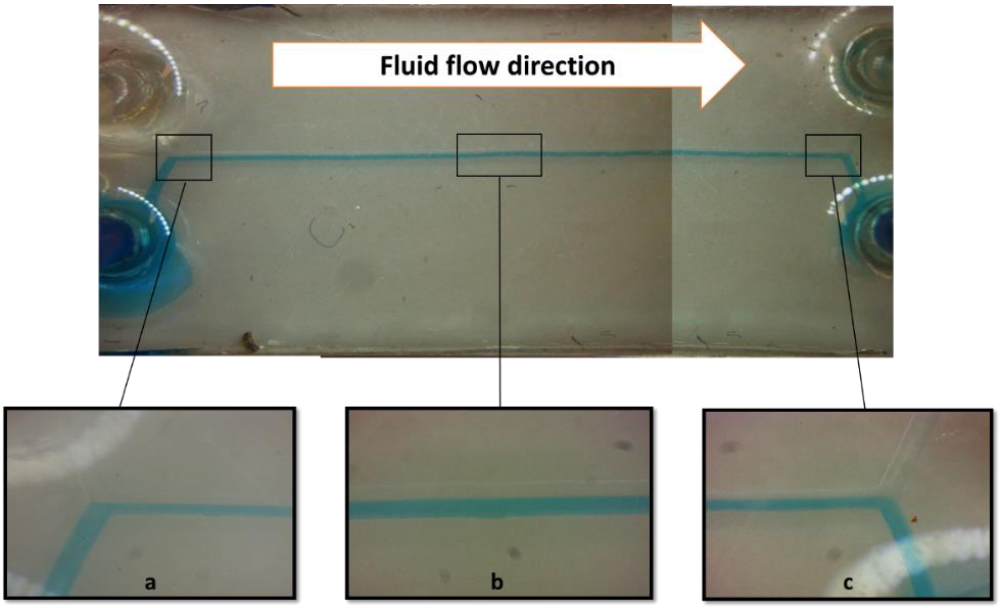

Figure 4:12 Testing the mixing level of a channel micromixer a) the inlets section, b) the mixing channel section, and c) the outlets section.

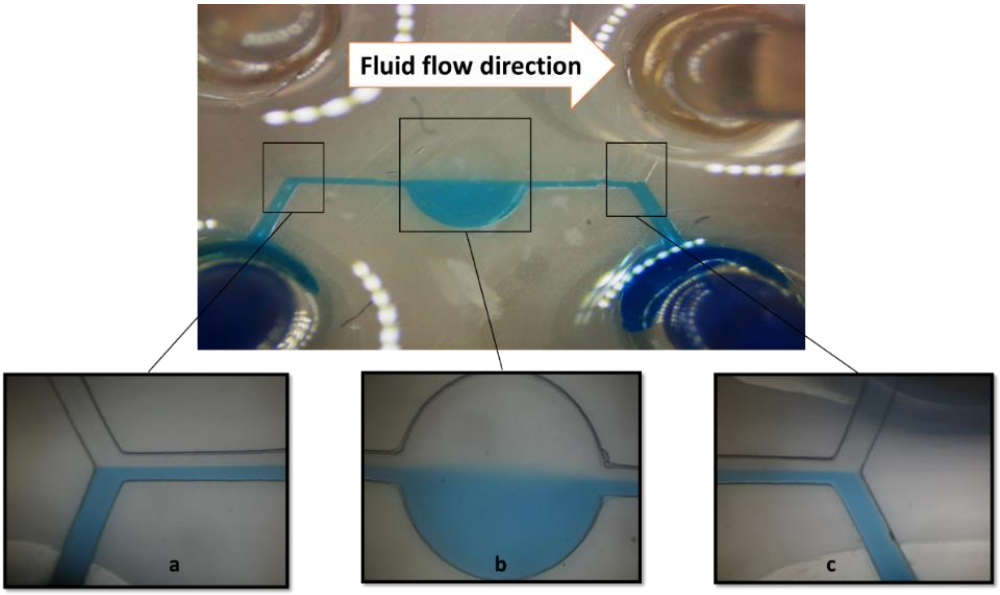

Figure 4:13 Testing the mixing level of circle micromixer a) the inlets section, b) the mixing circle section and c) the outlets section.

Figure 4:12 and Figure 4:13 illustrate that the mixing of the two fluids was inefficient for the channel and circle micromixers, as shown throughout the micromixer parts inlets, mixing unit area and outlets. Conversely, as illustrated in Figure 4:14, the mixing was apparently enhanced by applying pillars to the mixing unit area. Finally, featuring walls within the mixing unit area shows a good mixing, as illustrated in Figure 4:15.

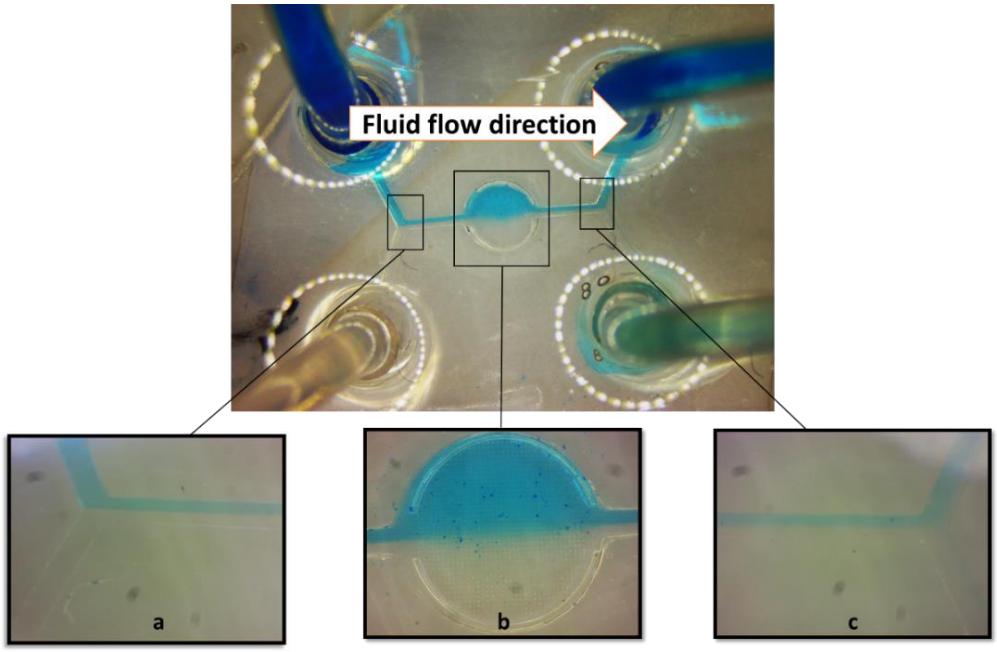

Figure 4:14 Testing the mixing level of circle-with-pillars micromixer a) the inlets section, b) the mixing circle-with-pillars section and c) the outlets section.

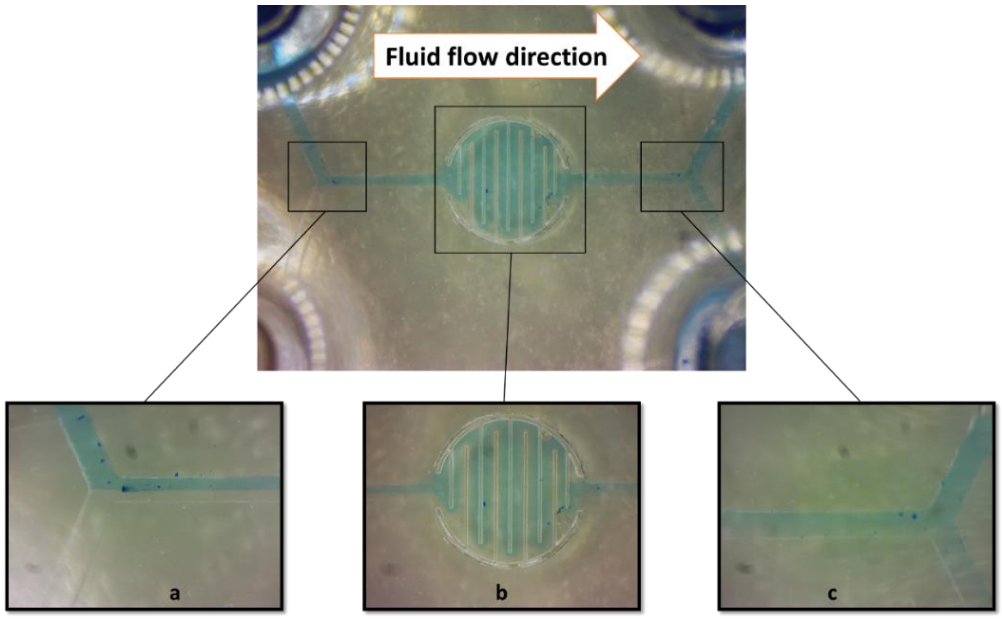

Figure 4:15 Testing the mixing level of circle-with-walls micromixer a) the inlets section, b) the mixing circle-with-walls section and c) the outlets section.

4.5.2.1. Concentration measurements by UV/Vis spectroscopy

All the created micromixers were tested for mixing efficiency at different flow rates (*1-6*) *µl/min*, using the mentioned system in *section 3.5*.

The concentrations of the collected samples for each flow rate were measured using the UV/Vis spectroscopy. The two outlets were named (a) and (b), and the samples were marked by the value of flow rate and outlet name for each flow rate (example: 1a and 1b refer to the collected sample of flow rate *1 µl/min* for (a) and (b) respectively, and so on….).

For all experiments, the used fluid was aqueous solution of methylene blue, which was prepared by concentration $c = 2 \times 10^{-5}\ mol/dm^{3}$. Aqueous solution of methylene blue has absorbance spectra with a maximum absorbance intensity peak at wavelength *664 nm* as shown in Figure 4:16.

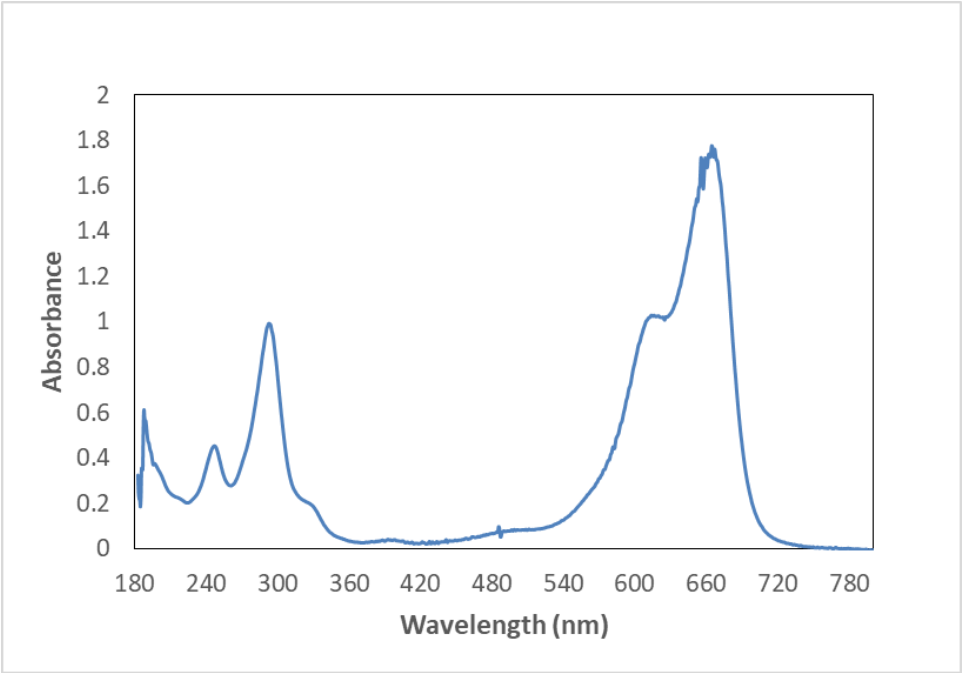

Figure 4:16 Absorption spectra of Methylene Blue (original concentration) before mixing process.

By using micromixers, the concentration of the input fluids will change due to the mixing, which depends on the structure of the used micromixer (channel, circle, pillars and walls). The heights of peaks at wavelength *664 nm* for the absorbance spectrum show different absorbance value, which refer to change the concentrations of the collected samples.

The absorbance peak height of the collected samples at outlets (a) and (b) represent the mixing efficiency value for the used flow rate and micromixer type. So in Figure 4:17- Figure 4:20, the mixing can be perfect g (*100%*) if there is identical overlapping between the two outlets (a and b) absorbance spectra (the heights of the two peaks (at *664 nm*) are equal), and the mixing goes worse if there is a shift between the two absorbance spectra (difference between the peaks heights (at *664 nm*) become larger).

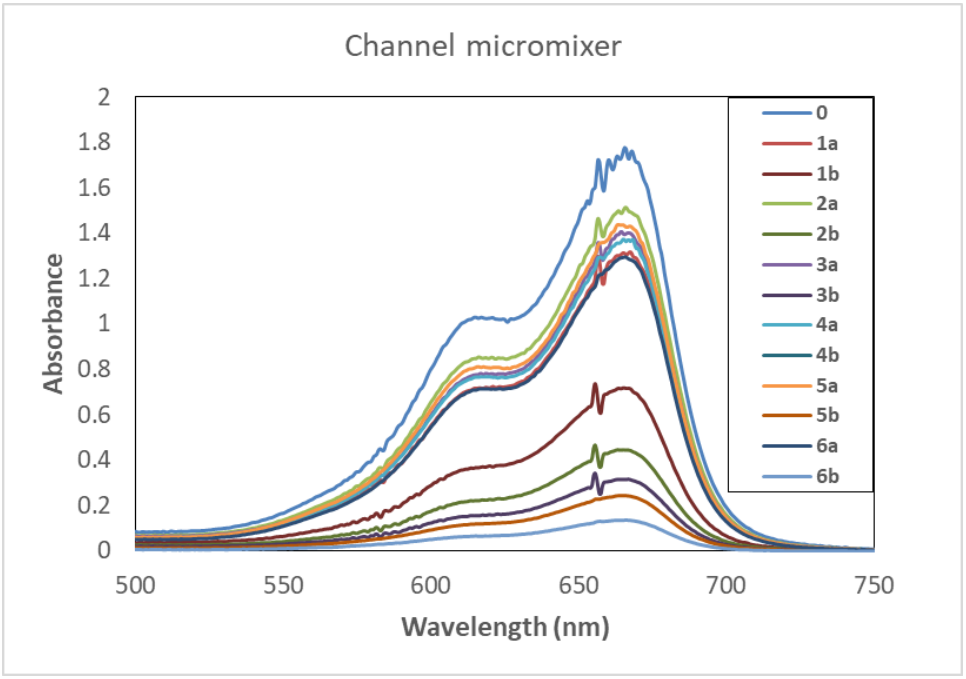

Figure 4:17 The absorbance variation at wavelength 664 nm with different flow rate for channel micromixer.

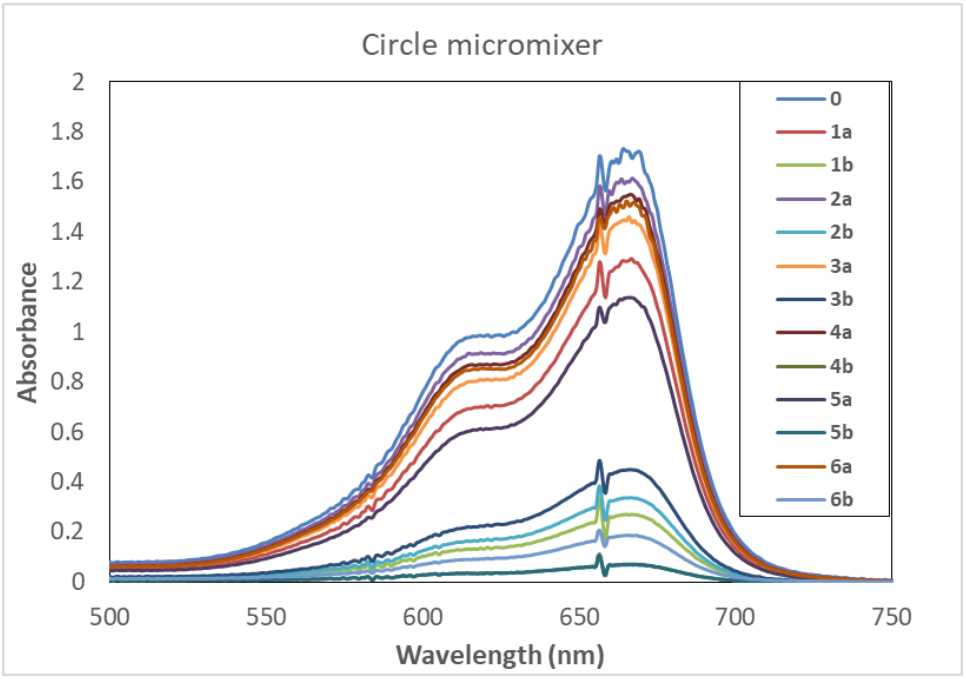

Figure 4:18 The absorbance variation at wavelength 664 nm with different flow rate for circle micromixer.

According to the type of micromixer, there are different efficiencies of mixing at different flow rates, which appear for low mixing efficiency of channel micromixer (Figure 4:17) and circle micromixer (Figure 4:18). The low mixing efficiency of those two micromixers can be understood from the high difference absorbance values (at *664 nm*) at outlets (a) and (b), as shown in Figure 4:21.

The mixing efficiency improved using pillars micromixer (Figure 4:19) and walls micromixer (Figure 4:20). Where the shift between the absorbance spectra of outlets (a) and (b) become smaller, and the peaks heights (at *664 nm*) become comparable which leads to the low values of the difference between the outlets absorbance values, especially at the low flow rate as shown in Figure 4:21.

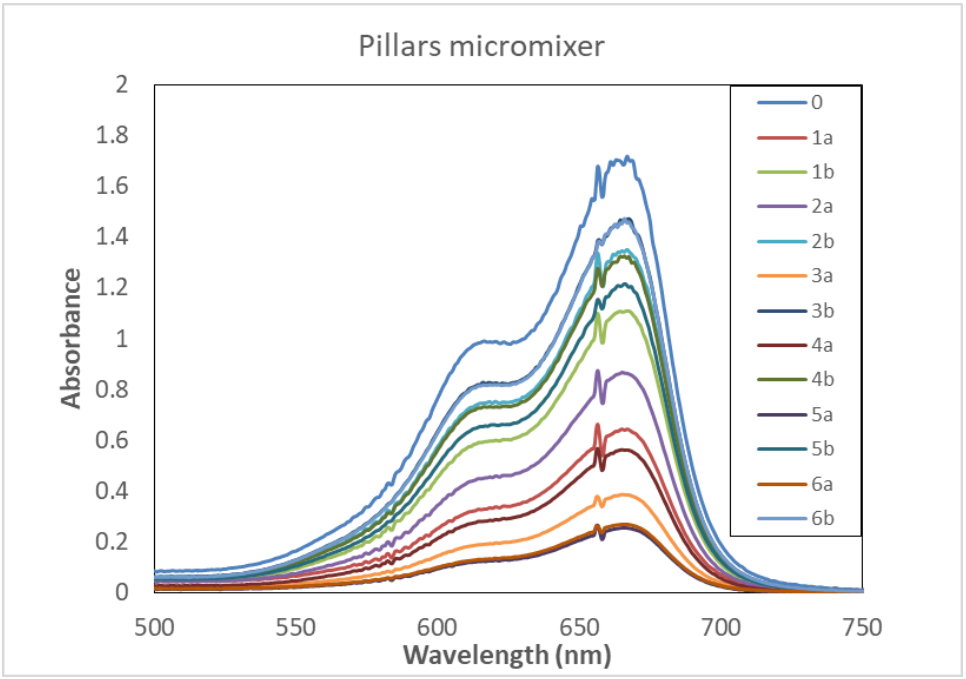

Figure 4:19 The absorbance variation at wavelength 664 nm with different flow rate for pillars micromixer.

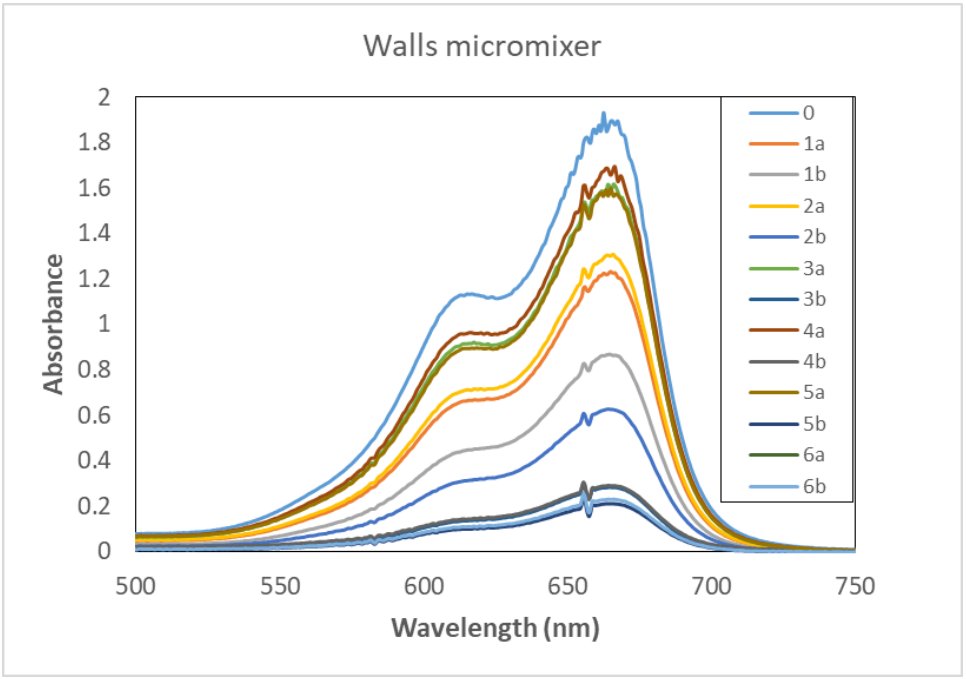

Figure 4:20 The absorbance variation at wavelength 664 nm with different flow rate for walls micromixer.

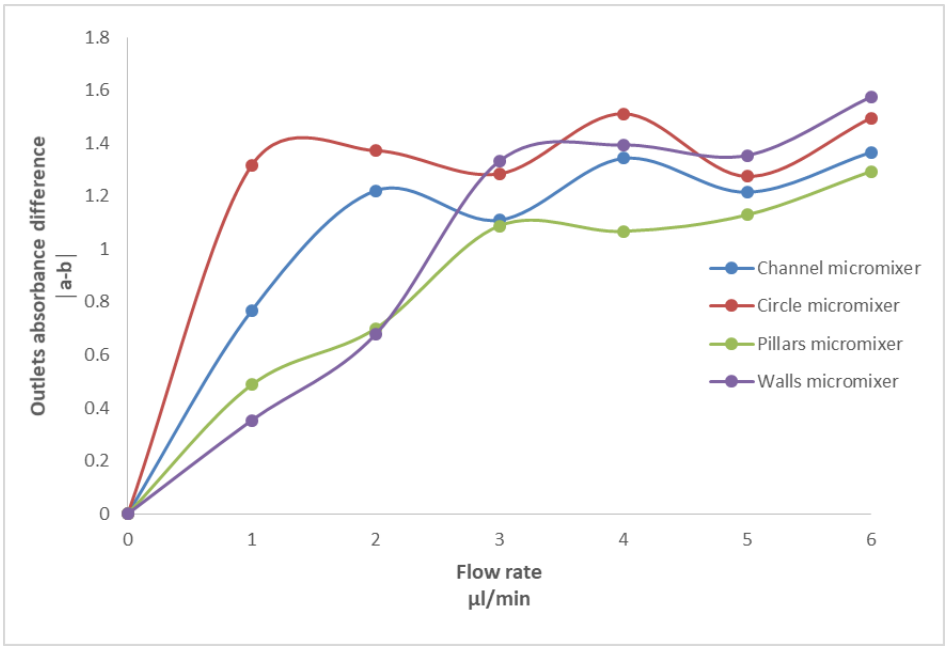

Figure 4:21 the difference of the absorbance values (around the wavelength 664 nm) between the two outlets (a) and (b) for the different shape micromixers at different flow rates.

4.5.2.2. Mixing efficiency calculations.

Firstly, UV/vis spectrophotometry was used to evaluate the methylene blue concentrations at the two chips' outputs. Then, based on the changes in concentrations at the two outlets, the mixing efficiencies were determined using *equation 5* for all the fabricated micromixers.

The mixing efficiency value $M = 0\ \%$, according to *equation 5*, refers to the totally unmixed condition of the species, and $M = 100\ \%$ refers to the totally mixed condition. The accepted value for mixing efficiency in practical applications is between $80 – 100\ \%$.

Because of the relatively low concentration of the methylene blue (2×10^{-5} mol/dm^3), the density (ρ) and dynamic viscosity (μ) of water and methylene blue solution were assumed to be equivalent for the mixing efficiency measurements.

4.5.2.3. Mixing efficiency vs flow rate and velocity

The efficiency of mixing for our created different micromixers (channel, circle, circle-with-pillars, and circle-with-walls) were determined experimentally using flow rate ranging from *1* to *6* $\mu l/min$.

The mixing efficiency values of the channel micromixer were low for the mentioned flow rate range, due to low molecular diffusion between the used two fluids through the length of the channel. The mixing efficiency value goes worse using the circle micromixer due to the increasing dimensions of the mixing part. While the pillars enhance the mixing efficiency to higher value comparing to the channel and circle micromixer as shown in Figure 4:22, as the pillars increase the molecular diffusion through the splitting and recombination of the fluids.

The good result of mixing efficiency can be obtained using walls (Figure 4:22), as the walls work to force the flow in a very narrow micro channel, that reduces the cross-diffusion length and maximizes the contact area of the two fluids which helps to enhance the fluids mixing.

As illustrated in Figure 4:22, the mixing efficiency drops with increasing the flow rate for all the mentioned micromixers. The mixing efficiency value at flow rate *1 µl/min* was used for comparison of the different fabricated micromixers, and the mixing efficiency values were found *58 %*, *29 %*, *72 %* and *82 %* for the micromixers channel, circle, circle-with-pillars and circle-with-walls, respectively.

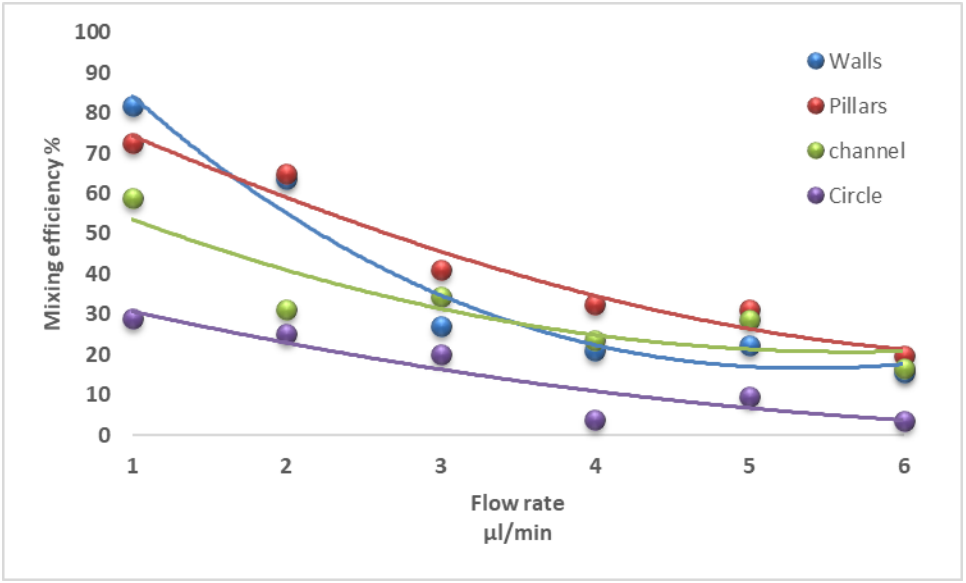

Figure 4:22 Mixing efficiency variation with flow rate for different shape micromixer

So, the circle-with-walls micromixer design produces more suitable mixing efficiency, due to its geometry increases the contact area and reduces the diffusion length between the used different fluids. The experimental results follow the trend of the simulated results.

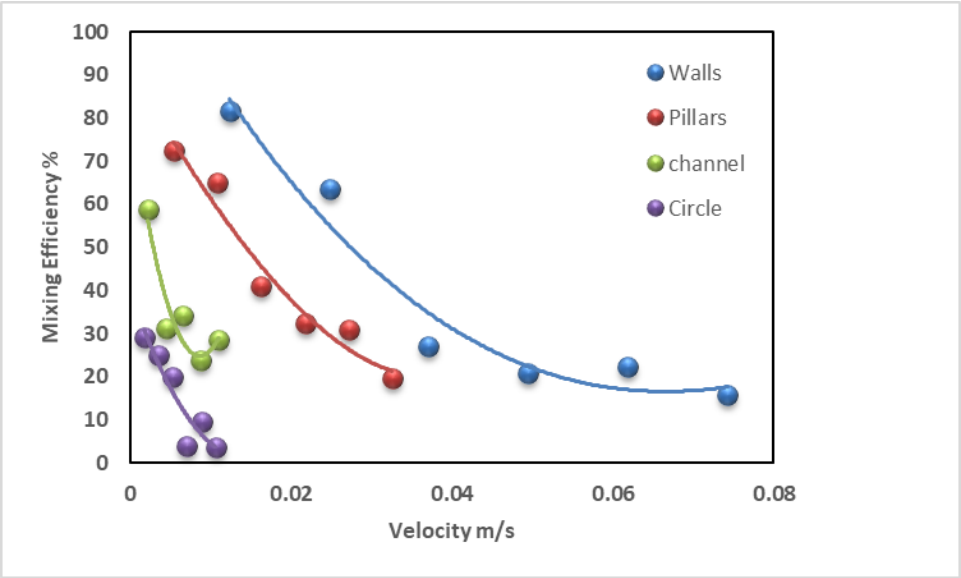

Figure 4:23 Mixing efficiency difference at various fluid velocity, according to the dimensions of the structure for the used micromixer.

The geometrical structure of the designed micromixers affects the velocity of the fluids through the micromixer as shown in Figure 4:23, which shows the dependence of velocity on the dimensions of the used micromixers channel, circle, pillars and walls. Where the smallest dimension of walls characterized by the highest velocity while the largest dimension of the circle has the lowest velocity.

Also, Figure 4:23 shows that the mixing efficiency for all micromixers decreases with increasing velocity of the fluids through the micromixer, and the mixing efficiency at a fixed speed depends on the structure type of the used micromixers.

4.5.3. COMSOL simulation and mixing efficiency of different walls structures micromixers.

The 2-dimensional designs illustrated in section 3.2.3 are simulated to get the results of mixing efficiency with highest possible accuracy and reliability by using modules and *equation*s *7-9* presented previously in chapter 2.

For COMSOL simulation, the value of used parameters like fluid density and viscosity are *1000 kg/m*^{3} and *10*$^{-3}$ $\frac{kg}{m*s}$, respectively. Also, the value of molecular diffusion coefficient used in this model is *10*$^{-11}$ *m*^{2} */s*.

The molar concentration of the entering fluids to the two side inlets are set to *0* and *1*, where in all simulated figures the blue circle refer to 0 and dark red circle refer to 1 as shown in (Figure 4:24-Figure 4:28). For simplicity, we assume that the fluid flows are in steady state and there are no slips at micromixer's walls. The model boundary conditions have a constant velocity of *0.01 m/s* at the two inlets.

The indicated two cut lines at positions distance = *0* and *5*, illustrated in Figure 4:24 - Figure 4:28 , were very useful to find the mixing values around inlets and outlets respectively. The values of mixing efficiency were calculated by *equation 5*, where the normalized concentration and the inlet's average concentration described in *equation 5* are extracted from y- coordinate vs concentration diagrams (the right side of Figure 4:24-Figure 4:28) for each structure separately.

The graph of y- coordinate vs concentration studies the change of the fluid's concentration (refer to mixing value) through the used two cut lines, which contains two lines for investigation the mixing enhancement through the simulated structure, the blue line refers to the cut line close to inlets (distance = *0*) and the green line refers to the cut line close to the outlets (distance = *5*).

It is self-evident that there is low value of mixing efficiency at inlets for all simulated structures as shown by the blue line in Figure 4:24-Figure 4:28, while there is an improvement of the mixing efficiency at outlets as indicated by the green line. The improvements of the mixing efficiencies depend on the geometry of used structures, the good mixing could be observed by the tendency of the green line around the half value of concentration ($50\ mol/m^3$).

Concentration profile through the cut line are shown in figures (Figure 4:24-Figure 4:28) for micromixers [SC], [CLSW], [CHSW], [CLTW] and [CHTW] respectively, by which the value of concentration at each point of the cut line of each micromixer separately was exported from the simulated data to Excel file, then the mixing efficiency for each point of the cut line was calculated individually by using *equation 5*. The average of the mixing efficiency values for all cut line points was calculated, to find the exact mixing efficiency for the used micromixer.

For the mentioned structures, the mixing efficiency values were calculated, and the results showed that *38.17 %* efficiency of mixing for simple circle [SC] and it illustrated by Figure 4:24, so SC structure has a poor mixing efficiency as the value of mixing efficiency (M) for accepted devices should be at the range *[80-100] %*.

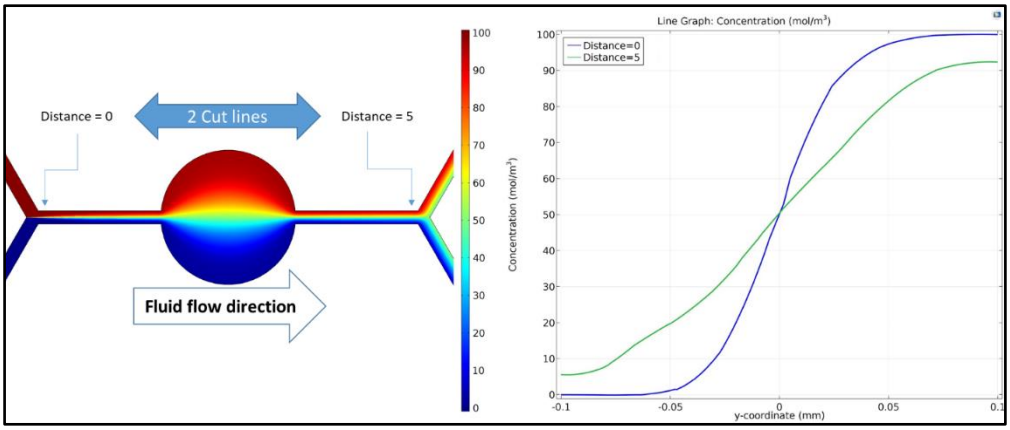

Figure 4:24 Left: COMSOL simulation for mixing of two fluids for SC structure with 2 cut lines at distance = 0 (near inlets) and distance = 5 (near outlets). Right: Concentration variation with y coordinate (Channel width) for distance = 0 (blue line) and distance = 5 (green line).

Using circle with walls improves the value of mixing efficiency for higher value *73.18 %* for circle with low number and same level walls [CLSW] as shown by Figure 4:25, but still not in the accepted mixing efficiency range, this leads to increase the number of walls for the same structure and the new structure is circle with high number and same level walls [CHSW] as shown by Figure 4:26, which gives an excellent value of mixing efficiency *99.44 %*.

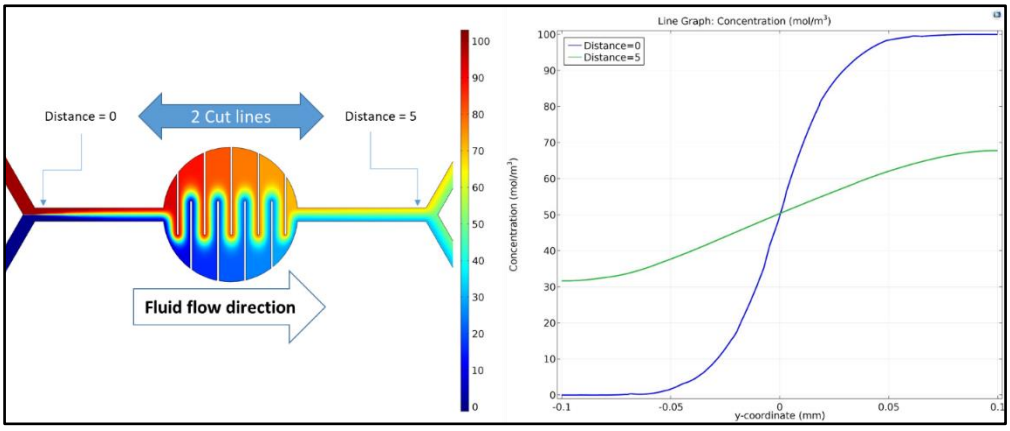

Figure 4:25 Left: COMSOL simulation for mixing of two fluids for CLSW structure with 2 cut lines at distance = 0 (near inlets) and distance = 5 (near outlets). Right: Concentration variation with y coordinate (Channel width) for distance = 0 (blue line) and distance = 5 (green line).

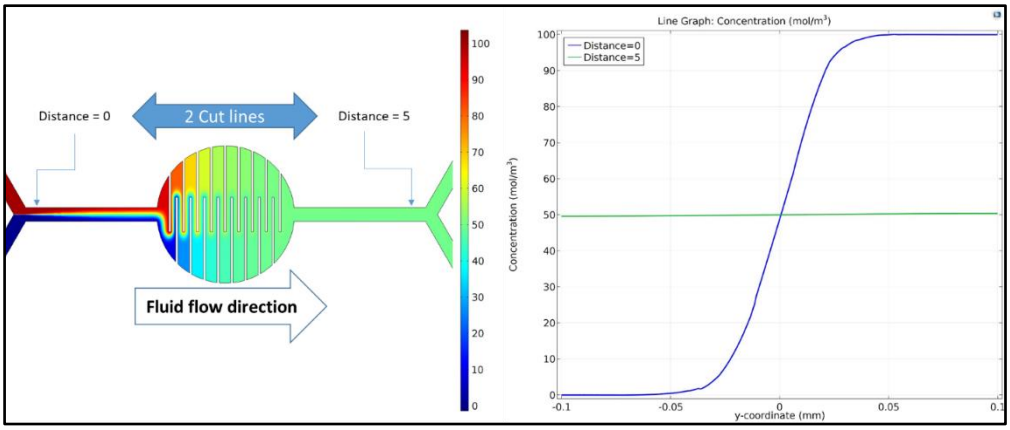

Figure 4:26 Left: COMSOL simulation for mixing of two fluids for CHSW structure with 2 cut lines at distance = 0 (near inlets) and distance = 5 (near outlets). Right: Concentration variation with y coordinate (Channel width) for distance = 0 (blue line) and distance = 5 (green line).

Another parameter was studied to improve the efficiency, using walls longer than the previous same level walls (but the same number) as described Figure 4:27 for circle with low number and tall (length) walls [CLTW], which helps to increase the mixing efficiency to accepted value *91.36 %* comparing to *73.18 %* of CLSW structure. And of course, increasing the number of tall (length) walls was the best value of mixing efficiency *99.99 %* as found in Figure 4:28 for circle with high number and tall (length) walls [CHTW].

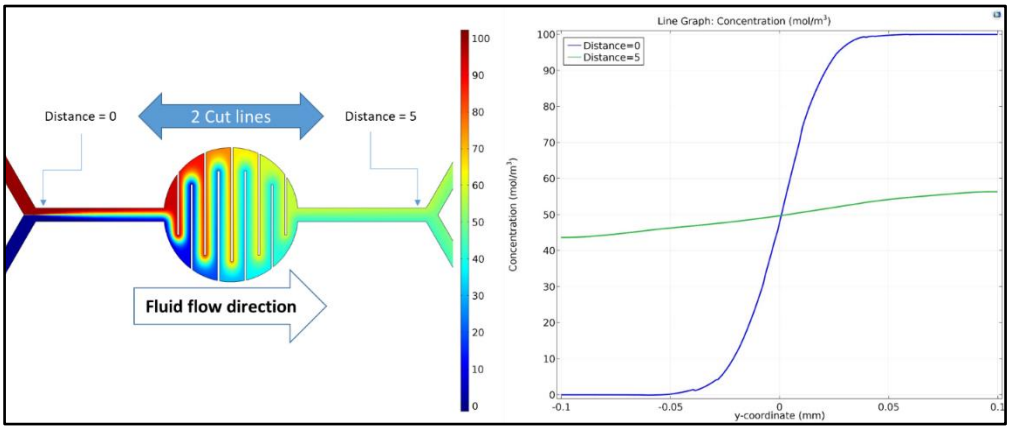

Figure 4:27 Left: COMSOL simulation for mixing of two fluids for CLTW structure with 2 cut lines at distance = 0 (near inlets) and distance = 5 (near outlets). Right:

Concentration variation with y coordinate (Channel width) for distance = 0 (blue line) and distance = 5 (green line).

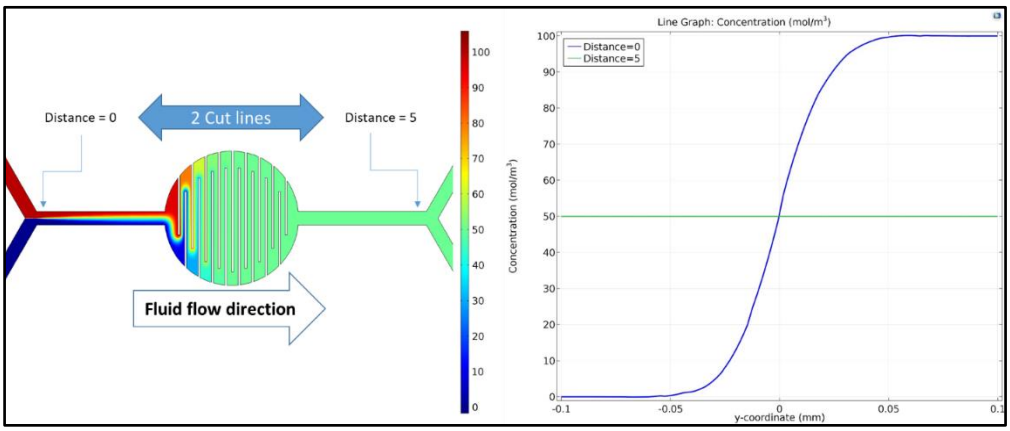

Figure 4:28 Left: COMSOL simulation for mixing of two fluids for CHTW structure with 2 cut lines at distance = 0 (near inlets) and distance = 5 (near outlets). Right: Concentration variation with y coordinate (Channel width) for distance = 0 (blue line) and distance = 5 (green line).

For conclusion, using the fact of accepted mixing efficiency range [80-100] %, the simulation results for the mentioned geometries, fixed velocity and fixed diffusion coefficient shows poor mixing efficiency of [SC] and [CLSW] micromixers, while it improves to accepted value for [CLTW] micromixer and to excellent mixing efficiency values for [CHSW] and [CHTW] micromixers. Due to the calculated results of mixing efficiency for different structures, there are two important factors, the number and the length of walls, which should be taken in account for the construction of the micromixers due to their importance to restructure the flow of the fluids in the way that increase the contact area between fluids and increase the molecular diffusion to enhance the mixing.

4.5.3.1. Pressure drop values in different walls micromixer

Using the dimensions of the real different walls micromixers (CLSW, CHSW, CLTW and CHTW), at different flow rate (*1-6 μl/min*) the pressure

drop using *equation 6* was calculated for the different walls micromixers and the values are listed in Table 5. The results show the dependency of the pressure drop on the structure of the micromixer, so the structures of high number of walls have a higher pressure drop than the low number of walls, also the length of the walls have the same influence where the longer walls increase the pressure drop. It is obvious the dependency of the pressure drop on the flow rate.

Figure 4:29 shows the simulated pressure values for the different walls micromixers (CLSW, CHSW, CLTW and CHTW), in which the pressure goes higher for the larger number and longer walls, so CLSW has the lowest pressure drop and CHTW has the highest pressure drop

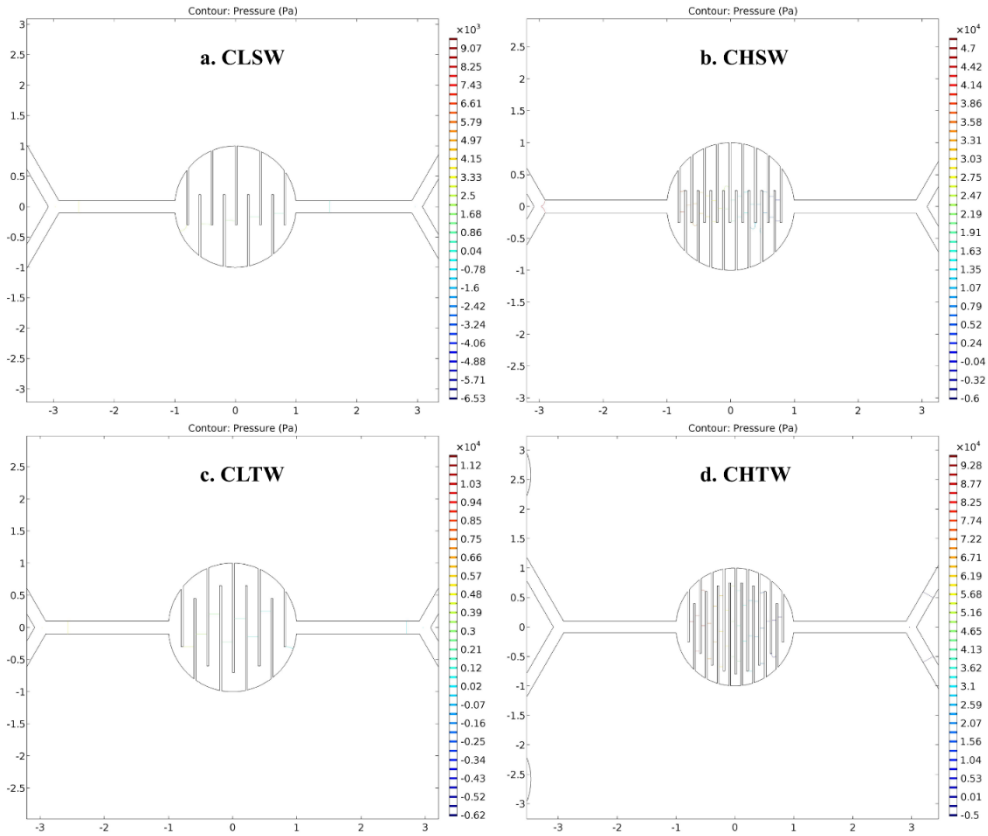

Figure 4:29 Pressure contour and the bar of pressure change for different wall micromixers: a) CLSW, b) CHSW, c) CLTW and d) CHTW.

Table 5 the calculated pressure drop at different flow rates for different walls micromixers.

Micromixer type	Flow rate (µl/min)	Pressure drop ΔP (kPa)	Micromixer type	Flow rate (µl/min)	Pressure drop ΔP (kPa)
CLSW	1	0.58	CHSW	1	1.26
	2	1.16		2	2.51
	3	1.74		3	3.77
	4	2.33		4	5.03
	5	2.91		5	6.29
	6	3.49		6	7.54
CLTW	1	1.19	CHTW	1	1.87
	2	2.38		2	3.74
	3	3.56		3	5.61
	4	4.75		4	7.48
	5	5.94		5	9.34
	6	7.13		6	11.21

4.5.4. Mixing test of the fabricated chips of different walls structures micromixers

For mixing efficiency investigation, a syringe pump shown in Figure 3:15 is used to pump two fluids at the inlets of the fabricated micromixers with a flow rate ranges from *1* to *6 µl/min*, the mixed samples are collected at outlets of micromixers, then the concentration of the two fluids before and after mixing were investigated by UV/vis spectroscopy, the mixing efficiency (M) were calculated by *equation 5* using the previous measured concentrations.

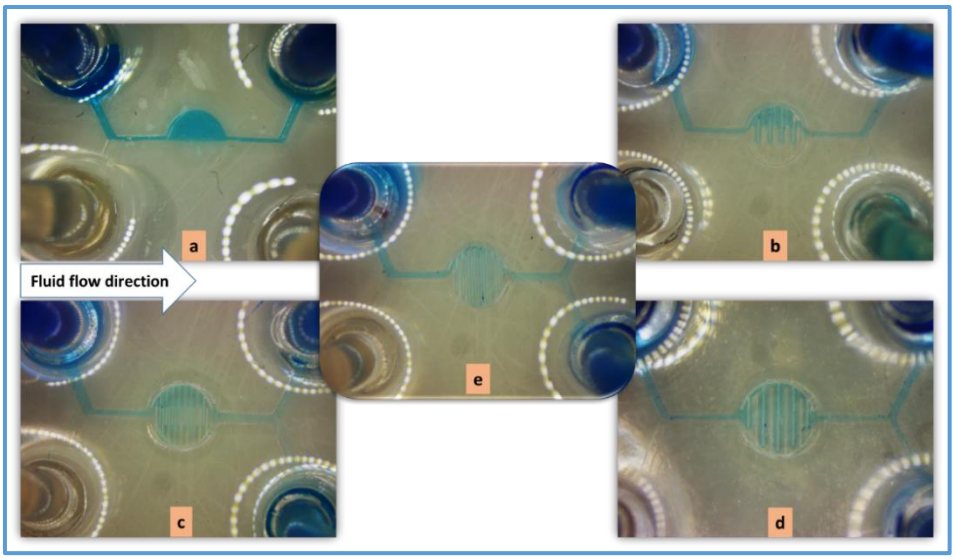

Figure 4:30 Optical microscope image of whole chip micromixer (2 inlets + 2 outlets + mixing unit area) to Show the mixing level for different micromixers: a) simple circle [SC], b) circle with low number and same level walls [CLSW], c) circle with high number and same level walls [CHSW], d) circle with low number and e) tall (length) walls [CLTW] and circle with high number and tall (length) walls [CHTW].

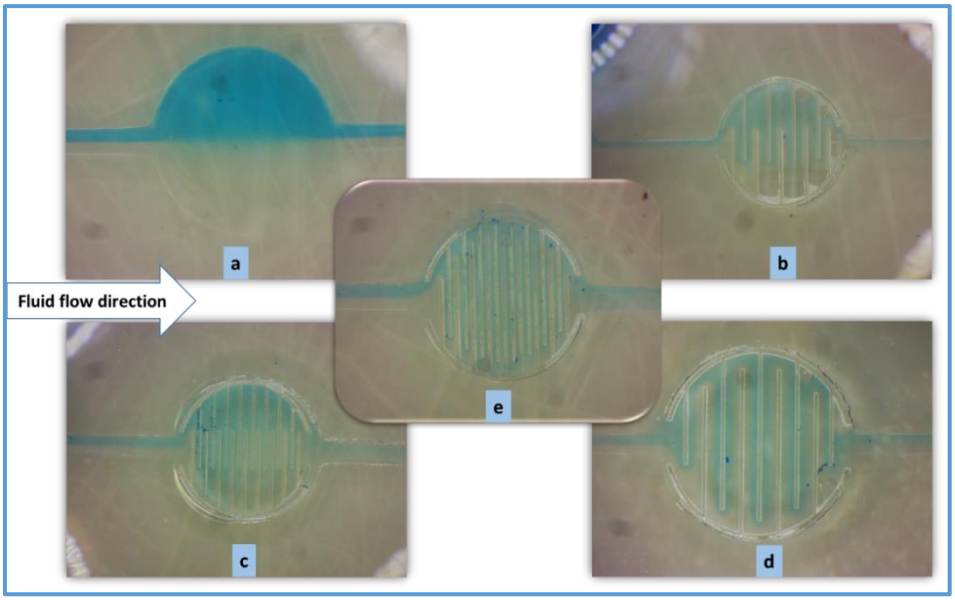

Figure 4:31 Focused optical microscope image of different mixing unit areas to Show the mixing level for different micromixers: a) simple circle [SC], b) circle with low number and same level walls [CLSW], c) circle with high number and same level walls [CHSW], d) circle with low number and e) tall (length) walls [CLTW] and circle with high number and tall (length) walls [CHTW].

All of the fabricated microfluidic chips of simple circle [SC], circle with low number and same level walls [CLSW], circle with high number and same level walls [CHSW], circle with low number and tall (length) walls [CLTW] and circle with high number and tall (length) walls [CHTW] micromixers are shown in Figure 4:30 and Figure 4:31.

In SC micromixer, the mixing efficiency of two fluids (water and methylene blue) was poor, where the two fluids pass separately with low mixing initiated around the two fluids contact area due to low molecular diffusion, and this happens through the micromixer as indicated all over the micromixer portions inlets, mixing unit area and outlets.

While the mixing efficiency improved a little bit through the fabricated microstructures walls as shown in CLSW and CLTW micromixers, in which the walls work to increase the molecular diffusion and consequently enhance the mixing efficiency. In fact, the walls restructure the flow path of the two fluids in a narrow channel (serpentine shape) which increase the fluids contacts area. And by increasing the number of used walls, the serpentine path become longer for the same area and consequently the mixing efficiency can be reached to excellent values through CHSW and CHTW micromixers with a fixed mixing area.

4.5.4.1. Concentration measurements by UV/Vis spectroscopy

Due to the good results of mixing efficiency which achieved by using the walls micromixer as reported in *sections 4.5.2.1* and *4.5.2.2*, the followed step was to focus the study in this structure and investigation the mixing performance of new structures using some parameters like the number of walls and changing the tall (length) of walls.

For the done micromixers which has different walls structures, using the described system in *section 3.5* and using the different micromixers which had

been shown in the previous *section 4.5.4*, the mixed samples were collected at outlets for different flow rate *(1-6) µl/min.*

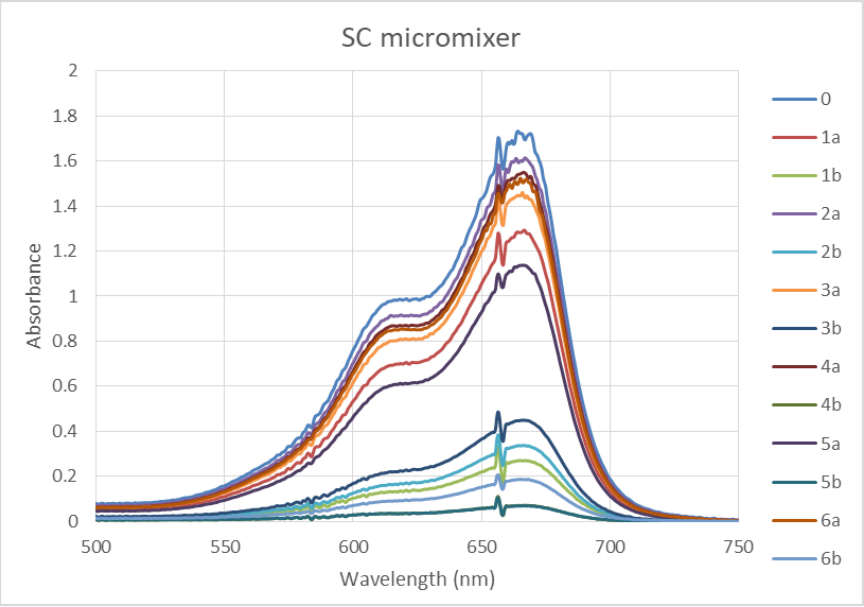

Figure 4:32 The absorbance variation at wavelength 664 nm with different flow rate for SC micromixer

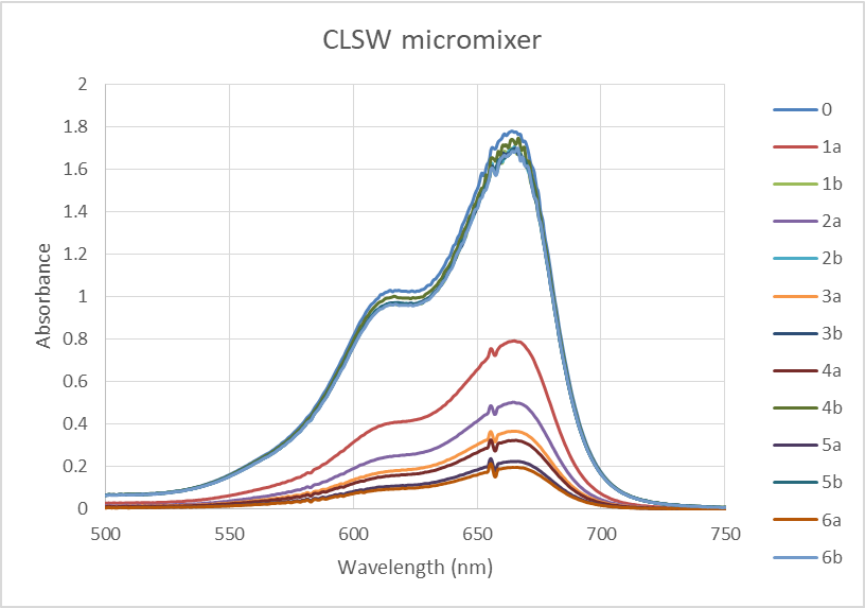

Figure 4:33 The absorbance variation at wavelength 664 nm with different flow rate for CLSW micromixer

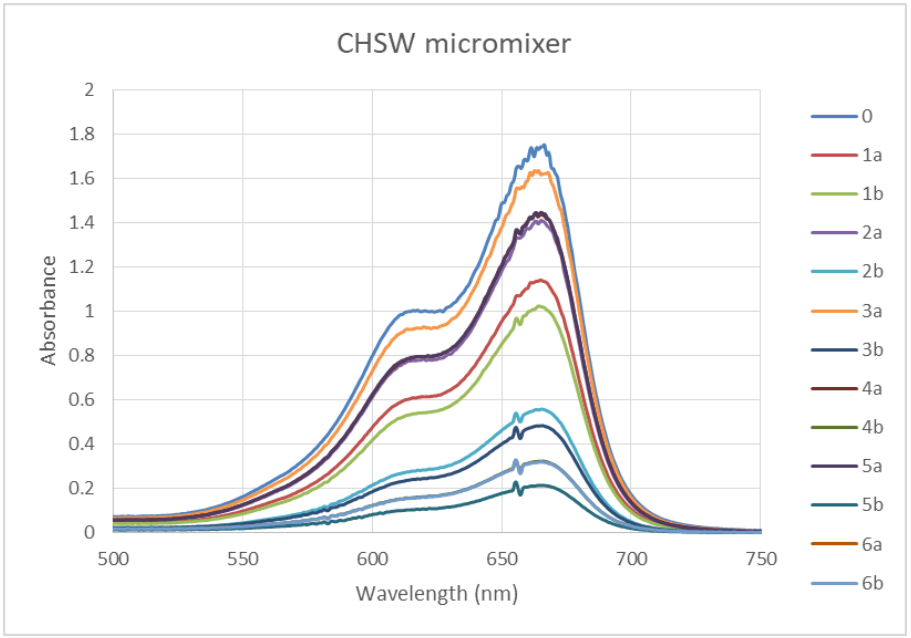

Figure 4:34 The absorbance variation at wavelength 664 nm with different flow rate for CHSW micromixer

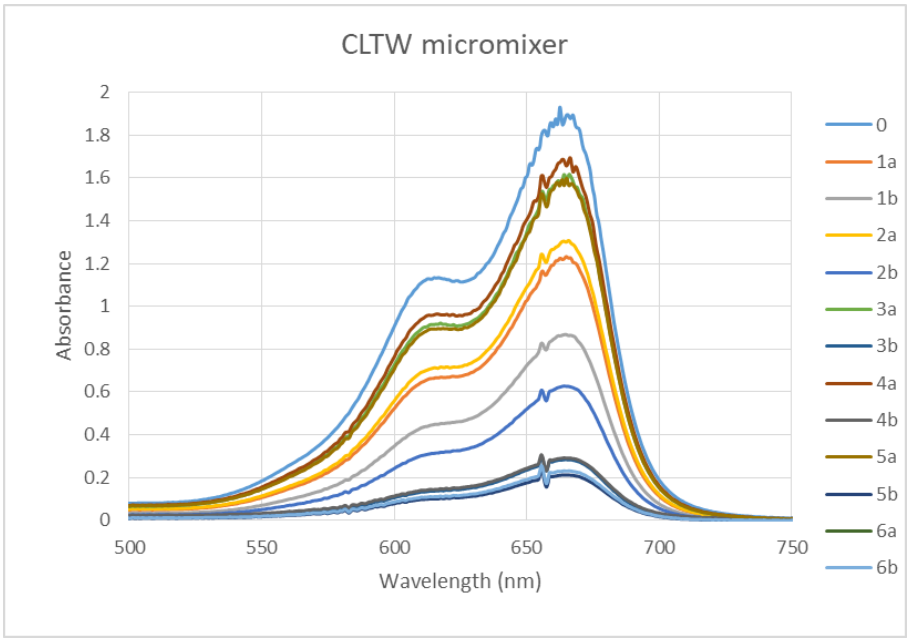

Figure 4:35 The absorbance variation at wavelength 664 nm with different flow rate for CLTW micromixer

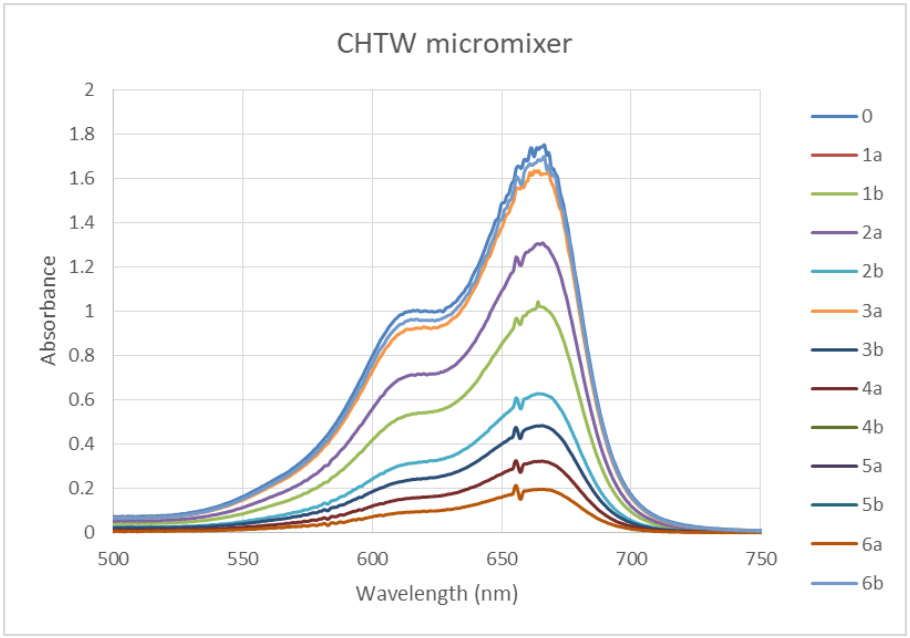

Figure 4:36 The absorbance variation at wavelength 664 nm with different flow rate for CHTW micromixer

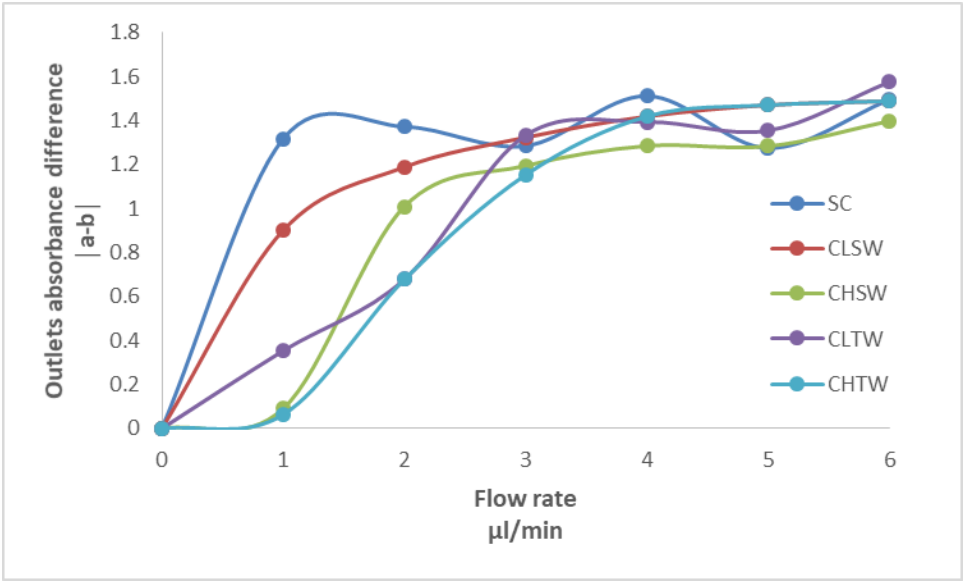

Figure 4:37 the difference of the absorbance values (around the wavelength 664 nm) between the two outlets (a) and (b) for the different walls micromixers at different flow rates.

4.5.4.2. Reynolds number and mixing efficiency calculations.

Reynolds number (Re) was calculated for all the fabricated micromixers to investigate the type of flow (laminar or turbulent) through the designed micromixers, the calculations were done using *equation 1,* which depends on the type of used fluids and the dimension of used micromixer.

The used fluids were water and diluted methylene blue, and the density (ρ) and dynamic viscosity (μ) for water and methylene blue assumed to be equally since the latter was diluted to low concentration, so the values of $\mu = 0.99987\ g/cm^3$ and $\rho = 0.0089\ dyn{\cdot}s/cm^2$ can be used for calculation for both fluids.

The dimensions of the different created micromixers are reported in Table 6, using the dimensions of each micromixer individually beside the values of fluids density and dynamic viscosity, (Re) described in *equation 1* can be calculated for the flow rates range of *1-6 µl/min*.

The velocity (*V*) of the fluids through the designed micromixer, described by the following relations (*equation 12* and *equation 13*), depends on the flow rate (*Q*) and the hydraulic diameter of the used structure (D_h), which can be calculated by the height (*a*) and width (*b*) of the designed walls. The calculated results of velocity were listed in Table 6,

$$V = \frac{4Q}{\pi D_h} \qquad (12)$$

$$D_h = \frac{2ab}{a+b} \qquad (13)$$

The Reynolds number were calculated for all design and geometries as a function of the flow rates (*1-6 µl/min*). The calculations showed that Re ranges (*0.19-1.15), (0.43-2.61), (0.49-2.960, (0.51-3.06)* and (*0.49-2.96)* for SC, CLSW, CHSW, CLTW and CHTW, respectively. This low value of Re indicates that in our work the flow is laminar.

The characteristics of the designed micromixers and the results of the mixing efficiency for the designs are summarized in Table 6,

Table 6. Results of the mixing efficiencies for different mixer walls designs.

Structure	Mixing unit area dimensions (Width /Height) *(μm/ μm)*	Inlets and outlets dimensions (Width/Height) *(μm/ μm)*	Flow Rate Range *(μL/min)*	Velocity Range *(m/s)*	Reynolds Number Range	Mixing Efficiency (%) at flow rate=1*μL/min*
SC	*2000/65*	*200/65*	*1-6*	*0.0017-0.0106*	*0.19-1.15*	*29.11*
CLSW	*170/28*	*200/28*	*1-6*	*0.0089-0.0539*	*0.43-2.61*	*63.67*
CHSW	*70/27*	*200/27*	*1-6*	*0.0116-0.0700*	*0.49-2.96*	*95.86*
CLTW	*170/25.5*	*200/25.5*	*1-6*	*0.0123-0.0742*	*0.51-3.06*	*81.72*
CHTW	*70/27*	*200/27*	*1-6*	*0.0116-0.0700*	*0.49-2.96*	*97.08*

At the end of the fabricated micromixers described in the previous *section 4.5.4*, there is two outlets, by which the mixed samples were collected. The mixing efficiency of collected mixed samples, at flow rates from *1-6 μl/min* for different micromixers structures, was calculated by *equation 5*. The concentrations of the collected samples for each flow rate can be investigated by UV/Vis Spectroscopy, then the mixing efficiency is calculated for each flow

rate individually. The results of mixing efficiency of mentioned flow rate range for each micromixer were figured out as shown in Figure 4:38.

As illustrated in Figure 4:38, the graphs show that the mixing efficiency is decreasing when the flow rate increases for all micromixers.

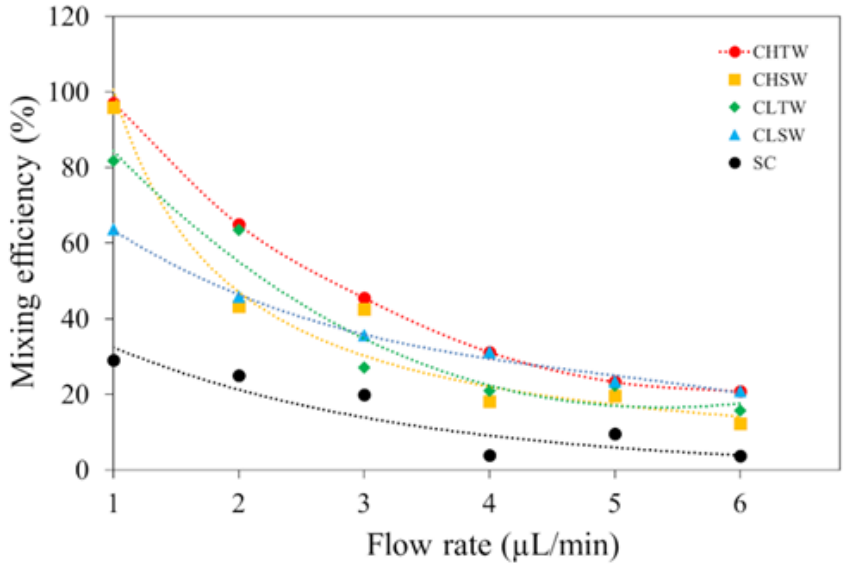

Figure 4:38 Mixing efficiency VS flow rate of different wall micromixers: a) simple circle [SC], b) circle with low number and same level walls [CLSW], c) circle with high number and same level walls [CHSW], d) circle with low number and e) tall (length) walls [CLTW] and circle with high number and tall (length) walls [CHTW].

From the mixing efficiency VS flow rate graph shown in Figure 4:38, the values of mixing efficiency at flow rate *1 µl/min* were *29.11 %, 63.67 %, 95.86 %, 81.72 % and 97.08 %* for the micromixers SC, CLSW, CHSW, CLTW and CHTW respectively.

The efficiency of mixing for micromixers SC and CLSW are poor and not good enough to be used for mixing purposes as the accepted value of efficiency should be at the range [80-100] %, while the efficiency value improved a little bit for CLTW micromixer to reach 81.72% which is accepted for mixing purposes.

The highest mixing efficiency can be achieved using CLTW and CHTW micromixers due to the fact of its geometry which increases the contact area between the different fluids and decreases the diffusion path.

Figure 4:39, shows that there is a match to some extent of the simulated and experimental mixing efficiency values for the variety different micromixers at the same velocity (*0.01 m/s*).

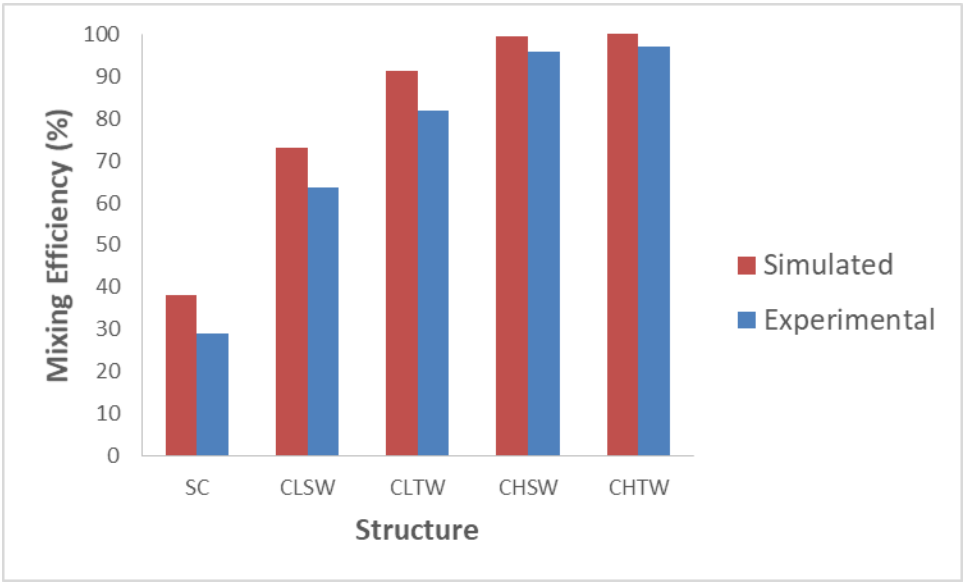

Figure 4:39 Comparison of simulated and experimental mixing efficiency for different microstructures micromixers.

Chapter 5

5. Summary

In this PhD dissertation I presented my studies of proton beam lithography and UV lithography on materials. My goal was to study the irradiation effects of proton beam and ultraviolet radiations on polymer especially PDMS and SU-8 polymers. The results of those irradiation processes of polymers were useful for some applications like microfluidic chips fabrication, which were used for mixing purposes as passive micromixers.

Due to the crosslinking of the used polymers, by the irradiation of proton beam or UV rays, any micro patterns can be fabricated in efficient way. Poly (dimethyl-siloxane) (PDMS) microstructures were inserted into PDMS microdevices using a novel microfluidic chips fabrication process that combined proton beam lithography and traditional UV lithography. This allows microstructures and microdevices to be manufactured from the same material, which is not only advantageous but also necessary in some applications.

This research focuses on the design of passive mixing microfluidic devices with and without embedded microstructures. The study covers computer simulation and optimization, followed by microfluidic chips production using the mentioned lithography techniques. Finally, UV/vis spectroscopy was used to investigate the mixing efficiency of the micromixer devices at a range of fluid flow rates. Compared to the small size of the whole mixing chip, high mixing efficiency could be achieved.

In thesis, there are two work directions which can be summarized as following:

a) Different microstructures

For micro-mixing simulations study, using COMSOL software, different microfluidic devices with and without integrated microstructures (channel, circle, circle-with-pillars and circle-with-walls micromixers) were constructed, optimized, and compared.

Real mixing tests were performed to compare the mixing functionality of the suggested microstructure designs. The mixing efficiencies were determined based on the results of these tests and to compare the performance of different microfluidic chips, at flow rate *1 µl/min*, the calculated efficiency values are found to be *58 %*, *29 %*, *72 %* and *82 %* for channel, circle, circle-with-pillars and circle-with-walls, respectively.

As a conclusion, we successfully integrated PDMS microstructures into PDMS microfluidic devices. With a proper design of the microstructures, the mixing efficiencies could be significantly improved, and reached as high as *82%*, keeping the size of the chip in the order of a few millimetres. The presented method opens the opportunity to further improve mixing efficiencies and to further decrease chip dimensions, by the development of new designs and by fabricating smaller and finer structures by nano-lithography (nano sized proton beam lithography).

b) Different walls microstructure

Different passive micromixer devices were designed, simulated and fabricated. The mixing unit area was functionalized by different walls microstructures (simple circle [SC], circle with low number and same level walls [CLSW], circle with high number and same level walls [CHSW], circle with low number and tall (length) walls [CLTW], circle with high number and tall (length) walls [CHTW]), whose shapes and layouts were designed in the simulations to improve the mixing efficiency of the chips.

In this work part, the length and the areal density of the walls in the micro wall array were varied in order to find good mixing performance. The devices were then created with ion microlithography and UV lithography techniques. Mixing test were performed from which the mixing efficiencies were determined. It was found, that the mixing efficiency of the fabricated passive micromixers can be improved to an excellent value by more densely distributed and longer micro-walls.

It was found that the so-called micro-wall-array is a promising candidate for passive mixing tasks, because it forces the fluid to flow along a very narrow serpentine shape. So, the length and the areal density of these walls were varied in order to find a better mixing performance.

The results showed that, generally, the more densely distributed and the longer walls are more efficient and their combination (long walls, densely distributed) showed the highest performance.

It was found, that the mixing efficiency of the fabricated passive micromixers, the densely distributed short walls and the densely distributed long walls, improves to an excellent value of *95.86 %* and *97.08 %*, *1 µl/min* flow rate. From these results, we conclude that the distribution of the walls has the higher effect on the mixing.

Finally, enhancements the mixing efficiency to an excellent value were reached with the simulated and fabricated designs, where the results show the dependence of the mixing efficiency on the geometry of the designed structure. And there is matching to a large extent for the mixing efficiency values, which investigated experimentally and simulation for the different walls micromixers.

Acknowledgement

First and foremost, praises and appreciations to the Almighty God for showering His blessings on me during my study effort, allowing me to successfully complete the research.

I really would like to express my sincere thankfulness to my research supervisor, *Dr. Huszánk Róbert*, for providing me with the opportunity to do research and for offering invaluable guidance throughout my research work. His deep understanding, creativity, sincerity, and motivation have exerted a great influence on me. He has educated me how to perform research and to convey my thoughts in the clearest and most concise right manner. It was a great privilege and honour to work and study under his guidance. I am extremely grateful for what he has offered me. Even beyond work, also I would like to express my gratitude for his friendship, empathy, and great sense of humour.

I thank my fellow lab mate, *Dr. Nagy Gyula*, for his valuable guidance of using the available instruments at this moment (*Van de Graaff* accelerator) to do my research, beside his encouragement, insightful comments and the stimulating discussions.

I express my gratitude to the Atomki institute and the doctoral school of physics, Faculty of Science and Technology, Debrecen University, for offering me the opportunity and providing me the necessary means to accomplish my work.

I am extremely grateful for who are behind-the-scenes, the administrative staff and the operators of the Van de Graaff and Tandetron accelerator, for their

patience and long-term work, without their assistance this work would have never been accomplished.

I must also thank colleagues at the Atomki institute, *Dr. Csík Attila*, *Szarka Máté* and *Dr. Döncző Boglárka*, for their friendship, sacrificing their precious time, and their personal and professional help for vital measurements using available devices in their lab.

Last but not the least, I like to express gratefulness to *my dear Father*, *precious Wife* and *Daughter* for their love, understanding, prayers and continuing support to complete this research work.

List of Figures

Scientific Publications

❖ Publications on the results of the present thesis

- **[A1]: Emad Nady**, Gyula Nagy, Róbert Huszánk, (2021). Functionalization of microfluidic devices by microstructures created with proton beam lithography. Vacuum, 190, 110295. https://doi.org/10.1016/j.vacuum.2021.110295

  IF^{2021}=3.627

- **[A2]: Emad Nady**, Gyula Nagy, Róbert Huszánk, (2021). Improvement in mixing efficiency of microfluidic passive mixers functionalized by microstructures created with proton beam lithography, Chemical Engineering Science Journal.
  https://doi.org/10.1016/j.ces.2021.117006

  IF^{2021}=4.311

❖ Publications not related to the dissertation

- **Emad N. Saad**, M. F. Eissa, Emad A. Badawi, M. A. K. El-Fayoumi (2014); Investigation of the physical properties of polymeric materials induced by alpha radiation Int. J. of Adv. Res. 2 (Dec). (ISSN 2320-5407).

- **Emad.N. Saad**, M. F. Eissa, Emad A. Badawi, M. A. K. El-Fayoumi. Study the effect of irradiation angle on the microstructure of CR-39 polymer, Applied Radiation and Isotopes Journal, submitted.

❖ Conferences

- **[C1]: Emad Nady**, Róbert Huszánk, Gyula Nagy: A Novel Passive Micromixer with Microstructure by Proton Beam Lithography for High Mixing Efficiency at Low Reynold Number, 17th International Conference on Nuclear Microprobe Technology and Applications (ICNMTA 2020),14-15 September 2020, Beld, Slovenia, on-line, poster.

- **[C2]: Emad Nady**, Gyula Nagy, Róbert Huszánk: Functionalization of microfluidic devices by microstructures created by proton beam lithography, 18th International Conference on Thin Films and 18th Joint Vacuum Conference (ICTF-JVC 2020), 22-26th November 2020, Budapest, Hungary, on-line, poster.

References

[1] J. Ouellette. (2003). A new wave of microfluidic devices. The Industrial Physicist, 9(4):14–17.

[2] Stephen R. Quake and Axel Scherer. (2000). From micro- to nanofabrication with soft materials. Science, 290:1536–1540.

[3] Marc A. Unger, Hou-Pu Chou, Todd Thorsen, Axel Scherer, and Stephen R. Quake. (2000). Monolithic microfabricated valves and pumps by multilayer soft lithography. Science, 288:113–116.

[4] Todd Thorsen, Sebastian J. Maerkl, and Stephen R. Quake. (2002). Microfluidic large-scale integration. Science, 298:580–584.

[5] Andreas Manz, D. Jed Harrison, Elisabeth M. J. Verpoorte, James C. Fettinger, Hans L¨udi, and H. Michael Widmer. (1991). Miniaturization of chemical analysis systems—a look into next century's technology or just a fashionable craze? Chimia, 45:103–105.

[6] P. M. Martin, D. W. Matson, and W. D. Bennett. (1999). Microfabrication methods for microchannel reactors and separations systems. Chemical Engineering Communications, 173:245–254.

[7] Peter Mitchell. (2001). Microfluidics-downsizing large-scale biology. Nature Biotechnology, 19:717–721.

[8] J. Michael Ramsey, Stephen C. Jacobson, and Michael R. Knapp. (1995). Microfabricated chemical measurement systems. Nature Medicine, 1(10):1093–1096.

[9] Sheila H. DeWitt. (1999). Microreactors for chemical synthesis. Current Opinion in Chemical Biology, 3:350–356.

[10] Klavs F. Jensen. (1999). Microchemical systems: Status, challenges, and opportunities. AIChE Journal, 45(10):2051–2054.

[11] Klavs F. Jensen. (2001). Microreaction engineering—is small better? Chemical Engineering Science, 56:293–303.

[12] Andrea W. Chow. (2002). Lab-on-a-chip: Opportunities for chemical engineering. AIChE Journal, 48(8):1590–1595.

[13] H. A. Stone and S. Kim. (2001). Microfluidics: Basic issues, applications, and challenges. AIChE Journal, 47(6):1250–1254.

[14] Janasek, D., Franzke, J., Manz, A. (2006). Scaling and the design of miniaturized chemical-analysis systems. In Nature (Vol. 442, Issue 7101, pp. 374–380). Nature Publishing Group. https://doi.org/10.1038/nature05059

[15] Kwapiszewski, R., Ziolkowska, K., Zukowski, K., Chudy, M., Dybko, A., Brzozka, Z. (2012). Effect of a high surface-to-volume ratio on fluorescence-based assays. Analytical and Bioanalytical Chemistry, 403(1), 151–155. https://doi.org/10.1007/s00216-012-5770-8

[16] Nguyen, N. T., Wereley, S. T., Shaegh, S. A. M. (2019). Fundamentals and applications of microfluidics. Artech house.

[17] Pennathur, S., Meinhart, C. D., Soh, H. T. (2007). How to exploit the features of microfluidics technology. In Lab on a Chip (Vol. 8, Issue 1, pp. 20–22). Royal Society of Chemistry. https://doi.org/10.1039/b717986n

[18] A. S. Utada, L.-Y. Chu, A. Fernandez-Nieves, D. R. Link, C. Holtze and D. A. Weitz, MRS Bull., 2007, 32, 702–708.

[19] Link, D.R., Grasland-Mongrain, E., Duri, A., Sarrazin, F., Cheng, Z., Cristobal, G., Marquez, M. and Weitz, D.A. (2006), Electric Control of Droplets in Microfluidic Devices. Angewandte Chemie International Edition, 45: 2556-2560. https://doi.org/10.1002/anie.200503540

[20] S.C. Terry, J.H. Jerman, J.B. Angell. (1979). A gas chromatographic air analyzer fabricated on a silicon wafer. IEEE Trans. Electron Dev. 26, 1880–1886.

[21] P. Yager, T. Edwards, E. Fu, K. Helton, K. Nelson, M.R. Tam, B.H. Weigl. (2006). Microfluidic diagnostic technologies for global public health. Nature 442 (7101), 412–418.

[22] G.M. Whitesides. (2006). The origins and the future of microfluidics, Nature 442 (7101), 368–373.

[23] B.H. Robertson, J.K. Nicholson. (2005). New microbiology tools for public health and their implications 1. Annu. Rev. Public Health 26, 281–302.

[24] Jeong, G. S., Chung, S., Kim, C. B., Lee, S. H. (2010). Applications of micromixing technology. In Analyst (Vol. 135, Issue 3, pp. 460–473). Royal Society of Chemistry. https://doi.org/10.1039/b921430e

[25] Hu, R. J., Lei, M., Xiong, H. S., Mu, X., Wang, Y. G., Yin, X. F. (2008). Highly selective acylation of ferrocene using microfluidic chip reactor. Tetrahedron Letters, 49(2), 387–389. https://doi.org/10.1016/j.tetlet.2007.11.035

[26] Beebe D.J., Mensing G.A., Walker G.M. (2002). Physics and application of microfluidic in biology. Annu. Rev. Biomed. Eng. 4, 261–286.

[27] Weigl B., Bardell R., Cabrera C. (2003). Lab-on-a-chip for drug development. Adv. Drug Deliv. Rev. 55(3), 349–377.

[28] Nguyen N., Wereley S. (2002). Fundamentals and applications of microfluidics. Artech House, Norwood.

[29] Einstein A., Fürth R. (1956). Investigations on the theory of the Brownian movement. Dover Publications, New York.

[30] Zhang Z., Zhao P., Xiao G., Lin M., Cao X. (2008). Focusing-enhanced mixing in microfluidic channels. Biomicrofluidics 2, 014101.

[31] Capretto, L., Cheng, W., Hill, M. and Zhang, X. (2011). Micromixing within microfluidic devices. Microfluidics, 27-68.

[32] Z. Yang, S. Matsumoto, H. Goto, M. Matsumoto, R. Maeda. (2001). Ultrasonic micromixer for microfluidic systems. Sens. Actuators, A 93, 266–272.

[33] H.H. Bau, J. Zhong, M. Yi. (2001). Aminute magneto hydro dynamic (MHD) mixer. Sens. Actuators, B 79, 207–215.

[34] J. Lin, K. Lee, G. Lee. (2005). Active mixing inside microchannels utilizing dynamic variation of gradient zeta potentials. Electrophoresis 26, 4605–4615.

[35] C. Tsouris, C.T. Culbertson, D.W. DePaoli, S.C. Jacobson, V.F. de Almeida, J.M.Ramsey. (2003). Electrohydrodynamic mixing in microchannels. AIChE J. 49, 2181–2186.

[36] L. Fu, R. Yang, C. Lin, Y. Chien. (2005). A novel microfluidic mixer utilizing electrokinetic driving forces under low switching frequency. Electrophoresis 5, 1814–1824.

[37] V. Hessel, S. Hardt, H. Löwe, F. Schönfeld. (2003). Laminar mixing in different interdigital micromixers: I. Experimental characterization. AIChE J. 49, 566–677.

[38] S.P. Sullivan, B.S. Akpa, S.M. Matthews, A.C. Fisher, L.F. Gladden, M.L. Johns. (2007). Simulation of miscible diffusive mixing in microchannels. Sens. Actuators, B 123, 1142–1152.

[39] J.B. Knight, A. Vishwanath, J.P. Brody, R.H. Austin. (1998). Hydrodynamic focusing on a silicon chip: mixing nanoliters in microseconds. Phys. Rev. Lett. 80, 3863–3866.

[40] F.G. Bessoth, A.J. deMello, A. Manz. (1999). Microstructure for efficient continuous flow mixing. Anal. Commun. 36, 213–215.

[41] A.D. Stroock, S.K.W. Dertinger, A. Ajdari, I. Mezi´ c, H.A. Stone, G.M. Whitesides. (2002). Chaotic mixer for microchannels, Science 295, 647–651.

[42] L. Wang, J. Yang, P. Lyu. (2007). An overlapping crisscross micromixer. Chem. Eng. Sci. 62, 711–720.

[43] D.G. Hassell, W.B. Zimmerman. (2006). Investigation of the convective motion through a staggered herringbone micromixer at low Reynolds number flow. Chem. Eng. Sci. 61, 2977–2985.

[44] X. Fu, S. Liu, X. Ruan, H. Yang. (2006). Research on staggered oriented ridges static micromixers. Sens. Actuators, B 114, 618–624.

[45] H. Sato, S. Ito, K. Tajima, N. Orimoto, S. Shoji. (2005). PDMS microchannels with slanted grooves embedded in three walls to realize efficient spiral flow. Sens. Actuators, A 119, 365–371.

[46] C. Hong, J. Choi, C.H. Ahn. (2004). A novel in-plane passive microfluidic mixer with modified Tesla structures. Lab-on-a-Chip 4, 109–113.

[47] Y. Liu, B.J. Kim, H.J. Sung. (2004). Two-fluid mixing in a microchannel. Int. J. Heat Fluid Flow 25, 986–995.

[48] A. Goullet, I. Glasgow, N. Aubry. (2006). Effects of microchannel geometry on pulsed flow mixing. Mech. Res. Commun. 33, 739–746.

[49] S. Park, J.K. Kim, J. Park, S. Chung, C. Chung, J.K. Chang. (2004). Rapid three-dimensional passive rotation micromixer using the breakup process. J. Micromech. Microeng. 14, 6–14.

[50] F. Jiang, K.S. Drese, S. Hardt, M. Küpper, F. Schönfeld. (2004). Helical flows and chaotic mixing in curved micro channels. AIChE J. 50, 2297–2305.

[51] S.H. Wong, M.C.L. Ward, C.W. Wharton. (2004). Micro T-mixer as a rapid mixing micromixer. Sens. Actuators, B 100, 359–379.

[52] H. Chen, J.-C. Meiners. (2004). Topologic mixing on amicrofluidic chip. Appl. Phys. Lett. 84, 2193–2195.

[53] Yaralioglu G., Wygant I., Marentis T., Khuri-Yakub B. (2004). Ultrasonic mixing in microfluidic channels using integrated transducers. Anal. Chem. 76(13), 3694–3698.

[54] Glasgow I., Aubry N. (2003). Enhancement of microfluidic mixing using time pulsing. Lab Chip 3(2), 114–120.

[55] Yang Z., Matsumoto S., Goto H., Matsumoto M., Maeda R. (2001). Ultrasonic micromixer for microfluidic systems. Sens. Actuators A Phys. 93(3), 266–272.

[56] Tsai H. Jr., Lin L. (2002). Active microfluidic mixer and gas bubble filter driven by thermal bubble micropump 1. Sens. Actuators A Phys. 97, 665–671.

[57] Bau H., Zhong J., Yi M. (2001). A minute magneto hydro dynamic (MHD) mixer. Sens. Actuators B Chem. 79(2–3), 207–215.

[58] Wu Z., Nguyen N. (2005). Convective–diffusive transport in parallel lamination micromixers. Microfluid Nanofluid 1(3), 208–217.

[59] Nguyen N., Wu Z. (2005). Micromixers – a review. J. Micromech. Microeng. 15(2):1, R1–R16.

[60] Kamholz A., Yager P. (2002). Molecular diffusive scaling laws in pressure-driven microfluidic channels: deviation from one dimensional Einstein approximations. Sens. Actuators B Chem. 82(1), 117–121.

[61] Schwesinger N., Frank T., Wurmus H. (1996). A modular microfluid system with an integrated micromixer. J. Micromech. Microeng. 6:99.

[62] Knight J., Vishwanath A., Brody J., Austin R. (1998). Hydrodynamic focusing on a silicon chip: mixing nanoliters in microseconds. Phys. Rev. Lett. 80(17), 3863–3866.

[63] Gunther A., Jhunjhunwala M., Thalmann M., Schmidt M., Jensen K. (2005). Micromixing of miscible liquids in segmented gas- liquid flow. Langmuir 21(4), 1547–1555.

[64] Song H., Tice J., Ismagilov R. (2003). A microfluidic system for controlling reaction networks in time. Angew. Chem .115(7), 792–796.

[65] Johnson T., Ross D., Locascio L. (2002). Rapid microfluidic mixing. Anal. Chem. 74(1), 45–51.

[66] Stroock A., Dertinger S., Ajdari A., Mezic I., Stone H., Whitesides G. (2002). Chaotic mixer for microchannels. Science 295(5555):647.

[67] Solliec C., Mouheb N. A., Montillet A., Malsch D. and Henkel T. (2012). Numerical and experimental investigations of mixing in T-shaped and cross-shaped micromixers Chem. Eng. Sci. 68 278–89.

[68] Cai, Gaozhe, Li Xue, Huilin Zhang, and Jianhan Lin. (2017). A Review on Micromixers. Micromachines 8, 274–301.

[69] Hossain, S.; Kim, K.-Y. (2014). Mixing analysis of passive micromixer with unbalanced three-split rhombic sub-channels. Micromachines, 5, 913–928.

[70] Li, J.; Xia, G.; Li, Y. (2013). Numerical and experimental analyses of planar asymmetric split-and-recombine micromixer with dislocation sub-channels. J. Chem. Technol. Biotechnol., 88, 1757–1765.

[71] Wang, L.; Ma, S.; Wang, X.; Bi, H.; Han, X. (2014). Mixing enhancement of a passive microfluidic mixer containing triangle baffles. Asia-Pac. J. Chem. Eng., 9, 877–885.

[72] Alam, Afroz, Arshad Afzal, and Kwang-Yong Kim. (2014). Mixing Performance of a Planar Micromixer with Circular Obstructions in a Curved Microchannel. Chemical Engineering Research and Design 9 (2), 423–434.

[73] Scherr, T.; Quitadamo, C.; Tesvich, P.; Park, D.S.; Tiersch, T.; Hayes, D.; Choi, J.W.; Nandakumar, K.; Monroe, W.T. (2012). A planar microfluidic mixer based on logarithmic spirals. J. Micromech. Microeng., 22, 55019.

[74] He, X.; Wei, D.; Deng, Z.; Yang, S.; Cai, S. (2014). Mixing performance of a novel passive micromixer with logarithmic spiral channel. Paiguan Jixie Gongcheng Xuebao/J. Drain. Irrig. Mach. Eng., 32, 968–972.

[75] Afzal, A.; Kim, K.-Y. (2014). Multi-objective optimization of a passive micromixer based on periodic variation of velocity profile. Chem. Eng. Commun., 202, 322–331.

[76] Wu, C.-Y.; Tsai, R.-T. (2013). Fluid mixing via multidirectional vortices in converging–diverging meandering microchannels with semi-elliptical side walls. Chem. Eng. J., 217, 320–328.

[77] Afzal, A.; Kim, K.-Y. (2012). Passive split and recombination micromixer with convergent–divergent walls. Chem. Eng. J., 203, 182–192.

[78] Tran-Minh, N.; Dong, T.; Karlsen, F. (2014). An efficient passive planar micromixer with ellipse-like micropillars for continuous mixing of human blood. Comput. Methods Programs Biomed., 117, 20–29.

[79] Chen, X.; Li, T. (2016). A novel design for passive misscromixers based on topology optimization method. Biomed. Microdevices, 18, 57.

[80] Chen, X.; Li, T. (2017). A novel passive micromixer designed by applying an optimization algorithm to the zigzag microchannel. Chem. Eng. J., 313, 1406–1414.

[81] The, H.L.; Le-Thanh, H.; Tran-Minh, N.; Karlsen, F. A novel passive micromixer with trapezoidal blades for high mixing efficiency at low reynolds number flow. In Proceedings of the 2014 Middle East Conference on Biomedical Engineering (MECBME), Doha, Qatar, 17–20 February 2014; pp. 25–28.

[82] The, H.L.; Ta, B.Q.; Thanh, H.L.; Dong, T.; Thoi, T.N.; Karlsen, F. (2015). Geometric effects on mixing performance in a novel passive micromixer with trapezoidal-zigzag channels. J. Micromech. Microeng., 25, 094004.

[83] Le The, H.; Tran-Minh, N.; Le-Thanh, H.; Karlsen, F. A novel micromixer with multimixing mechanisms for high mixing efficiency at low reynolds number. In Proceedings of the 2014 9th Ieee International Conference on Nano/Micro Engineered and Molecular Systems (NEMS), Waikiki Beach, HI, USA, 13–16 April 2014; pp. 653–656.

[84] Alam, A.; Kim, K.-Y. (2013). Mixing performance of a planar micromixer with circular chambers and crossing constriction channels. Sens. Actuators B Chem., 176, 639–652.

[85] Viktorov, V.; Mahmud, M.R.; Visconte, C. (2016). Numerical study of fluid mixing at different inlet flow-rate ratios in tear-drop and chain micromixers compared to a new h-c passive micromixer. Eng. Appl. Comput. Fluid Mech., 10, 182–192.

[86] Yang, J.; Qi, L.; Chen, Y.; Ma, H. (2013). Design and fabrication of a three dimensional spiral micromixer. Chin. J. Chem., 31, 209–214.

[87] Liu, K.; Yang, Q.; Chen, F.; Zhao, Y.; Meng, X.; Shan, C.; Li, Y. (2015). Design and analysis of the cross-linked dual helical micromixer for rapid mixing at low reynolds numbers. Microfluid. Nanofluid, 19, 169–180.

[88] Sheu, T.S.; Chen, S.J.; Chen, J.J. (2012). Mixing of a split and recombine micromixer with tapered curved microchannels. Chem. Eng. Sci., 71, 321–332.

[89] Li, X.; Chang, H.; Liu, X.; Ye, F.; Yuan, W. (2015). A 3-d overbridge-shaped micromixer for fast mixing over a wide range of reynolds numbers. J. Microelectromech. Syst., 24, 1391–1399.

[90] Yang, A.-S.; Chuang, F.-C.; Chen, C.-K.; Lee, M.-H.; Chen, S.-W.; Su, T.-L.; Yang, Y.-C. (2015). A high-performance micromixer using three-dimensional tesla structures for bio-applications. Chem. Eng. J., 263, 444–451.

[91] Feng, X.; Ren, Y.; Jiang, H. (2013). An effective splitting-and-recombination micromixer with self-rotated contact surface for wide reynolds number range applications. Biomicrofluidics, 7, 54121.

[92] Hossain, S.; Lee, I.; Kim, S.M.; Kim, K.-Y. (2017). A micromixer with two-layer serpentine crossing channels having excellent mixing performance at low reynolds numbers. Chem. Eng. J., 327, 268–277.

[93] Kamholz A. E. et al. (1999). Quantitative analysis of molecular interactive in microfluidic channel: the T-sensor Anal. Chem. 71 5340–7.

[94] Swickratha M. J., Burnsa S. D. and Wnekb G. E. (2009). Modulating passive micromixing in 2-D microfluidic devices via discontinuities in surface energy. Sensors Actuators. B140 656–62.

[95] Bothe D., Lojewski A. and Warnecke H. J. (2011). Fully resolved numerical simulation of reactive mixing in a T-shaped micromixer using parabolized species equations. Chem. Eng. Sci. 66 6424–40

[96] Hossain S., Ansari M. A. and Kim K. Y. (2009). Evaluation of the mixing performance of three passive micromixers. Chem. Eng. J. 150 492–501.

[97] Tofteberg T., Skolimowski M., Andreassen E. and Geschke O. (2010). A novel passive micromixer: lamination in a planar channel system. Microfluid. Nanofluid. 8 209–15.

[98] Kim K. Y. and Ansari M. A. (2007). Shape optimization of a micromixer with staggered herringbone groove. Chem. Eng. Sci. 62 6687–95.

[99] Kim K. Y., Hossain S. and Husain A. (2010). Shape optimization of a micromixer with staggered-herringbone grooves patterned on opposite walls. Chem. Eng. J. 162 730–7.

[100] Shih T. R. and Chung C. K. (2008). A high-efficiency planar micromixer with convection and diffusion mixing over a wide Reynolds number range Microfluid. Nanofluid. J. 5 175–83.

[101] Xua Z., Li C., Vadilloc D., Ruanb X. and Fub X. (2011). Numerical simulation on fluid mixing by effects of geometry in staggered oriented ridges micromixers. Sensors Actuators B. 153 284–92.

[102] Cho H. H., Kim B. S., Kwak B S., Shin S., Lee S., Kim K. M. and Jung H. I. (2011). Optimization of microscale vortex generators in a microchannel using advanced response surface method. Int. J. Heat Mass Transfer 54 118–25.

[103] Yu X., Lin Y., Wang Z., Tu S. T. and Wang Z. (2011). Design and evaluation of an easily fabricated micromixer with three-dimensional periodic perturbation. Chem. Eng. J. 171 291–300.

[104] Ohkawa K. et al. (2008). Flow and mixing characteristics of σ –type plate static mixer with splitting and inverse recombination. Chem. Eng. Res. Des. 86 1447–53.

[105] Lee S. W. and Lee S. S. (2008). Rotation effect in split and recombination micromixing. Sensors Actuators B 129 364–71.

[106] Chen Z., Bown M. R., Sullivan B. O., MacInnes J. M., Allen R. W. K., Mulder M., Blom M. and van't Oever R. (2009). Performance analysis of a folding flow micromixer. Microfluid. Nanofluid. 6 763–74.

[107] Chen J. J., Lai Y. R., Tsai R. T., Lin J. D. and Wu C. Y. (2011). Crosswise ridge micromixers with split and recombination helical flows. Chem. Eng. Sci. 66 2164–76.

[108] Nimafar M., Viktorov V. and Martinelli M. (2012). Experimental comparative mixing performance of passive micromixers with H-shaped sub-channels. Chem. Eng. Sci. 76 37–44.

[109] Karthikeyan K., L. Sujatha, and N. M. Sudharsan. (2017). Numerical Modeling and Parametric Optimization of Micromixer for Low Diffusivity Fluids. International Journal of Chemical Reactor Engineering 16 (3). 20160231.

[110] Nimafar, Mohammad, Vladimir Viktorov, and Matteo Martinelli. (2012). Experimental Investigation of Split and Recombination Micromixer in Confront with Basic T- and O- Type Micromixers. International Journal of Mechanics and Applications 2 (5), 61–69.

[111] Afzal, Arshad, and Kwang-Yong Kim. (2014). Three-Objective Optimization of a Staggered Herringbone Micromixer. Sensors and Actuators B 192, 350–60.

[112] Jen, Chun-Ping, Chung-Yi Wu, Yu-Cheng Lin, and Ching-Yi Wub. (2003). Design and Simulation of the Micromixer with Chaotic Advection in Twisted Microchannels. Lab on a Chip 3, 77–81.

[113] Tung, Kai-Yang, Li Chih-Chieh, and Jing-Tang Yang. (2009). Mixing and Hydrodynamic Analysis of a Droplet in a Planar Serpentine Micromixer. Microfluidics and Nanofluidics 7, 545–57.

[114] Madhumitha, R., S. Arunkumar, K. K. Karthikeyan, S. Krishnah, V. Ravichandran, and M. Venkatesan. (2017). Computational Modeling and Analysis of Fluid Structure Interaction in Micromixers with Deformable

Baffle. International Journal of Chemical Reactor Engineering 15 (3). 20160121.

[115] Chen, Xueye, and Xiaolei Wang. (2015). Optimized Modular Design and Experiment for Staggered Herringbone Chaotic Micromixer. International Journal of Chemical Reactor Engineering 13 (3), 305–09.

[116] Wang, Chin-Tsan, Yan-Ming Chen, and Shih-Syun Chen. (2016). Heart-Like Micro-Flow Mixer. International Journal of Chemical Reactor Engineering 14 (1), 343–49.

[117] Wang, Chin-Tsan, Yan-Ming Chen, Pei-An Hong, and Yi-Ta Wang. (2014). Tesla Valves in Micromixers. International Journal of Chemical Reactor Engineering 12 (1), 397–403.

[118] Cha, unghun, Jinseok Kim, Suk-Kyu Ryu, Jungyul Park, Yongwon Jeong, Sewan Park, Sukho Park, Hyeon Cheol Kim, and Kukjin Chun. (2006). A Highly Efficient 3D Micromixer Using Soft PDMS Bonding. Journal of Micromechanics and Microengineering 16(9), 1778–1782.

[119] Kapilmanoharan, Prabhatranjan, and Ramesh R. Lekurwale. (2014). Design & Development of a Micro-Mixer-Reactor for a LOC Application. International Journal of Advances in Science Engineering and Technology 2: 4.

[120] Svasek, P., E. Svasek, B. Lendl, and M. Vellekoop. (2004). Fabrication of Miniaturized Fluidic Devices Using SU-8 Based Lithography and Low Temperature Wafer Bonding. Sensors and Actuators A 115, 591–599.

[121] Saragih, Agung Shamsuddin, and Tae Jo Ko. (2009). Fabrication of Passive Glass Micromixer with Third-Dimensional Feature by Employing SU8 Mask on Micro-Abrasive Jet Machining. The International Journal of Advanced Manufacturing Technology 42 (6), 474–81.

[122] M. Stepanova and S. Dew, Nanofabrication: techniques and principles. 2011.

[123] X. Shi, Helium ion beam lithography. PhD thesis, University of Southampton, Southampton, United Kingdom, 2018.

[124] M. HATZAKIS, “Electron resists for microcircuit and mask production,” Electrochem SocJ, vol. 116, no. 7, pp. 1033–1037, 1969.

[125] D. L. Olynick, B. Cord, A. Schipotinin, D. F. Ogletree, and P. J. Schuck, “Electron beam exposure mechanisms in hydrogen silsesquioxane investigated by vibrational spectroscopy and in-situ electron beam induced desorption,” J.Vac. Sci. Technol. B, 2010.

[126] Harriott L.R., Hull R. (2004) Nanolithography. In: Di Ventra M., Evoy S., Heflin J.R. (eds) Introduction to Nanoscale Science and Technology. Nanostructure Science and Technology. Springer, Boston, MA

[127] H. Y. Liu and X. X. Zhu, “Lower critical solution temperatures of N-substituted acrylamide,” Polymer (Guildf)., vol. 40, p. 6985, 1999.

[128] M. A. Mohammad, T. Fito, J. Chen, S. Buswell, M. Aktary, M. Stepanova, and S. K. Dew, “Systematic study of the interdependence of exposure and development conditions and kinetic modelling for optimizing low-energy electron beam nanolithography,” Microelectron. Eng., vol. 87, no. 5–8, pp. 1104–1107, 2010.

[129] LaBianca, N.C.; Gelorme, J.D. High-aspect-ratio resist for thick film applications. Proc. SPIE 1995, 2438, doi:10.1117/12.210413.

[130] Lorenz, H.; Laudon, M.; Renaud, P. Mechanical characterization of a new high-aspect-ratio near UV-photoresist. Microelectron. Eng. 1998, 41, 371–374.

[131] Lin, C.H.; Lee, G.B.; Chang, B.W.; Chang, G.L. A new fabrication process for ultra-thick microfluidic microstructures utilizing SU-8 photoresist. J. Micromech. Microeng. 2002, 12, 590.

[132] Despont, M.; Lorenz, H.; Fahrni, N.; Brugger, J.; Renaud, P.; Vettiger, P. High-aspect-ratio, ultrathick, negative-tone near-UV photoresist for mems applications. In Proceedings of Tenth Annual International Workshop on Micro Electro Mechanical Systems, Nagoya, Japan, 26–30 January 1997; pp. 518–522.

[133] Lorenz, H.; Despont, M.; Vettiger, P.; Renaud, P. Fabrication of photoplastic high-aspect ratio microparts and micromolds using SU-8 UV resist. Microsyst. Technol. 1998, 4, 143–146.

[134] Genolet, G.; Brugger, J.; Despont, M.; Drechsler, U.; Vettiger, P.; De Rooij, N.; Anselmetti, D. Soft, entirely photoplastic probes for scanning force microscopy. Rev. Sci. Instrum. 1999, 70, 2398–2401.

[135] Carlier, J.; Arscott, S.; Thomy, V.; Fourrier, J.; Caron, F.; Camart, J.; Druon, C.; Tabourier, P. Integrated microfluidics based on multi-layered SU-8 for mass spectrometry analysis. J. Micromech. Microeng. 2004, 14, 619.

[136] Shew, B.; Kuo, C.; Huang, Y.; Tsai, Y. UV-LiGA interferometer biosensor based on the SU-8 optical waveguide. Sens. Actuators A Phys. 2005, 120, 383–389.

[137] Cho, S.H.; Lu, H.M.; Cauller, L.; Romero-Ortega, M.I.; Lee, J.B.; Hughes, G.A. Biocompatible SU-8-based microprobes for recording neural spike signals from regenerated peripheral nerve fibers. Sens. J. IEEE 2008, 8, 1830–1836.

[138] Cremers, C.; Bouamrane, F.; Singleton, L.; Schenk, R. SU-8 as resist material for deep X-ray lithography. Microsyst. Technol. 2001, 7, 11–16.

[139] Nallani, A.K.; Park, S.W.; Lee, J.B. Characterization of SU-8 as a photoresist for electron-beam lithography. Proc. SPIE 2003, 5116, doi:10.1117/12.499112.

[140] Van Kan, J.; Bettiol, A.; Watt, F. Three-dimensional nanolithography using proton beam writing. Appl. Phys. Lett. 2003, 83, 1629–1631.

[141] Lee, J. B., Choi, K. H. and Yoo, K. (2015). Innovative SU-8 lithography techniques and their applications. Micromachines, 6(1), 1-18.

[142] International Technology Semiconductor Roadmap (2003), http://public.itrs.net/Files/2003ITRS/Home2003.htm.

[143] Xia, Y., and Whitesides, G. M., Angew. Chem. Int. Ed. (1999) 37, 550

[144] Pease, R. F., Nature (2002) 417, 802

[145] Frank Watt, Mark B.H. Breese, Andrew A. Bettiol, Jeroen A. van Kan, Proton beam writing, Materials Today, Volume 10, Issue 6,2007, Pages 20-29, ISSN 1369-7021,https://doi.org/10.1016/S1369-7021(07)70129-3.

[146] Watt, F., et al., Nucl. Instr. Meth. Phys. Rev. B (2003) 210, 14

[147] Ziegler, J. F., The Stopping and Range of Ions in Matter, Vols. 2-6, Pergamon, Oxford, (1977-1985)

[148] Huszank, Robert ; Bonyár, Attila ; Kámán, Judit ; Furu, Enikő, Wide range control in the elastic properties of PDMS polymer by ion beam (H+) irradiation, Polymer degradation and stability 152 pp. 253-258. , 6 p. (2018)

[149] Van Kan, J. A., et al., Nucl. Instr. Meth. Phys. Rev. B (2007), in press

[150] Saifullah, M. S. M., Subramanian, K. R. V., Tapley, E., Kang, D. , Welland, M. E., & Butler, M. (2003). Sub-10 nm electron beam nanolithography using spin-coatable TiO 2 resists. Nano Letters, 3(11), 1587-1591.

[151] Namatsu, H., Yamaguchi, T., Nagase, M., Yamazaki, K., & Kurihara, K. (1998). Nano-patterning of a hydrogen silsesquioxane resist with reduced linewidth fluctuations. Microelectronic Engineering, 41-42, 331-334.

[152] Adesida, I. (1985). Fine line lithography using ion beams. Nuclear Inst.and Methods in Physics Research, B, 7-8(PART 2), 923-928.

[153] R. Giri, M.S. Sureshkumar, K. Naskar, Y.K. Bharadwaj, K.S.S. Sarma, S. Sabharwal, G.B. Nando, Electron beam irradiation of LLDPE and PDMS rubber blends: studies on the physicomechanical properties, Adv. Polym. Technol. 27 (2008) 98.

[154] C.N.B. Udalagama, S.F. Chan, S. Homhuan, A.A. Bettiol, T. Wohland, F. Watt, Fabrication of integrated channel waveguides in polydimethylsiloxane (PDMS) using proton beam writing (PBW): applications for fluorescence detection in microfluidic channels, in: Proc. SPIE (SPIE, 2008), vol. 6882, 68820D-8, 2008.

[155] W. Hellmich, J. Regtmeier, T.T. Duong, R. Ros, D. Anselmetti, A. Ros, Poly(oxyethylene) based surface coatings for poly(dimethylsiloxane) microchannels, Langmuir 21 (2005) 7551.

[156] S.D. Minteer, Microfluidic Techniques: Reviews and Protocols, Humana Press, New Jersey, 2006.

[157] J.-G. Lim, S.-S. Lee, K.-D. Lee, Polymeric arrayed waveguide grating using imprint method incorporating a flexible PDMS stamp, Opt. Commun. 272 (2007) 97.

[158] Z. Wu, H. Yan, H. Chen, H. Huang, One-stage fabrication of sub-micron hydrophilic microchannels on PDMS, Appl. Surf. Sci. 255 (2009) 4702.

[159] L.P. Wang, P.G. Shao, J.A. van Kan, A.A. Bettiol, F. Watt, Development of elastomeric lab-on-a-chip devices through Proton Beam Writing (PBW) based fabrication strategies, Nucl. Instrum. Methods B 267 (2009) 2312.

[160] R. Huszank, S.Z. Szilasi, I. Rajta, A. Csík, Fabrication of optical devices in poly(dimethylsiloxane) by proton microbeam, Opt. Commun. 283 (2010) 176.

[161] Y.-C. Chen, A.J. Crosby, High aspect ratio wrinkles via substrate prestretch, Adv. Mater. 26 (2014) 5626.

[162] S. Rahmouni, A. Lindner, F. Rechenmacher, S. Neubauer, T.R.A. Sobahi, H. Kessler, E.A. Cavalcanti-Adam, J.P. Spatz, Hydrogel micropillars with integrin selective peptidomimetic functionalized nanopatterned tops: a new tool for the measurement of cell traction forces transmitted through a vb3 - or a 5b1 - integrins, Adv. Mater. 25 (2013) 5869.

[163] J. Fu, Y.-K. Wang, M.T. Yang, R.A. Desai, X. Yu, Z. Liu, C.S. Chen, Mechanical regulation of cell function with geometrically modulated elastomeric substrates, Nat. Methods 7 (2010) 733.

[164] K.A.K. Beningo, Y.-L.Y. Wang, Flexible substrata for the detection of cellular traction forces, Trends Cell Biol. 12 (2002) 79.

[165] Huszank, R. (2014). Irradiation induced chemical and physical effects in silicones. Concise Encyclopedia of High Performance Silicones, 75-84.

[166] K. Saito, H. Hayashi, H. Nishikawa, Fabrication of curved PDMS microstructures on silica glass by proton beam writing aimed for micro-lens arrays on transparent substrates, Nucl. Instrum. Methods B 306 (2013) 284.

[167] R. Huszank, I. Rajta, CS. Cserháti, Proton beam lithography in negative tone liquid phase PDMS polymer resist, Nucl. Instrum. Methods B 348 (2015)213.

[168] Huszank, R., Szilasi, S. Z., and Szikra, D. (2013). Ion-energy dependency in proton irradiation induced chemical processes of poly (dimethylsiloxane). The Journal of Physical Chemistry C, 117(49), 25884-25889.

[169] R. Huszank, I. Rajta, Cs. Cserháti. (2015). Direct formation of high aspect ratio multiple tilted micropillar array in liquid phase PDMS by proton beam writing. European Polymer Journal 69, 396–402.

[170] Polydimethylsiloxane. https://en.wikipedia.org/wiki/Polydimethylsiloxane

[171] Schnabel, W.; Klaumu¨ nzer, S. Linear Energy-transfer Effects in the Radiolysis of Polymers: 2. Main-chain Degradation of Poly-methacrylonitrile and Crosslinking of Polystyrene. Radiat. Phys. Chem. 1989, 33, 323 − 328.

[172] LaVerne, J. A.; Baidak, A. Track Effects in the Radiolysis of Aromatic Liquids. Radiat. Phys. Chem. 2012, 81, 1287 − 1290.

[173] Giri, R.; Sureshkumar, M. S.; Naskar, K.; Bharadwaj, Y. K.; Sarma, K. S. S.; Sabharwal, S.; Nando, G. B. Electron Beam Irradiation of LLDPE and PDMS Rubber Blends: Studies on the Physicomechanical Properties. Adv. Polym. Technol. 2008, 27, 98 − 107.

[174] Satriano, C.; Conte, E.; Marletta, G. Surface Chemical Structure and Cell Adhesion Onto Ion Beam Modified Polysiloxane. Langmuir 2001, 17, 2243 − 2250.

[175] Grigoras, S. In Computational Modeling of Polymers; Bicerano, J., Ed.; Marcel Dekker: New York, 1993; p 161.

[176] Huszánk, R., Szikra, D.P., Simon, A., Szilasi, S., & Nagy, I.P. (2011). 4He+ ion beam irradiation induced modification of poly (dimethylsiloxane). Characterization by infrared spectroscopy and ion beam analytical techniques. *Langmuir : the ACS journal of surfaces and colloids, 27 7,* 3842-8 .

[177] COMSOL Multiphysics® v. 5.3a. www.comsol.com. COMSOL AB, Stockholm, Sweden.

[178] H. Darcy. (1856). Les fontaines publiques de la ville de Dijon. Victor Dalmont. pp. 304-311.

[179] H.C. Brinkman. (1949). A calculation of the viscous force exerted by a flowing fluid on a dense swarm of particles. Appl. Sci. Res. 1-27.

[180] Tóth, Eszter L., Eszter G. Holczer, Kristóf Iván, and Péter Fürjes. 2015. "Optimized Simulation and Validation of Particle Advection in Asymmetric Staggered Herringbone Type Micromixers" Micromachines 6, no. 1: 136-150.

[181] J. A. Van Kan, A. A. Bettiol, K. Ansari, E. J. Teo, T. C. Sum, and F. Watt. (2004). Proton beam writing: a progress review. Int. J. Nanotechnol. 1, 464-479.

[182] I. Rajta, I. Borbély-Kiss, Gy. Mórik, L. Bartha, E. Koltay, Á.Z. Kiss. (1996).The new ATOMKI scanning proton microprobe. Nucl. Instr. and Meth. B, 109/110, p. 148-153.

[183] Á.Z. Kiss, E. Koltay, G. Nagy and E. Somorjai, ATOMKI Közl. 20 (1978) 263.

[184] E. Koltay, Gy. Szabó. Nucl. ASYMMETRICAL QUADRUPOLE LENSES IN A BEAM TRANSPORT SYSTEM. Nucl. Instr. and Meths. 35 (1965), p. 88-92.

[185] G.W. Grime, M. Dawson, M. Marsh, I.C. McArthur, F. Watt. The Oxford submicron nuclear microscopy facility. Nucl. Instr. and Meths. B, 54 (1991), p. 52-63.

[186] K. Karthikeyan and L. Sujatha. (2018). Study of Permissible Flow Rate and Mixing Efficiency of the Micromixer Devices. International Journal of Chemical Reactor Engineering.

[187] Lambert, J.H. (1760). Photometria sive de mensura et gradibus luminis, colorum et umbrae [Photometry, or, On the measure and gradations of light intensity, colors, and shade]. Augsburg, (Germany): Eberhardt Klett.

[188] Beer (1852). "Bestimmung der Absorption des rothen Lichts in farbigen Flüssigkeiten" [Determination of the absorption of red light in colored liquids]. Annalen der Physik und Chemie (in German). 162 (5): 78–88.

[189] Viktorov V., Mahmud M.R., Visconte C. (2015). Comparative Analysis of Passive Micromixers at a Wide Range of Reynolds Numbers. Micromachines. 6(8):1166-1179.